Dipl.-Ing. Matthäus PEDIADITIS, BSc

Computerised Analysis of the Clinical Image of Absence Seizures

DISSERTATION

zur Erlangung des akademischen Grades
Doktor der Technischen Wissenschaften (Dr.techn.)

Doktoratsstudium an der Fakultät für Informatik und
Biomedizinische Technik
Doctoral School Biomedical Engineering

Technische Universität Graz

Betreuer/in:
Univ.-Prof. Dipl.-Ing. Dr.techn. Norbert LEITGEB

Institut für Health Care Engineering mit Europaprüfstelle für
Medizinprodukte

Graz, im November 2014

Eidesstattliche Erklärung

Ich erkläre an Eides statt, dass ich die vorliegende Arbeit selbständig verfasst, andere als die angegebenen Quellen/Hilfsmittel nicht benutzt, und die den benutzten Quellen wörtlich und inhaltlich entnommenen Stellen als solche kenntlich gemacht habe.

Graz, am ....
(Unterschrift)

Statutory Declaration

I declare that I have authored this thesis independently, that I have not used other than the declared sources/resources, and that I have explicitly marked all material which has been quoted either literally or by content from the used sources.

....
date (signature)

Acknowledgement

Most of all, I would like to thank those three persons who made it possible for me to accomplish this Dissertation: Dr. Norbert Leitgeb for the encouragement and fostering consultation, Dr. Manolis Tsiknakis for the essential support on any aspect and guidance in technical matters, and Dr. Pelagia Vorgia for the advice on clinical issues and the collaboration on data acquisition and annotation.

I would also like to express my gratitude to my lovely wife Eleni and our children, Panos and Ioannis, who have given me support through joy and sympathy. Many thanks are also addressed to all my friends and colleagues for their backup at times. Finally, I would like to especially thank my father, my mother and my brother for always being there for me since my birth.

Matthew Pediaditis
Graz, November 2014

"The scientific man does not aim at an immediate result. He does not expect that his advanced ideas will be readily taken up. His work is like that of the planter — for the future. His duty is to lay the foundation for those who are to come, and point the way. He lives and labors and hopes."

Nikola Tesla, "Radio Power Will Revolutionize the World" in Modern Mechanics and Inventions (July 1934)

Abstract

Epilepsy is one of the most common disorders of the brain. Its diagnosis is a challenging task, which relies on the experience of the attending doctor. Misdiagnosis of epilepsy reaches a rate of 30% and has tremendous consequences on the quality of life of the wrongly diagnosed patient. A precise diagnosis of epilepsy requires the assessment of both the clinical image and the Electroencephalogram (EEG). Although great advances in automatic EEG analysis have been made, the same cannot be stated for the clinical image. In current clinical practice the clinical image is assessed by the neurologist through either witnessing the epileptic seizure or watching recorded videos of the patient having an epileptic seizure, as well as taking observations delivered by caring persons into account. The aim of this work was to use image and video processing methods for a computerised analysis of the clinical image of absence seizures, a task that has not been performed before for this specific type of seizure. In contrast to the majority of related studies, which analysed epileptic seizures with distinct clinical characteristics involving motion of the extremities, this work focused on motion characteristics of subtle facial expressions. For this purpose, video recordings from 12 patients with a total of 350 seizures were analysed, incorporating state of the art object detectors for the eyes and mouth. Motion analysis in these areas was performed using dense optical flow and background-foreground segmentation with Gaussian mixture models. The two algorithms delivered nine motion-describing signals for four regions of interest. From each signal, 24 features from the time and frequency domain were extracted on a basis of a sliding window. Finally, 22 experiments with initially seven classifiers were performed in order to find the relevant features that lead to seizure detection and therefore constitute measurable facial characteristics of absence seizures.

The result was a set of features for the eye and mouth regions, that differentiate the facial expression of absence seizures from other expressions in the recorded video. It could be shown that under the condition of a robust detection of the eyes and the mouth, absence seizures can be detected automatically. Finally, issues that are related to long-term monitoring, which have not been yet explicitly taken into account by the research community in this field were exposed.

Zusammenfassung

Epilepsie ist eine der häufigsten Krankheiten des zentralen Nervensystems. Ihre Diagnose stellt eine herausfordernde Aufgabe dar, welche auf die Erfahrung des behandelnden Arztes beruht. Die Fehldiagnoserate von Epilepsie erreicht 30% und hat enorme Auswirkungen auf die Lebensqualität der falsch diagnostizierten Patienten. Für eine genaue Diagnose von Epilepsie ist die Beurteilung sowohl der klinischen Erscheinungen, als auch des Elektroenzephalogramms (EEG) ein Voraussetzung. Obwohl die Forschung große Fortschritte in der automatischen EEG-Analyse zählt, kann dasselbe nicht für die computerunterstützte Analyse der klinischen Erscheinungen belegt werden. In der Praxis werden die klinischen Erscheinungen vom Neurologen entweder durch Beobachtung des epileptischen Anfalls während seines Auftretens oder im Nachhinein durch aufgenommene Videos beurteilt, unter Berücksichtigung jeglicher Beobachtungen von Personen aus dem Umfeld des Patienten. Das Ziel dieser Arbeit war es, Bild- und Videoverarbeitungsmethoden zu nutzen, um eine Computerunterstützte Analyse der klinischen Erscheinungen von Absencen durchzuführen, eine Aufgabe, die noch nicht zuvor für diese apezifische Art von Anfällen durchgeführt wurde. Im Gegensatz zu den meisten verwandten Studien, in denen epileptische Anfälle mit deutlichen klinischen Charakteristika im Sinne von Bewegungen der Extremitäten behandelt werden, konzentriert sich diese Arbeit auf feine Bewegungsmerkmale von Gesichtsausdrücken. Es wurden Videoaufnahmen von 12 Patienten mit insgesamt 350 Anfällen analysiert. Dafür wurden Objektdetektoren aus dem Stand der Technik benutzt um Augen und Mund zu erkennen. Die Bewegungsanalyse in diesen Bereichen wurde mit dichtem optischen Fluss und Hintergrund-Vordergrundsegmentierung mit Gaußschen Mischverteilungen durchgeführt. Diese Methoden lieferten neun verschiedene Bewegungsbeschreibende Signale für insgesamt vier Bereiche von Interesse. Aus jedem Signal wurden 24 Merkmale aus dem Zeit- und Frequenzbereich mithilfe von einem gleitenden Fenster extrahiert. Schließlich wurden 22 Experimente mit anfangs sieben Klassifikatoren durchgeführt um die relevanten Merkmale, die zur Detektion von Anfällen führen und somit messbare Bewegungsmerkmale von Absencen im Gesicht darstellen, zu erkennen.

Es ergab sich eine Zusammenstellung von Merkmalen für die Augen- und Mundbereiche, welche den Gesichtsausdruck von Absencen von den anderen Ausdrücken im aufgezeichneten Video differenzieren. Es wurde gezeigt, dass Absencen automatisch erkennt werden können, unter der Bedingung einer robusten Detektion der Augen- und Mundregionen. Zusetzlich wurden Probleme aufgedeckt die in Zusammenhang mit der Langzeitüberwachung von Patienten stehen und bisher noch nicht von der Forschungsgemeinschaft in diesem Gebiet berücksichtigt wurden.

Executive summary

Diagnosis of epilepsy is a challenging task, which is based on the experience of the attending doctor. It is prone to the subjective or biased judgement of the neurologist or caring person. Misdiagnosis of epilepsy reaches a rate of 30% [5] and has tremendous consequences on the quality of life of the wrongly diagnosed patient, experiencing side effects of medication, unnecessary driving restrictions and serious employment problems [13]. Indicating the importance of the diagnostic precision, the International League Against Epilepsy (ILAE) presented a revised terminology and concepts for the organization of seizures and epilepsies on the basis of the level of specificity, i.e. the diagnostic precision [7]. Moreover, "(...) one-third or more of all epilepsies are the most poorly understood, and represent perhaps the most fertile area for future research (...)" [7]. This indicates the need for a higher diagnostic precision, which is the main problem being addressed in this thesis, on the level of analysing and quantifying the ictal phenomenology (i.e. the clinical image). This is done by applying methods of computer vison, which include image processing, video analysis, pattern recognition and machine learning, in order to perform a computerised analysis of the clinical image of absence seizures, a task that has not been performed before for this specific type of seizure.

A thorough introduction into the problem is given by describing the motivation behind this work and providing information on the diagnostic procedure of epilepsy with a detailed description of absence seizures. The largest part of the introduction is a systematic review on seizure detection and analysis based on computer vision (Section 1.6). This review offers an insight into methodology, achievements and challenges of existing approaches for motion detection, analysis and seizure recognition in epilepsy. This gives valid guidelines for approaching the problem at hand and formulating the research question, asking:

Which are the measurable facial characteristics of absence seizures, delivered by a computerised analysis of a patient's facial expression from video sequences and is it possible to use them for detecting at least two seizures for each patient?

The term "measurable" represents the quantitative aspect of the study, while the methodological boundaries are set by the terms "computerised", "facial expression" and "video". Finally the diagnostic aspect is covered by investigating the possibility to detect at least two seizures per patient, as defined by the ILAE (cf. Section 1.3).

The long-term video-EEG was recorded at the the University Hospital in Heraklion, Crete and consisted of 12 patients with 350 seizures. The video pre-processing step included deinterlacing and smoothing for noise reduction. The analysis focused on four regions of interest (ROIs), the eye-pair, the left eye, the right eye and the mouth. The feature extraction process was based on frame-differencing using Gaussian mixture models and dense optical flow. These two techniques delivered nine different signals describing motion patterns in each ROI, for each signal a total of 24 features were extracted in terms of a sliding window. This resulted in a total of 864 features, which were evaluated with initially nine classifiers in 22 experiments, grouped in four phases. The first three phases used data from eight patients and the regions of interest were annotated semi-automatically with a self-developed annotation tool. The final phase introduced fully automatic ROI detection, as well as the additional four patients. In particular, the first phase used a subset of the annotated seizures in order to limit the capturing conditions and isolate interfering factors including noise from bad illumination, heavy occlusions etc. The main aim of this phase was to select the window size and step for feature extraction, to test the different classifiers and to perform feature selection. The second phase used all annotated seizures, including those captured under varying conditions and tested the performance of the final selected classifier in the previous phase. It also performed tests with various sub-sampling ratios for the training set and a mapping of the classified instances to seizure events as a whole. The third phase analysed the influence of the different ROIs in seizure detection performance. The final phase introduced automatic ROI detection and applied the gained information from the previous phases on the four remaining patients as a final evaluation step.

The results demonstrate the existence of several features that differentiate motion patterns of the eyes and the mouth from seizure and seizure-free epochs, although the number and type of features is influenced by noise introduced as a result of the high variance in capturing conditions, as well as the inter-person variability of the seizure manifestation (characteristics and duration) by itself. The biggest challenge when it comes to detecting individual seizures in a video sequence with a duration of several hours is the dataset imbalance (many negatives and few positives). Even a few percentage of false positives may easily exceed the total number of actual positives. In order to account for that, an extremely high true negative rate would be necessary. Three possible solutions to that problem include methods that statistically model normal data/behaviour, such as semi-supervised anomaly detection (e.g. that only uses the normal labels), the partition of the negative class into multiple subclasses, including "sleeping", "eating", "talking", "reading" etc. or even a multimodal approach that uses the EEG as an additional channel of information.

Finally, the following answer can be given to the research question: Based on the analysed data, the most relevant measurable characteristics that differentiate the facial expression of absence seizures from other (unknown) expressions include the variance of time inter-

vals between adjacent spikes, derived from the mean angle, the mean magnitude weighted by the mean angle and the maximum magnitude weighted by the angle for the left and right eye. The minimum, maximum and median of the same signals is mainly relevant for the mouth region. Additional characteristics include the power in the band between 3 an 6 Hz and the dominant frequency derived from signals measuring the angle at maximum magnitude, the mean angle, the mean magnitude weighted by the mean angle, and the pixel area from background-foreground segmentation for the left eye, right eye and mouth. Considering the detection of at least two seizures for each patient, the results showed that under the conditions of a robust detection of the left eye, the right eye and the mouth (whenever visible), and given an initial position of an assumed existence of a seizure with a period of approximately 3 times the seizure duration, at least 2 seizures can be detected with an average precision of 0.86.

Contents

List of publications

This Chapter presents a list of relevant publications, written by the author, with a short description of the relevance of each publication to this thesis.

Journals

- **M. Pediaditis**, M. Tsiknakis, and N. Leitgeb. Vision-based motion detection, analysis and recognition of epileptic seizures — A systematic review. *Computer methods and programs in biomedicine*, 108(3):1133–1148, 2012.

  This publication formed the core of the systematic review on the research domain related to this thesis. It offered an understanding of the state of the art, the applied methods and challenges in the domain at hand. The contents of this review have been updated and contribute to Section 1.6.

- G. Vavoulas, **M. Pediaditis***, C. Chatzaki, E. G. Spanakis, and M. Tsiknakis. The MobiFall Dataset: Fall Detection and Classification with a Smartphone. *International Journal of Monitoring and Surveillance Technologies Research (IJMSTR)*, 2(1):44–56, 2014.

  Although the main subject of this publication is not related to video analysis or epilepsy, the feature extraction and classification methods are similar to some of those implemented for this work and described in Section 2.5.

  *Corresponding author

Conferences

- **M. Pediaditis**, M. Tsiknakis, P. Vorgia, D. Kafetzopoulos, V. Danilatou, and D. Fotiadis. Vision-based human motion analysis in epilepsy - Methods and challenges. In *10th IEEE International Conference on Information Technology and Applications in Biomedicine (ITAB)*, 2010.

  This is a publication of first results from the investigation of the research domain related to vision-based human motion analysis in epilepsy, as an effort to recognize problems and open questions.

- **M. Pediaditis**, M. Tsiknakis, V. Bologna, and P. Vorgia. Model-free vision-based facial motion analysis in epilepsy. In *10th International Workshop on Biomedical Engineering (BioEng)*, 2011.

  This publication presents preliminary results on methods for vision-based facial motion analysis in epilepsy. The main goal was to select an initial set of relevant features describing epileptic-like motion in the area of the face.

- **M. Pediaditis**, M. Tsiknakis, L. Koumakis, M. Karachaliou, S. Voutoufianakis, and P. Vorgia. Vision-based absence seizure detection. In *34th Annual International Conference of the IEEE EMBS*, 2012.

  This is the first publication presenting actual results on the detection of epileptic seizures, based on methods that have been implemented in this thesis.

- **M. Pediaditis**, M. Tsiknakis, V. Kritsotakis, M. Góralczyk, S. Voutoufianakis, and P. Vorgia. Exploiting advanced video analysis technologies for a smart home monitoring platform for epileptic patients: Technological and legal preconditions. In *International Conference on Telecommunications and Multimedia (TEMU)*, 2012.

  As an effort to produce a complete picture of possible applications of a video-based seizure detection system, this paper describes the exploitability and legal preconditions related to home monitoring of epileptic seizures, based on video.

Book chapters

- G. Giannakakis, V. Sakkalis, **M. Pediaditis**, and M. Tsiknakis. *Neuromethods, Chapter 68 - Methods for Seizure Detection and Prediction: An Overview.* Springer Science + Business Media New York, 2014.

  The author contributed to a section related to video-based analysis of epileptic seizures.

List of figures

List of tables

List of abbreviations

Abbreviation	Full term
25SPF	25% Spectral power frequency
2D	Two-dimensional
3D	Three-dimensional
AMXM	Angle at maximum magnitude
ANN	Artificial neuronal network
ANOVA	Analysis of variance
ATHP	Adaptive thresholded pixels (area of adaptive thresholded magnitudes)
DBSCAN	Density-based spatial clustering of applications with noise
EEG	Electroencephalogram
ENR	Energy ratio (last 75% to first 25% of samples of the autocorrelation)
FFNN	Feed forward artificial neuronal networks
FLE	Frontal lobe epilepsy
FN	False negatives
FP	False positives
HP	High-pass
HSV	Hue Saturation Value
ID	Identification
ILAE	International League Against Epilepsy
IR	Infra-red
KLT	Kanade-Lukas-Tomasi (tracking algorithm)
LP	Low-pass
MA	Mean angle
MMW	Mean magnitude weighted (by angle)
MNMR	Movement to non-movement ratio
MPEG-2	Motion Picture Experts Group 2
MRF	Markov random field
MXM	Maximum magnitude
MXMW	Maximum magnitude weighted (by angle)

PBFS	Pixels background-foreground segmentation
PPV	Positive predictive value
ROI	Region of interest
SM	Sum of magnitudes
SMO	Sequential minimal optimization
SVAT	Simple video annotation tool
SVM	Support vector machine
THP	Thresholded pixels (area of thresholded magnitudes)
TLE	Temporal lobe epilepsy
TN	True negatives
TP	True positives
TV	Television
VTI	Variance of time intervals (between adjacent spikes)

CHAPTER 1

Introduction

Parts of the contents of this chapter have been published in [46, 108, 110, 111, 112].

1.1 Problem overview

Epilepsy is one of the most common disorders of the brain. The estimated number of children and adolescents in Europe with active epilepsy is 0.9 million (prevalence 4.5–5.0 per 1000) [43]. Diagnosis of this disorder is a challenging task, which is based on the experience of the attending doctor. It is prone to the subjective or biased judgement of the neurologist or caring person. Misdiagnosis of epilepsy reaches a rate of 30% [5] and has tremendous consequences on the quality of life of the wrongly diagnosed patient, experiencing side effects of medication, unnecessary driving restrictions and serious employment problems [13].

A widely accepted classification of epileptic seizures [19] and epileptic syndromes [20] has been established, respectively in 1981 and 1989, by the International League Against Epilepsy (ILAE) and provides a common language that facilitates epilepsy diagnosis. These proposals are and will be subject to continuous revisions [7, 35, 36], which underline the fact that epilepsy diagnosis is characterized by practical, e.g. not being able to give a recognized syndromic diagnosis to every patient, and dynamic aspects, as seizure types and syndromes change while advances in neuroscience (e.g. genomics, molecular biology) provide new information [35]. The special report of the ILAE on this subject presented a revised terminology and concepts for the organization of seizures and epilepsies on the basis of the level of specificity, i.e. the diagnostic precision, indicating the importance of the latter [7]. Moreover, "(...) one-third or more of all epilepsies are the most poorly understood, and represent perhaps the most fertile area for future research (...)" [7].

This indicates the need for a higher diagnostic precision, which is the main problem being addressed in this thesis, on the level of analysing and quantifying the ictal phenomenology (i.e. the clinical image). This is done by applying methods of computer vison, which include image processing, video analysis, pattern recognition and machine learning.

In this scope focus is being set on automated facial expression analysis for a quantitative description of epileptic seizures. Facial expressions have been an active research topic in behavioural science, as they correlate well with self-reported emotion and emotion related physiology, while expressive changes in the face are a rich source of clues about intra and interpersonal indicators and functions of emotion [18, 132]. With respect to epilepsy, facial expressions such as grimacing, starring, laughing etc. as well as face-related motion patterns, such as lip smacking, eye deviation and eyelid flickering are frequently used in descriptions of a patient's clinical image of epileptic seizures [105].

The first step towards such a scheme is the detection of a deviation or anomaly in the facial expression, which is characteristic to an epileptic seizure. The second step includes the study of the parameters, upon which the detection scheme achieves its goal, to produce quantifiable information and new knowledge on the seizure. For the work at hand **absence seizures**, which described in depth in Section 1.4, are analysed. They exhibit a stereotypical expression and occur frequently enough. This allows the generation of an adequate dataset in size. The focus on a single seizure has proven necessary, primarily for the reduction of problem dimensionality, as more than 20 different seizure types[1] exist [7] with more than 40 possible either simple or complex facial expression descriptions [31, 105].

1.2 Motivation

As mentioned above, misdiagnosis of epilepsy reaches a rate of 30% [5], which needs to be lowered. For a precise diagnosis of epilepsy the assessment of both the clinical image and the Electroencephalogram (EEG) is required. Although great advances in the area of EEG analysis have been made [134], the same cannot be stated for the field of automated analysis of the clinical image of a patient. In current clinical practice the clinical image is assessed by the neurologist through either witnessing the epileptic seizure or watching video episodes, from long-term video-EEG recordings, of the patient having an epileptic seizure, and taking into account the observations delivered by caring persons. In this framework a reliable video analysis tool provides additional information leading to correct diagnosis. In many cases, especially if the epileptic events are rare, videos of a person's seizure are captured at home with a smartphone or a camcorder. The automatic analysis of this video as well provides information to be utilized for a correct diagnosis. Moreover, the new ILAE definition of epilepsy, as it is described in Section 1.3, demands for at least two seizures being 24 h apart, as well as a seizure recurrence risk

[1] Although generalized seizures can be categorized, the new concepts in classification of the epilepsies recommend that focal seizures should be described accurately according to their semiologic features without trying to fit them into artificial categories. This, in connection to the existence of non characterizable seizures makes it impossible to number all the existing seizure types [6].

assessment, which sometimes is only possible if documented recordings of longer periods are available. The latter asks for longer stays in hospitals or epilepsy centres for Video-EEG recording, which can be shortened if the presence of a seizure can be documented from video recordings only, taken anywhere.

A further related application of the video analysis capabilities lies within a smart home monitoring environment. Currently such environments exist, providing home care services for the elderly and patients with chronic diseases. Digital imaging, interactive webcams and camera-nursing are about to be established as standard components of a promising healthcare scheme that aims to extend the time people can live independent in their own home, thus dealing with the consequences associated to the demographical challenge, namely the higher needs in care services and the rising health-care expenditures due to a growing population of the aged [131]. For epilepsy, a smart monitoring environment will enhance the patient-related behavioural information originating at his/her home[2]. It will provide answers to questions regarding seizure frequency, duration, terms of occurrence (while awake, during sleep or both) and finally it may also serve as an alarming system for severe seizure episodes [111]. Finally, the extraction of new knowledge considering characteristics of the clinical image that are not visible by the human eye will contribute to the research community.

1.3 Epilepsy diagnosis

The word epilepsy originates from the Greek verb "epilambanein" (επιλαμβάνειν), which means "to seize, possess, or afflict" [84]. "Epilepsy is a disorder of the brain characterized by an enduring predisposition to generate epileptic seizures and by the neurobiologic, cognitive, psychological, and social consequences of this condition. (...) An epileptic seizure is a transient occurrence of signs and/or symptoms due to abnormal, excessive and synchronous neuronal activity in the brain." [41]. This conceptual definition, proposed by the ILAE in 2005 marks the existence of epilepsy if after the first unprovoked seizure there is a high risk for another seizure. The required risk is hard to define and depends on each case. Practically this requires the occurrence of a second unprovoked seizure at least after 24 h [52]. In its latest official report in April 2014 [42], the ILAE considered the difficulties of defining the required risk and other problems such as the fact that a diagnosis of epilepsy is not linked to a decision for treatment and vice versa. Moreover the above definition does not allow a patient to "outgrow" epilepsy. It provides the following definition [42]:

[2]In some cases seizures will manifest only at the familiar home environment [8].

Epilepsy is a disease of the brain defined by any of the following conditions

1. At least two unprovoked (or reflex) seizures occurring more than 24 h apart
2. One unprovoked (or reflex) seizure and a probability of further seizures similar to the general recurrence risk (at least 60%) after two unprovoked seizures, occurring over the next 10 years
3. Diagnosis of an epilepsy syndrome

Epilepsy is considered to be resolved for individuals who had an age-dependent epilepsy syndrome but are now past the applicable age or those who have remained seizure-free for the last 10 years, with no seizure medicines for the last 5 years.

In contrast to the commonly employed definition, epilepsy is defined as a disease and not a disorder. The term disease is more suitable according the the ILAE, since it conveys a more lasting derangement of normal function, while the term disorder implies a not necessarily lasting functional disturbance and minimizes the serious nature of epilepsy. The first item of the new definition includes the past definition. The second item introduces circumstances that, based on the experts, lead to managing patients as if epilepsy is present after the first unprovoked seizure. This includes e.g. patients after a stroke or with epileptiform EEG. The defined threshold of 60% is based on epidemiological studies and provides the freedom to the neurologist to specify the recurrence risk for special circumstances. The third item links the existence of an epileptic syndrome to epilepsy even if the recurrence risk is low. The final comment in the definition allows for epilepsy to "disappear". The term "resolved" implies that a person no longer has epilepsy, but it does not guarantee that it will not reappear.

As mentioned above, the decision of treatment is distinct from diagnosis but if decided, the type of treatment relies heavily on the outcome of the diagnostic process, which defines the type and dose of antiepileptic drug prescription or the possibility of brain surgery. The most important questions that a neurologist has to answer when seeing a new patient with a suspicion of epilepsy are the following:

- Are the seizures of epileptic origin[3]?
- Do seizures happen when the patient is awake, during sleep or both?
- How frequent are the seizures?
- Based on assessment of the clinical image and the EEG, which type of seizure does the patient exhibit?
- Does the patient have more than one type of seizure?
- Where is the origin (in the brain) of a focal seizure?

[3]Many seizures may have other causes than epilepsy, e.g. as a reaction to anesthesia or a strong drug, or may be caused by narcolepsy, Tourette syndrome, cardiac arrhythmia and other medical conditions. Other non-epileptic events are psychological in origin and may be referred to as psychogenic seizures.

These questions are not always easy to answer and require follow-up and/or long-term monitoring procedures. In order to obtain an assured diagnosis, usually long-term video-EEG is performed at a health care facility, giving the physician the possibility to retrospectively assess the clinical image recorded on video in synchronization to the EEG. During this process the neurologist compares any eplieptiform finding (e.g. epileptiform discharges) in the EEG with the clinical image visible in the video during ictal and interictal phases.

1.4 Absence seizures

Absence seizures are generalized seizures with three subtypes, according to the ILAE [7]: typical absences, atypical absences and absences with special features (myoclonic absence and eyelid myoclonia). Typical absences are brief, generalized epileptic seizures of sudden onset and termination. They present a cluster of clinico-EEG manifestations that may be syndrome-related, as for example in Childhood Absence Epilepsy, in which typical absences persist as the only seizure type. Typical absences most frequently occur between 4 and 9 years of age. Transient impairment of consciousness (severe, moderate, mild or inconspicuous) is an essential component of typical absences and may be the only clinical symptom (simple absences). When the transient impairment of consciousness is combined with other manifestations (clonic, myoclonic, atonic, autonomic components and automatisms) absences are characterized as complex [106].

Clonic and myoclonic symptoms are particularly frequent at the seizure onset. The most common are clonic or myoclonic jerking of the eyelids, eyebrows, and eyeballs, including random or repetitive eye closures and horizontal or vertical nystagmus-like ocular movements. Perioral myoclonias at the corner of the mouth and jerking of the jaw are less common, while clonic or myoclonic jerks of the head are even less frequent. Tonic components may affect extensor or flexor muscles symmetrically or asymmetrically. The eyes and the head may be drawn backwards (retropulsion) or to one side. Atonic symptoms are not unusual and may lead to drooping of the head. Autonomic components consist of pallor and less frequently sweating, flushing, salivation etc. Automatisms usually occur when cognition is impaired and may be delayed, 4-6 sec after onset. The most common automatisms are lip licking, smacking, swallowing, chewing, shoulder shrug and mute speech movements. [104]

The above descriptions reveal the complexity of the problem at hand, but they also indicate that head motion, eye- and mouth-related motion is heavily involved in absence seizures.

1.5 Seizure detection and prediction based on computerised EEG analysis

EEG is with no doubt the most established instrument in analysing epileptic brain activity. The first application of EEG in epilepsy was performed in 1934, by Frederic A. Gibbs and his colleagues Hallowell Davis and William G. Lennox. They reported EEG findings in epilepsy and states of altered consciousness [138]. Since then, EEG evolved to play a central role in diagnosis and management of patients with seizure disorders. It is a convenient and relatively inexpensive way to measure the physiological manifestations of abnormal cortical activity as a result of epilepsy [128]. Since EEG is an important component of the epilepsy diagnosis process, a brief overview of the involved methods is given in this section.

Until recently, seizures were identified only visually by an expert neurologist. However, this procedure constitutes a laborious task especially in the case of long-term EEG recordings. Therefore, automatic computer-based algorithms have evolved in order to shorten and automate this procedure and many seizure detection methods are reported in the literature [2, 125, 134]. Most studies present a solution to the problem of seizure detection in the context of a potential decision support system for the neurologist expert. As there are many types of seizures, this is sometimes a difficult task, taking into account the nature, the duration and singularities of each seizure type. When a patient experiences seizures of different types one needs to categorize ictal EEG periods into specific types, although some epileptic syndromes are difficult to be characterized as being of specific category. A more demanding task, which is considered an open scientific question, is the prediction of a seizure [143], which will obviously improve the quality of life of people suffering from severe seizures. Besides, the perfect understanding of underlying mechanisms leading to seizures does not jet exist, while and the determination of the exact location in the brain of the origin of a seizure is a much sought-after problem.

Towards this direction, many EEG analysis algorithms have been proposed. They include linear methods, which have been widely used, based mainly on synchronization features, as a primer and straightforward approach. Although these methods can detect in some cases epileptic seizures, they have some limits if someone takes the nature of real human EEG signal into account [59, 102]. Under this prism, EEG signals can be interpreted as the result of a system consisting of highly non-linear elements. The study of non-linear EEG dynamics can reveal hidden information and provide a more complete picture of underlying brain processes [40]. As a result non-linear methods have been used with increased accuracy over the last decade in the area of seizure detection and prediction.

In order to detect or predict an epileptic seizure, various features are extracted, which are either thresholded or fed into a classifier, trained to detect the event under investigation. A summary of the extracted features is given in the following two Subsections. The most common approach for determining a threshold is the product of a constant and the standard deviation of the feature space distribution. In terms of machine learning, classifiers including expert systems [103], decision trees [116], artificial neural networks [74, 129, 135] and support vector machines [14] have been used.

1.5.1 Seizure detection

For seizure detection, linear methods have been widely used due to their simplicity and versatility. One of the simplest linear statistic metrics is the variance of the signal. It offers an insight into dynamics underlying the EEG and is usually calculated in consecutive windows. A further linear method is based on the autocorrelation function, exploiting the periodic nature of seizures. Liu et al. [80], using scored autocorrelation moment analysis, distinguished EEG epochs containing seizures with an accuracy of 91.4% although the signals did not present differences in terms of spectral properties. Further linear methods include linear prediction filters [4] discrete wavelet transform [39], relative fluctuation index [145] and time-frequency methods [51].

On the other hand, non-linear analysis of EEG has attracted the interest by many research groups mainly because it incorporates the non-stationary nature of a signal. It perceives brain mechanisms as part of a macroscopic system in a way to understand its spatio temporal dynamic properties. The revealed underlying information of ongoing EEG leads to promising results not only in the detection but also in the prediction of upcoming seizures [130]. Such methods include the fractal dimension [37] and the Lyapunov exponent [48]. Finally, coming from the information theory domain, entropy has been widely used for automatic seizure detection [2, 74] to address and describe the irregularity, complexity, or unpredictability characteristics of a signal.

1.5.2 Seizure prediction

The notion of seizure prediction was firstly introduced in 1975 based on spectral analysis of EEG data collected from two electrodes [140]. In 1981, Rogowski et al. [123] investigated preictal periods using pole trajectories of an autoregressive model, while Gotman et al. [47] reported rates of interictal spiking as indicators of upcoming seizures.

In the category of linear methods, Mormann et al. [94] investigated, among other methods, the statistical moment of the EEG amplitudes in order to detect the pre-ictal state. Among other linear measures, the power has been used in [137] and the signal variance has been used in [88] to predict seizure onset. Further approaches include Hjorth parameters [107], accumulated energy [79] and autoregressive models [17].

Non-linear approaches for seizure prediction include the Lyapunov exponent [53], dynamical similarity index [75], correlation dimension [85], entropy [147] and phase synchronization [93].

1.6 Seizure detection and analysis based on computer vision

This Section presents a systematic documentation of research related to the main subject of this thesis. Its purpose is to report on the methodology, achievements and challenges

of existing approaches in vision-based human motion analysis, motion detection, as well as seizure recognition in epilepsy with a strong focus on utilized methodologies and associated feature sets. The following questions are addressed:

- What is the objective behind each reported work?
- Which technological/algorithmic tools are applied?
- Which features are being analysed?
- What constraints or assumptions are being set?
- What is the quality of the results so far obtained?

1.6.1 Methodology

The period of interest for this review spans from 2000 to 2014 (to date). The following search string was used in the SCIRUS[4] search engine as an initial search action in July 2010: human* AND epilepsy AND (video OR vision) AND (motion OR movement OR seizure) AND (analysis OR detection OR recognition) ANDNOT ("case report" OR animal* OR mri OR fmri). The results were filtered based on their title and abstract. Additionally searching of publications by the same authors of initially identified relevant papers, following references, and using the "cited by" function whenever available by the search engine resulted to a total of 28 articles from journals and conferences. In classifying the available literature, the functional taxonomy presented in the 2001 survey by Moeslund and Granum [91], dealing with vision-based human motion capture, has been taken into account. It distinguishes between initialization, tracking, pose estimation and recognition. This taxonomy was however rearranged to fit the purposes of this review. Specifically, the articles here are first grouped into marker-based and marker-free methods (cf. Subsection 1.6.4). Within each group, methods dealing with either motion detection, analysis or recognition are then separately described, although for marker-based approaches no explicit motion detection tasks were reported. Subsequently for each subgroup references to initialization and tracking are made within the text if available. Table 1.1 shows an overview of all included publications sorted according to type (i.e. marker-based and marker-free) and year. It also summarizes the algorithms each study presents and the respective methods that were applied for the evaluation of results.

1.6.2 Vision-based human motion detection, analysis and recognition of epileptic seizures

Research so far can be divided into three groups, each dealing with motion detection, analysis or recognition. Regarding motion detection, there are efforts for normal and seizure-like (not strictly epileptic) motion detection with the aim of developing intelligent patient monitoring (e.g. alarm triggering) systems, for which the reliable detection of the

[4]http://www.scirus.com/, Accessed 2011

onset of a seizure or any abnormal movement is important [118]. Moreover, motion detection can be used for data reduction purposes by detecting and discarding video sections that do not contain information relevant to human motion. Although motion detection is implicitly a part of any study dealing with motion analysis, for this review, only publications with detection of movement as their main objective were assigned to the first group. With regard to motion analysis, the second group, research focuses on extracting objective information which quantitatively describes a patient's motoric pattern for facilitating diagnosis and enhancing treatment, while offering a refinement of the characterization of motion. Finally, in terms of motion recognition, the third group, the identification of specific seizure types and the distinction between epileptic and non-epileptic motion is being explored in the corresponding studies. Performance and robustness of this task is crucial since it provides the main functionality of a decision support system with significant clinical utility in supporting the diagnosis and management of epilepsy. Hence generalization of such a system to the whole spectrum of epileptic syndromes is a major challenge towards an integrated health care scheme for this disease.

1.6.3 Features for motion detection, analysis and recognition of epileptic seizures

Features are measurable properties of the phenomenon being observed. They enable the quantification and subsequent classification of an observation and therefore should be discriminating and independent [11]. The chosen features for vision-based human motion analysis are usually physical quantities such as displacement (motion trajectories), velocity, area, angle, angular speed and duration. The time-dependent signal derived from these features is usually further decomposed into parameters such as the variance of time intervals between subsequent peaks or the number of peaks per time unit. The following features are utilized so far in studying epilepsy-related motion, based on video:

The most commonly analysed feature is the motion trajectory, the path of a moving object through space as a function of time. In marker-based methods x- and y-components of 2D marker trajectories [76] and derivatives, like the relative amplitude as a difference to first frame [144], the distance of selected markers to a reference marker [23, 16] and the power spectrum [16, 89, 136, 144] are often used. Recently, an approach using 3D trajectories was proposed, measuring the Euclidian distance of a marker position in each frame to the position in the first frame [27]. The dominant frequency and the accumulated displacement of arm motion are used in motion recognition [82]. For motion analysis without markers, trajectories, also called "temporal motor activity" signals, are extracted by automatic tracking of either manually or automatically selected anatomical sites [60, 65, 69, 97]. The location of selected anatomical sites is usually projected into the horizontal-vertical plane in order to achieve data reduction from the 3D to the 2D space. Regarding seizure recognition, the time-dependent projections of motion trajectories are the basis for the extraction of further features [69]: (a) The variance of the time intervals between any two subsequent peaks or transients. This feature is used for estimating the periodicity of the movements based on the observation that rhythmic movements would produce variances close to zero. (b) The energy ratio of the autocorrelation sequence

Table 1.1: Publications on vision-based motion detection, analysis and recognition of epileptic seizures from 2000 onwards, sorted according to category (maker-based or marker-free) and year.

Author	Year	Seizure type, motion type	Category	Dimensions	Methods for main objective			Features	Evaluation
					Motion detection	Motion analysis	Motion recognition		
Li et al. [76]	2002	Epileptic seizures, not specified	Marker-based, 22 markers	2D	-	Thresholding; 2D ballistic model; Kalman filter; Greedy algorithm	-	Motion trajectory; Speed	Based on graphical visualization
Cunha et al. [23]	2003	Epileptic seizures, not specified	Marker-based, 30 markers	2D	-	Thresholding; 2D ballistic model; Kalman filter; Greedy algorithm; commercial tool; Reference markers;	-	Distance to reference markers	Based on graphical visualization; Comparison to manual tracking
Wagner et al. [142]	2004	Frontal and temporal lobe epilepsy	Marker-based, 2 points were tracked	2D	-	Manual tracking with a commercial tool as in [31]	-	Angular speed and duration of head movements. Duration from seizure onset to occurrence of movements	Statistical analysis; Mann-Whitney-Wilcoxon-test
Meier et al. [89]	2005	Automotor and hypermotor seizures	Marker-based	2D	-	Manual tracking with a commercial tool as in [31]	Thresholding	Relative wrist-trunk speed; Relative wrist extend; Power spectrum	Statistical analysis
Ulowetz et al. [136]	2005	Automotor and hypermotor seizures	Marker-based	2D	-	Manual tracking with a commercial tool as in [31]	Thresholding	Relative wrist-trunk speed; Wrist extend; Trunk extend; Power spectrum	Statistical analysis

O'Dwyer et al. [99]	2005	Temporal lobe epilepsy	Marker-based	2D	-	Manual tracking (cf. [98])	-	Angle, duration, angular speed of head movement	Statistical analysis; Mann-Whitney-Wilcoxon-test
O'Dwyer et al. [100]	2007	Temporal lobe epilepsy	Marker-based, 2 points were tracked	2D	-	Manual tracking with a commercial tool: MaxTraQ x.2, Innovation Systems Inc. (cf. [98])	-	Angle, ipsilateral and contralateral angular speed. Duration of head movement	Statistical analysis; Mann-Whitney-Wilcoxon-test; Pearson's product-moment correlation; frame-by-frame inspection
Cunha et al. [24]	2009	Epileptic seizures, not specified	Marker-based	3D	-	Commercial system	-	Not specified	Comparison to previous 2D method [23]
Yang et al. [144]	2009	Temporal lobe epilepsy	Marker-based	2D	-	Manual marker coordinate selection	-	Power spectrum; Relative amplitude	Statistical analysis (t-test); Distal vs. proximal limb amplitude ratio; Shoulder vs. abdominal amplitude ratio

Chen et al. [16]	2009	Supplementary motor area seizures of frontal lobe epilepsy; Temporal lobe epilepsy; Psychogenic/non-epileptic seizures	Marker-based	2D	-	Manual marker coordinate selection	-	Power spectrum; Relative amplitude	Statistical analysis (one-way ANOVA); Distal vs. proximal limb amplitude ratio; Shoulder vs. abdominal amplitude ratio
Cunha et al. [25]	2009	Automotor and hypermotor seizures	Marker-based, 3 markers	2D	-	Thresholding; Thresholding 2D ballistic model; Kalman filter; Greedy algorithm		Wrist extent; Maximum; Average wrist motion velocity	Statistical analysis; Mann-Whitney-Wilcoxon-test
Cunha et al. [26]	2010	Upper limb automatisms, temporal and frontal lobe epilepsy	Marker-based	2D		Manual tracking with a commercial tool as in [99]	-	Duration of automatisms in relation to total seizure duration; Movement speed; Total distance traveled of marked points during a seizure; Dominant frequency	Statistical analysis
Mirzadjanova et al. [90]	2010	Upper limb automatisms, temporal lobe epilepsy	Marker-based	2D	-	Manual tracking with a commercial tool	-	Wrist extent; Dominant frequency, Maximum and average speed; Accumulated displacement during a seizure; Seizure duration	Statistical analysis

Rémi et al. [121]	2011	Automotor and hypermotor seizures	Marker-based	2D	-	Thresholding; 2D ballistic model; Kalman filter; Greedy algorithm; as in [76], [23]	Thresholding	Trunk, wrist movement extent; Trunk, wrist movement speed	Statistical analysis
Rémi et al. [122]	2011	Frontal and temporal lobe epilepsy	Marker-based	2D	-	Automatic and manual tracking; Commercial system	-	Time between clinical onset and head turning; Duration; Angular speed	Statistical analysis; Mann-Whitney Wilcoxon-test
Lu et al. [82]	2011	Epileptic seizures, not specified	Marker-based (colored pajama)	2D	-	HSV modeling and Gaussian mixture models for limb segmentation; Boundary point detection; Edge detection	Thresholding	Motion trajectories; Arm orientation; Accumulated displacement; Dominant frequency	Graphical visualization
Cunha et al. [27]	2012	Simulated motor paradigm; Complex motor seizure	Marker-based	3D	-	Commercial system	-	Euclidian distance	Comparison to previous 2D method [23]

Karayiannis et al. [65]	2001	Neonatal myoclonic; Focal clonic; Random movement	Marker-free; Holistic view	2D	-	Sub-band decomposition; Non-linear filtering (median); Segmentation for gaining the pixel area of moving body parts, Kanade-Lucas-Tomasi for site selection and tracking for gaining the motion trajectories	-	Pixel area of moving body parts (average, relative speed), Motion trajectories	Frame-by-frame inspection
Karayiannis [60]	2002	Neonatal myoclonic; Focal clonic	Marker-free; One site/body part	2D	-	Sub-band decomposition for Pixel area of moving body parts; Kanade-Lucas-Tomasi for gaining the motion trajectories	-	Pixel area of moving body parts, motion trajectories	Frame-by-frame inspection
Karayiannis et al. [61]	2003	Neonatal myoclonic; Focal clonic	Marker-free; One site/body part	2D	-	Optical flow	-	Max. velocity (maximum velocity)	Frame-by-frame inspection
Karayiannis et al. [64]	2003	Neonatal myoclonic; Focal clonic	Marker-free; One site/body part	2D	-	Deformable motion model for tracking compared to translational motion model	-	Motion trajectories	Frame-by-frame inspection

Liu et al. [81]	2004	Synthetic data and real epilepsy monitoring video	Marker-free	2D	Markov random field theory; Mean field theory	-	-	Change detection maps	Frame-by-frame inspection
Karayiannis et al. [67]	2004	Neonatal myoclonic	Marker-free; Holistic view (all pixels above a level)	2D	-	Optical flow (discrete formulation compared to Horn-Schunck); Thresholding for gaining the pixel area of moving body parts	-	Pixel area of moving body parts	Frame-by-frame inspection
Karayiannis et al. [66]	2004	Neonatal myoclonic	Marker-free; One site/body part	2D	-	Predictive block matching for site tracking	-	Motion trajectories	Root-mean-square error and frame-by-frame inspection
Sami et al. [126]	2004	Neonatal myoclonic; Focal clonic; Random movement	Marker-free; Multiple sites/body parts	2D	-	Optical flow for site selection; Predictive block matching for tracking	-	Motion trajectories	Frame-by-frame inspection
Karayiannis et al. [70]	2005	Neonatal myoclonic; Focal clonic; Random movement	Marker-free; Holistic view (all pixels above a level)	2D	-	Optical flow; Thresholding for gaining the pixel area of moving body parts	-	Pixel area of moving body parts	Frame-by-frame inspection
Karayiannis et al. [72]	2005	Neonatal myoclonic	Marker-free; One site/body part	2D	-	Translational motion model for tracking	-	Motion trajectories	Frame-by-frame inspection

Karayiannis et al. [71]	2005	Neonatal myoclonic, focal clonic; random movement	Marker-free; One site/body part	2D	-	Fractional and generalized fractional block motion model for tracking compared to translational and deformable motion models	-	Motion trajectories	Root-mean-square error and frame-by-frame inspection
Karayiannis et al. [62]	2005	Neonatal myoclonic; Focal clonic, random movement	Marker-free; One site/body part	2D	-	Frame differencing; Non-linear filtering (median); Clustering; Morphological filtering	-	Pixel area of moving body parts	Frame-by-frame inspection
Karayiannis et al. [69]	2005	Neonatal myoclonic; Focal clonic	Marker-free; One site/body part	2D	-	Frame differencing; Non-linear filtering (median); Clustering; Morphological filtering and optical flow plus thresholding for gaining the pixel area of moving body parts; Predictive block matching and block motion tracking for the motion trajectories	Feed-forward neural networks	Pixel area of moving body parts (Variance of time intervals, energy ratio, maximum peak duration, number of peaks); Motion trajectories (Energy ratio, maximum peak duration, variance of time intervals, number of extrema)	Scatter plots, Fisher ratio, Generalized Fisher ratio for feature selection; Sensitivity, specificity for recognition

Karayiannis et al. [68]	2005	Neonatal myoclonic; Focal clonic; Random movement	Marker-free; Multiple sites/body parts	2D	-	Optical flow for site selection; Adaptive block matching for tracking compared to Kanade-Lucas-Tomasi (translational motion model)	-	Motion trajectories	Root-mean-square error and frame-by-frame inspection
Karayiannis et al. [73]	2006	Neonatal myoclonic; Focal clonic; random movement	Marker-free	2D	-	Optical flow with direct thresholding; Clustering of velocities and clustering of motion model parameters.	Feed-forward neural networks	Pixel area of moving body parts (energy ratio, variance of time intervals, maximum peak duration, 10% spectral power frequency)	Scatter plots for feature selection; Sensitivity; Specificity
Karayiannis et al. [63]	2006	Neonatal myoclonic; Focal clonic; Random movement	Marker-free	2D	-	Frame differencing; Non-linear filtering (median), Vector clustering; Morphological filtering	-	Pixel area of moving body parts (Variance of time intervals, energy ratio, maximum peak duration)	Scatter plots; Fisher ratio; Generalized Fisher ratio; t-test
Cuppens et al. [28]	2008	Simulated video for normal sleep movement and seizure-like movement	Marker-free	2D	-	Optical flow	-	Max. velocity (Average of 0.06 % of the highest magnitudes)	Movement vs. non-movement ratio; Absolute value

Cuppens et al. [29]	2010	Epileptic convolution during night; normal movement	Marker-free 2D	-	Optical flow	Global/ variable threshold	Max. velocity (Optimal percentage of the averaged highest motion vector magnitudes)	Movement vs. non-movement ratio; ROC-curves; sensitivity; positive predicted value
Cuppens et al. [30]	2010	Not specified epileptic events during night	Marker-free 2D	-	Optical flow	Threshold	Max. velocity (mean of the magnitude of the largest motion vectors)	Three-fold cross validation for determining the optimal values for the number of vectors and the threshold
Ntonfo et al. [96]	2012	Neonatal seizures	Marker-free 2D	-	Frame differencing	Threshold	Average motion signal; Difference between normalised autocorrelation and Yin estimator	Preliminary results; 10 video recordings
Ntonfo et al. [97]	2012	Neonatal seizures	Marker-free 2D	-	Optical flow for location of point with maximum velocity; Template matching and optical flow for tracking; DBSCAN clustering	-	Geisture trajectories: length, location, angle, speed	Preliminary results; Only two videos; Cardinality of a cluster

Kalitzin et al. [58]	2012	Major motor seizures, clonic and tonic-clonic seizures	Marker-free 2D	-	Optical flow; Principal components extraction through the maximum eigenvalue of the covariance matrix; wavelets responses at various frequencies in a time window	Threshold	Global properties of the velocity field: rates of rotation, translation and shear as primary features; Final feature: "spectral contrast"	Statistical separation test: non-parametric Kolmogorov-Smirnov test
Pisani et al. [114]	2014	Neonatal seizures of clonic type; Other seizure types; Noise	Marker-free 2D	-	Background-foreground segmentation; Erosion	Thresholding	Average motion signal	

which is calculated as the ratio of the energy contained by the last 75% of the samples of the autocorrelation sequence to the energy contained by the first 25%. It is a measure for the rhythmicity of motion manifested as quasiperiodic peaks [69]. (c) The maximum peak duration as a quantitative measure of the speed of the movement. (d) The number of peaks per time unit, e.g. by shifting a time window counting the peaks over the entire sequence.

A further common feature is the velocity, as well as statistical quantities (average, maximum) derived from it [25]. This feature is being employed for motion analysis in marker-based methods [76, 121], alongside with the relative velocity between two markers (e.g. the relative wrist-trunk speed) alongside with the relative velocity between two markers [89, 136]. In marker-free approaches the velocity feature is also used for motion analysis and is obtained from the velocity vector-fields computed, e.g. by optical flow, from successive frames of the video. The so-called "temporal motion velocity" signal, used in [61] consists of the maximum velocity over time of any pixel or pixel block in a given region of each frame. The region is defined as the region that contains the moving body part. Instead of defining a region and calculating the maximum velocity, the average of a percentage of all maximum velocities can be calculated [28, 29]. For describing the relative speed of motion, the relative speed signal is obtained by multiplying the areas of the moving parts by the distance covered by them between adjacent frames [65].

Some marker-based techniques also use the area change over time of a rectangle containing a marker trajectory (maximum in all directions) for motion analysis. It is called the "movement extent", e.g. of the wrist [25, 89] or the trunk [136]. During motion analysis in marker-free applications, the so-called "temporal motion strength" signals are extracted from video sequences by measuring the pixel area of the moving body parts within successive frames [60, 65]. The temporal area change signal is obtained by averaging areas containing motion whose centroids are present within a small radius between successive frames, in order to prevent contribution of spurious noisy patches. The area can also be regarded as the area containing all pixels with velocities exceeding a certain threshold [67, 70] or as the minimum of clustered displacement areas [62, 63]. Other methods for calculating the area include clustering of the pixel velocities or clustering the model parameters obtained by fitting a motion model to the pixel velocities [73]. For seizure recognition, the time-dependent area change signal is the basis for the extraction of further features, i.e. the features (a) – (d) as described in first paragraph plus the 10% spectral power frequency, by determining the upper band containing the 10% of the total spectral power of the power spectral density. Seizures containing isolated sharp peaks generate high values of the upper band (slow reduction of the power spectral density) while seizures with many (near periodic) peaks produce low values (fast reduction of the power spectral density) [63, 69, 73].

One more feature is the angle, measured between lines connecting tracked points [99] and/or reference lines, as well as the angular speed. These features are used in [98, 99, 100, 142], along with the duration of movements and duration from seizure onset to occurrence of movement for an approach where the tracked points are labeled manually, supported by a software tool. Duration measures are often based on EEG or clinical onset and EEG end, as reported in [90].

Finally, a feature also used for marker-free motion detection, the "change detection maps" are 2D binary random fields whose optimal configuration is being sought in terms of applying Markov random field theory [81].

1.6.4 Methods and algorithms: marker-based and marker-free approaches

Vision-based human motion analysis and seizure recognition in epilepsy can be divided into two main categories, which consider marker-based and marker-free approaches. Marker-based approaches use one or more cameras that track easily detectable (e.g. infra-red) objects/markers of various shape and size. These markers are placed on motion relevant positions of the human body, like joints or extremities. Marker-free methods rely solely on the content of image sequences taken by one or more video cameras. The video is usually analysed with automatic methods. Some authors perform tracking of motion relevant points by manually labelling such positions in the video. Since markers are not physically attached, it is theoretically a marker-free approach, although it is actually closer related to marker-based systems, which are based on tracking points, and since automatic image analysis is not performed, papers using this method have been assigned to the group of marker-based approaches.

Marker-based approaches

Marker-based systems have been utilised for motion analysis and motion recognition in epilepsy. As mentioned in Subsection 1.6.2, motion analysis offers a quantitative description of a patient's kinematic image, while in motion recognition the classification of a motion pattern to a limited number of classes (e.g. seizures) and the interpretation of movement over time is the kernel of interest.

a) Motion analysis

Li et al. [76] introduced a marker-based approach for quantifying motion of epileptic patients using 22 infra-red (IR) reflecting markers, symmetrically positioned over the whole body. In an initialization phase the marker pixel patches were segmented by calculating a threshold using an entropy measure. Subsequently, the centroids of these patches were calculated and the markers were labeled manually. The movement of a marker was modeled using a 2D ballistic model, whose initial parameters were calculated from the first three frames and were employed in a Kalman filter for predicting the positions of the labeled markers in every next frame. For estimation of the correspondence between successive markers a distance criterion optimization algorithm between the predicted and the measured position was used. In coping with complexity of the correspondence algorithm, the authors implemented a modified version of a non-iterative Greedy algorithm where the normalized distance is used as a cost function. The motion (in pixels) of the markers in the x- and y-direction and the velocity (pixels/s) were graphically displayed in form of tracings mimicking the EEG. The velocity was also visualized as a 2D color-coded graph on a human silhouette. The tracking method revealed some weaknesses

during marker occlusions due to non-optimal patient position (e.g. sideways). Based on the same methodology and in combination with a commercial tool, Cunha et al. [23] used 8 additional IR-markers in the scene for providing distance calibration and a reference for the measurements (maximum displacement measurement error: 8%). The distance of relevant markers to a reference marker was analysed graphically. Similar methods were used for extracting the timing, duration and speed of head movement in a clinical study analysing differences in ictal head turning in FLE and TLE [122], revealing significant differences between the two patient groups. Furthermore, based on the above methods, automatisms in TLE and FLE were studied in [26, 90] by means of the same features, including the dominant frequency.

Head movements in patients with temporal lobe epilepsy (TLE) have been analysed by O'Dwyer et al. [98, 99, 100] in order to evaluate the lateralizing significance. The motion of a marker positioned on the nose in relation to a reference marker on the trunk was analysed. Primarily, the angle between the straight line connecting both markers and the horizontal image axis was investigated. From this parameter, the ipsilateral and the contralateral angular speed and duration were extracted and statistically analysed. Similar comparisons between ipsilateral and contralateral head movements were also carried out in patients with TLE and frontal lobe epilepsy (FLE) and differences in the movement characteristics and seizure evolution were found [142].

The set-up for marker-based recording, as described by Cunha et al. [23] was adopted by Yang et al. [144] and Chen et al. [16] using a slightly revised marker positioning system with 20 markers. Marker coordinates were collected manually for each marker on each frame. Yang et al. [144] analysed the movement trajectories in automatisms of TLE and FLE. They investigated distal vs. proximal limb motion ratios, shoulder vs. abdominal motion ratios, and the frequency and relative amplitude (difference to the first frame) of the trajectories. Statistically significant differences (t-test, $p<0.05$) in distal vs. proximal limb motion ratios and shoulder vs. abdominal motion ratios were found between patients with TLE and FLE. Using the same features, Chen et al. [16] analysed the movement trajectories of hyperkinetic, tonic posturing, fencing posture and tonic head turning seizures of the supplementary motor area and compared them with temporal lobe seizures and psychogenic non-epileptic seizures. One-way ANOVA revealed statistically significant ($p<0.05$) differences in average amplitude and distal vs. proximal limb motion ratios.

Cunha et al. [22, 24] reported on a 3D marker-based motion quantification system for epileptic seizures within the "MovEpil3D" project by synchronizing a video-EEG device with a commercial movement tracking system (Vicon, Oxford, UK) using 4 high frame-rate cameras offering higher accuracy. In [27] a comparison to the previous 2D method [23] is performed for two cases: a) a simple simulated motor paradigm and b) a complex epileptic seizure, characterized by a movement of both legs. The calculation of the error rate was based on the Euclidian distance between the position of each marker in each frame and its respective position in the first frame. The 3D method showed its superiority, especially for motion patterns perpendicular to the 2D plane. Mean error rates of the 2D method for the complex epileptic seizure varied from 22.4% in the best case and 161.7% in the worst case, with regard to different distance reference measures.

b) Motion recognition

Based on the initial tracking method presented by Li et al. [76], the classification of automotor and hypermotor seizures was investigated in [25] using three markers, one on the trunk and one on each wrist. A joint-model of the trunk-arm-wrist segment for compensating the trunk movement was used for calculating the wrist extend (area change over time of a rectangle containing a marker trajectory) and the maximum and average wrist motion speed. These parameters were statistically analysed (Wilcoxon rank sum test) and thresholds for classification were set. The results showed that thresholding the wrist extend and the maximum speed yields accuracies of 100% and 90% respectively, while the average wrist speed could not provide a clear separation. Similar features including the relative wrist-trunk speed, power spectra of movements and the extend of trunk had been evaluated at first for their capability in differentiating automotor from hypermotor seizures, resulting in statistically significant differences between $p<0.001$ and $p<0.2$ [89], and a sensitivity above 65% with a specificity greater than 70% (unknown set) [136]. The approach described above was further investigated in [121], supporting the applicability of the speed and extend of wrist and trunk movement for identifying hyperkinetic seizures through thresholding.

Another type of marker-based method was presented by Lu et al. [82]. Although the authors titled the method as markerless they utilized a coloured suit worn by the patient in bed in order to facilitate the tracking procedure, which implies a certain degree of marking. For initialization, the user indicates two colors/regions for the foreground (arms) and one background color/region. Body parts are detected using a coarse-to-fine approach [56]. In the coarse phase the foreground is segmented based on hue, saturation, value (HSV) color space modelling, which returns two foreground, one background and one gray mask through thresholding median values. Forming the union of the respective masks produces regions for the foreground and background. The fine segmentation stage performs foreground-background classification using two Gaussian mixture models, one for each class (GrabCut algorithm [57]), and keeping only one connected region with the largest normalized area for each foreground color. For motion analysis, the trajectories (position) of shoulders over time are estimated by using domain knowledge for identifying the body parts and subsequently calculating an average body part position. The orientation (angle) of the arms in each frame is also estimated by using edge detection. The analysis of these features was done graphically (plotting). Out of these signals, two features, namely the accumulated absolute displacement and the dominant frequency, were calculated for 5 sec. windows in order to design a seizure detector. The detection was based on selecting suitable thresholds (no further detection performance stated).

Marker-free approaches

As a first step prior to motion analysis and recognition, marker-free approaches have also been applied for motion detection. In relation to epilepsy, this means the detection of seizure-like motion that e.g. could trigger an alarm during monitoring of a patient (see also Subsection 1.6.2).

a) Motion detection

Cuppens et al. [28, 29, 30] applied optical flow for detecting movement of epileptic patients during sleep. In a preprocessing step, histogram equalization was performed. The authors used the average of a portion of all velocities calculated using the Horn-Schunck implementation for optical flow [40] in order to distinguish between epochs with- and without movement via thresholding. Initially, the effects of variations in spatial resolution, frame-rate, video compression, illumination and camera point-of-view were studied using videos of an adult simulating epileptic and non-epileptic movement [28]. In that study 0.06% of the highest velocities were averaged with the purpose of achieving noise rejection. A measure for comparison was the ratio of the maximum average velocity in a movement epoch to the maximum average velocity in a non-movement epoch (MNMR). In a second study [29] the authors determined the optimal threshold for detecting movement epochs as well as the optimal percentage of the averaged highest motion vector magnitudes. A global threshold and a variable threshold as a multiple of the standard deviation added to the mean of a non-movement epoch at the start of each sequence were analysed against the percentage of magnitudes. The MNMR, the sensitivity and the positive predictive value (PPV) were evaluated in a three-fold cross validation at a labeled dataset of 11 sequences of 8 epileptic patients by plotting ROC-curves and examining the maximum PPV at a sensitivity of 1. The variable threshold returned better results than the global, giving a PPV between 0.86 and 1 at a sensitivity of 1.

Having the same objective as Cuppens et al. [28, 29], namely the detection of local motion or otherwise called "change detection", Liu et al. [81] applied Markov random field theory (MRF) in order to avoid thresholding. Images were modeled as MRFs. The change detection problem was deduced to the estimation of the optimal configuration of a 2D binary random field, called the change detection map. For finding the optimal solution, using the maximum a posteriori criterion, a mean field theory approach was adopted. The problem was subsequently solved in an iterative manner minimizing the energy at each pixel until convergence was reached. The algorithm was tested on a synthetic image sequence, reporting a very low error rate (rate of pixels with false labels to all pixels), as well as on a segment of a real epilepsy monitoring video reporting accurate movement detection.

b) Motion analysis

Karayiannis et al. [61] used optical flow to extract temporal motion strength signals for motion analysis purposes. Initially, three different methods for the computation of optical flow, namely the block motion model method, the Horn-Schunck method and a modified Horn-Schunck method using median filtering, were tested successfully on two videos showing a myoclonic and a focal clonic seizure of an infant, with the objective of obtaining quantitative information regarding the seizure [61]. The authors further proposed in [67] a discrete formulation of the optical flow that relied on the discrete approximation of the quadratic functionals describing the smoothness constraint, relying on the squared Laplacian operator as mentioned by Horn-Schunck [40]. Motion strength signals of a specific region were used for comparison to the regular Horn-Schunck-method in videos of neonatal seizures. Errors in the computation of the optical flow resulted in abrupt fluctuations of the area of the moving body part, a criterion according to which the proposed modified method produced better results. A further implementation of the optical flow was tested in [70], by forming the smoothness constraint in terms of

a second order spline functional and using various masks for the approximation of the Laplacian, utilized in solving the minimization problem. This implementation showed a lower sensitivity of the motion strength signals to the threshold used for their extraction in comparison to the Horn-Schunck-method. Considering the optical flow computation the authors state that its performance is mainly affected by the specific smoothness constraint employed. The velocity field estimated by optical flow was used by Karayiannis et al. [73] in order to calculate the temporal motion strength signals also by a) clustering of the pixel velocities and b) clustering the model parameters obtained by fitting a motion model to a block of pixel velocities, thus providing the basis for assigning pixels of each frame to either the background or to a moving body part. Optical flow in the Horn-Schunck implementation together with morphological filtering was furthermore used for selecting anatomical sites for extraction of motor activity signals from video recordings of neonatal seizures [68, 126]. The areas in each frame containing moving body parts were segmented by thresholding the magnitudes of the velocity vectors, thus producing velocity patches. Spurious patches were reduced by employing morphological opening and closing operations [68]. Initially, the location selected for tracking was a) the center of the velocity patch with the largest area and b) the center of the velocity patch with the maximum average velocity [126]. Due to the problem of losing track of sites in homogenous areas of a moving body part, texture analysis was performed, based on the concept of entropy, which was in turn defined in terms of a co-occurrence matrix [68]. The final selected anatomical site was located at the point with the highest texture within the initial velocity patch. This method was applied within the same study for additionally selecting anatomical sites of multiple moving body parts, though a labeling procedure was necessary for eliminating overlapping velocity patches. Another study, using optical flow, is described by Kalitzin et al. [58]. From the velocity fields, global motion parameters, i.e. the real and imaginary part of the three affine transformation rates (translation, rotation and shear), were initially extracted. The next step included principal components extraction, which were represented through the maximum eigenvalue of the covariance matrix of the wavelet responses at various frequencies in a time window. For the detection a feature called the "spectral contrast" was used. It represents the relative difference between the sum over the frequency of the maximum Eigenvalues, weighted by a spectral weight function, once with and once without its sign. The spectral weight function was heuristically defined in order to highlight the seizures, which were of clonic and tonic-clonic type (72 seizures in total). The final evaluation was based on statistical separation tests (non-parametric Kolmogorov-Smirnov tests) and a simple detector based on thesholding. The results showed a sensitivity of 95%.

A further approach for motion analysis is based on spatiotemporal sub-band decomposition, which was performed by Karayiannis et al. [60, 65] in order to utilize the redundancy between adjacent frames and within each frame for identifying the moving body parts of an infant during a seizure. In this case, 11-band spatiotemporal sub-band decomposition was performed for extracting temporal motion strength signals. The first step, the temporal decomposition split the video signal into a low-pass (LP) temporal and a high-pass (HP) temporal sub-band using a Haar filter. In a subsequent spatial decomposition phase, each temporal sub-band was passed through an LP and HP filter along the horizontal dimension and each of the resulting sub-bands was passed again through an LP

and HP filter along the vertical dimension. For the spatial decomposition, a Daubechies wavelet filter was used. Each HP and LP operation in the spatial decomposition process was followed by a down-sampling by a factor of two, since the half of the frequencies has been removed. Motion was detected and measured on the sub-band that contained the LP spatial components in both horizontal and vertical dimensions of the initial HP temporal sub-band, where a median filter was employed for removing spurious patches. The filtered sub-band was clustered into foreground and background using a k-means algorithm. The area of the foreground patches was used for the estimation of the temporal motion strength signals. The authors comment that although limb motion could be traced successfully, the experimental results indicated that the segmented frames may still contain a few spurious patches due to noise. Further processing in terms of considering only those areas, whose centroids were present within a small radius between successive frames, was necessary. Frame-by-frame inspection indicated that myoclonic seizures and focal clonic seizures can be distinguished from non-seizure events, such as tremor and posturing of the extremities, by detecting the most significant peaks, though the method may not be suitable for types of seizure involving subtle movements such as ocular and orobuccolingual seizures.

An alternate way to perform motion analysis is frame differencing. A series of frame differencing, non-linear filtering, clustering and morphological filtering were performed in [62] on videos of neonatal seizures in order to extract temporal motion strength signals. For motion extraction each current frame was subtracted from the previous and the resulted frame difference was filtered using a median filter for removing spiky noise. The filtered frames were then segmented into 4 clusters using the k-means algorithm: A cluster corresponding to pixels of positive intensity values of large magnitude, a cluster corresponding to pixels of negative intensity values of large magnitude, a cluster containing background pixels and a cluster containing pixels that do not belong to the background but are not relevant to the motion. The last two clusters were merged together. Further reduction of spurious patches was achieved throughout the application of a sequence of morphological opening and closing operations. The displacement area of the moving body part was calculated as the minimum of the areas occupied by the patches of the first two clusters. As reported by the authors, this method offered effective noise reduction but during the noise elimination attempt it may underestimate the area. This procedure was improved in [63] by using vector clustering instead of scalar clustering. Vectors containing the 9 pixels of a 3ÃŮ3 window were used. The features extracted out of the motion strength signals (variance of time intervals, energy ratio, maximum peak duration) were evaluated statistically based on their ability to separate between myoclonic seizures, focal clonic seizures and random movement using the Fisher ratio, the generalized Fisher ratio as well as a t-test. The differentiation of random movements from either myoclonic or focal clonic seizures was identified as being the most challenging problem rather than distinguishing between focal clonic and myoclonic seizures. Another study, using frame differencing, is described by Ntonfo et al. [96]. The difference image was thresholded, producing a binary image or mask (1 = white). The threshold was set heuristically in order to maximize the ratio between the number of white pixels of the moving body part most affected by the seizure, and the number of remaining white pixels in the frame. Noisy pixels were filtered by the erosion operation. Finally the average motion signal was calculated as the sum of

all remaining white pixels. For the detection of neonatal seizures, the periodicity of the signal was analysed in terms of a difference between the normalised autocorrelation function and a fundamental frequency estimator (Yin estimator). The detection of a seizure was based on counting minima below a certain threshold within overlapping windows and was preliminary tested on 10 video recordings. This approach was utilized by Pisani et al. [114] with a larger dataset (23 videos, 12 patients, 78 seizures), obtaining a sensitivity of 71% (specificity of 69%) with 50% window overlap.

A further approach to motion analysis is based on tracking moving objects. This can be performed with the well known Kanade-Lucas-Tomasi (KLT) tracking algorithm [83, 133]. Karayiannis et al. [60, 65] used a modified version of the KLT algorithm in order to extract temporal motor activity signals. The initial algorithm selects suitable sites in the first frame based on the requirement that the spatial gradient matrix computed on the corresponding frame location is above noise level and well-conditioned. The noise requirement implies that both eigenvalues of the gradient matrix must be sufficiently large, while the conditioning requirement means that the eigenvalues cannot differ by several orders of magnitude. The sites are then tracked through the image sequence by using a Newton-Raphson optimization method to minimize the difference between windows in successive frames. The modification included an extension of the Newton-Raphson method to operate under affine image transformations. This algorithm was tested on two myoclonic and two focal clonic neonatal seizures as well as two video recordings of random movement through frame-by-frame inspection. In some cases the algorithm lost some of the sites, which means that moving body parts containing large amount of lost sites could not be tracked through the entire sequence. This motivated the simultaneous tracking of a sufficiently large number of spots from the selected anatomical site within a predetermined radius. The temporal motor activity signals provided information regarding the frequency and rhythmicity of motion enabling the quantification of the two seizure types under investigation.

Moving objects can also be tracked with a method called block or template matching. The purpose of a block matching algorithm is to search and find a matching block of pixels from one frame in a second frame, which may usually appear after the first one. In [68], adaptive block matching was applied for extracting motor activity signals on a set of videos of two types of seizures (myoclonic, focal-clonic) and random movement in order to track selected anatomical sites. Block matching, a correlation-based approach relies on the assumption, that a block of pixels remains constant over time and motion, an assumption which is only valid at sufficiently high sampling rates. A reference block is tracked using window searching for the most similar block in subsequent frames according to a similarity measure. In [68] adaptive block matching, taking the mean square error as a similarity measure was used, where the reference block was additionally updated to take into consideration changes in the appearance of the target. Various update strategies were tested in that study including a single-frame update strategy, a multi-frame update strategy, a finite impulse response filtering update strategy and a Kalman filtering update strategy. The results were compared to reference data coming from manual tracking. The performance of adaptive block matching depended on the update strategy employed for the reference block. Ultimately Kalman filtering proved to be the most reliable strategy for this study. Compared to the KLT tracking method mentioned earlier, adaptive

block matching was more accurate, providing a lower mean square error, and reliable, having less failures in tracking the anatomical site. A combined approach was nevertheless suggested, where a displacement-estimation method (e.g. KLT) could initiate the search for the best matching block in the next frame, which then would be performed by adaptive block matching. As an alternative to adaptive block matching, predictive block matching was applied during extraction of temporal motor activity signals in videos of neonatal myoclonic and focal-clonic seizures [66, 126]. The approach, used for tracking of selected anatomical sites, employed a translational motion model in order to estimate the displacement of a block of pixels before initiating the search for a matching block. The search itself relied on adaptive block matching, using the Kalman filtering update strategy. Predictive block matching turned to be more reliable than adaptive block matching when the video recordings contained high-amplitude movements of the infants' extremities affected by seizures. Another study, using predictive block matching for detecting neonatal seizures, is described by Ntonfo et al. [97]. The search area of the block to be matched was defined according to the direction of the optical flow of the point to be tracked, which was initially located as the point with the maximum magnitude, since the seizures under analysis manifested with sudden movements. This approach returned the motion trajectory, from which features including length, location, angle and speed were extracted. Further analysis included clustering of the features in order to reveal similarities.

c) Motion recognition

Karayiannis et al. [69] trained multiple feed forward artificial neuronal networks (FFNNs) for classifying myoclonic from focal clonic neonatal seizures. The inputs used for training the FFNNs were formed in terms of a) three features extracted from temporal motion strength signals (variance of time intervals, energy ratio and maximum peak duration), b) three features extracted from temporal motor activity signals (energy ratio, maximum peak duration and variance of time intervals), and c) all the six features extracted from temporal motion strength and motor activity signals. Sensitivity and specificity results showed values above 85% when applied to the test set. Based on these findings the authors suggest that it is feasible to develop an automated system for the recognition and characterization of the types of neonatal seizures based on video recordings. They furthermore report that the performance of neural network models trained to perform seizure recognition and characterization is affected mainly by the existence of uncertain events as a result of the lack of contextual information such as EEG recordings.

Using temporal motion strength signals, Karayiannis et al. [73] studied the classification between myoclonic, focal clonic neonatal seizures and random infant movement in two experiments: a) the classification between a neonatal seizure in general and random infant movement using either the energy ratio, the variance of time intervals and maximum peak duration (time-domain measures only) or the same plus the 10% spectral power (time- and frequency-domain measures) and b) the classification between myoclonic seizure, focal clonic seizure and random infant movement, again using either time-domain measures only or the time- and frequency-domain measures. The authors reported that training with a feature set including time- and frequency-domain metrics improved the performance of the FFNNs (increased average specificity by 5%). Additionally, using two output units, i.e. the classification between a neonatal seizure and random infant move-

ment, rather comprised the network's ability to distinguish between these two classes due to the disparity between the manifestations of myoclonic and focal clonic seizures which in this case were fused into one class. In other words, choosing the correct number of possible decisions (output nodes) is crucial to the performance of the network.

1.6.5 Conclusion

It is noticeable that there is only a small number of research groups (2 for marker-based and 5 for marker-free methods) active in the specific subject, probably defined by the limited access to video data, usually derived from video-EEG sessions, in conjunction with the need of a consent for usage of this data in research. As an alternative, simulated epileptic motion can be captured but its relation to complex epileptic motion is questionable. To date, researchers have focused on the following seizure and/or motion types: epileptic (not specified), automotor, hypermotor, supplementary motor area seizures of FLE, non-epileptic seizures, myoclonic, focal clonic, random movement and motion related to FLE and TLE. This is a limited set not covering all the seizure types and by far not addressing all electroclinical syndromes proposed by the report of the ILAE Commission on Classification and Terminology [49]. It points out that a holistic approach utilizing vision-based human motion analysis for epilepsy is missing. Moreover the fact that the concentration of the researchers is quite exclusive on the analysis and quantification respectively of selected motion patterns in epilepsy, reveals a low level of advances in terms of integrated clinical decision support, based on recognition. During the motion analysis phase the main problem seems to be the selection and extraction of the appropriate features that are likely to reveal quantifiable information on the captured motion. The most common features utilized are the motion trajectories and velocities of markers, separate pixels or pixel blocks. A two-level approach considering the features is distinguishable in marker-free methods where specific "secondary" features are extracted from basic "primary" features (i.e. the motion signals) in means of signal processing. These secondary features prove useful for feeding a classifier as in the case of Karayiannis et al. [69, 73]. Considering efforts in motion/seizure recognition, a classification performance of up to 94% sensitivity and 87% specificity based on test data has been achieved [73]. The reported results have been validated in trials involving 20 to 240 video sequences taken from 17 to 54 patients respectively [25, 69, 73].

The number of publications dedicated to either marker-free or marker-based methods is more or less equally distributed, affirming the still existing trade-off (closer described in [16]) that is usually taken between high reliability and easy application of marker-based systems on the one hand and ubiquity and versatility of marker-free systems on the other, whilst the only 3D method reported is a marker-based system [24]. Combined approaches were not reported.

While following the evolution of methods for the capture of human movement, that leads to marker-free motion capture for biomechanical applications [95] and the great advances in the field of computer vision [92, 117], algorithms used for human motion analysis in epilepsy without utilizing markers are of special interest. Although the lack of human model usage, i.e. an a priori human model with relevant anatomic and kinematic

information that is tracked or matched to 2D image planes or 3D representations, is noticeable and raises the question whether these methods would be better suited or not to the domain at hand. Model-free approaches, i.e. the direct extraction of motion relevant information, can benefit from already available image and video analysis tools as e.g. optical flow or the KLT tracker, which are indeed frequently employed in the related literature. Among the reported methods, optical flow seems to be the most promising approach because of the rich motion-related information that is hidden behind the extracted velocity field. Given the fact that cameras during video-EEG recording are usually fixed, simple frame differencing is with no doubt the most effective method in terms of computational cost for extracting any region containing motion in the video sequence (e.g. human silhouettes).

Within the reported methods, the more demanding model-free pose estimation task has not been addressed yet. A general observation is that vision-based human motion analysis in epilepsy up to now is limited to the extraction of abstract, but still quantitative, information without an automatic inference to specific body parts. Only one publication reported the analysis of multiple moving body parts or rather different regions with motion in the sequence without actually detecting the body parts [68]. Nevertheless the detection of body parts and related motion is a necessary step for future extraction of the clinically relevant knowledge of "how", in a quantitative manner, specific body parts are moving and the relation of this movement to certain ictal phenomena. A model-based approach on the other hand would, once the human model is fitted to the observation, return through its parameters all the relevant information describing the motion of each body part. Here the quality of the fitting process and complexity of the model define the accuracy of the resulting information. Moreover the usage of a priori knowledge and assumptions for the model might not correlate with the complex epileptic motion patterns. A general problem of vision-based human motion analysis is the self-occlusion of body parts, as a result of improper positioning of the patient or the occlusion by other objects or persons [76]. As to clinical experience it is quite often the case, that during a seizure, intervention is required by a caring person, nurse or a physician. This introduces an additional problem, not addressed within the reported studies, of distinguishing multiple persons within a scene in the case of marker-free analysis.

Considering recognition, there are positive results using thresholding [25] and ANN's [69, 73] that prove the feasibility of a vision-based system for classification of some specific seizure types. The question that remains open in this context is to what extent vision-based human motion recognition can support generalized classification within the whole domain of epileptic syndromes. Besides thresholding and ANN's, the usage of probabilistic methods as e.g. the Transferable Belief Model used for human action recognition [120] or MRF theory already used for motion detection [81] might be a suitable alternative while dealing with uncertainty. Moreover, the applicability of vision-based human motion analysis in non-motor or autonomic events is limited. In such a case a combined approach using EEG analysis is likely to be successful.

Concluding, it can be deduced that it is feasible to use automated video analysis in extracting quantifiable information of a patient's clinical manifestations and recognizing various kinematic patterns related to epileptic seizures. The main characteristic of current

approaches is that they address only a limited set of epileptic phenomena. Moreover there is no automatic inference of which body part is producing which signal (displacement, velocity, angle etc.), especially in the case of marker-free approaches, while marker-based systems still need manual marker labelling. This inference âĂŞ if available âĂŞ would be the key in producing information that can lead to clinically relevant knowledge. The answer to the question whether the whole spectrum of epileptic activity can be covered, depends on the ability of a vision-based system to combine quantifiable motion information that is robustly extracted from several automatically detected body regions (extremities, face, head etc.).

1.7 Facial expression analysis in epilepsy

Advances in facial expression analysis are mainly driven by research efforts in human emotion recognition. Based on a thorough review, which is presented in [132], most automatic facial expression analysis systems attempt to recognize a small set of prototypic emotional expressions (e.g. disgust, fear, joy etc.), although emotion is more often communicated by subtle changes in one or a few discrete facial features, such as tightening of the lips in anger or obliquely lowering the lip corners in sadness. Therefore the Facial Action Coding System [34], a human-observer-based coding system designed to detect subtle changes in facial features as a result of facial muscle activity, is often adopted.

Considering facial expression analysis in epilepsy, only one reference can be found by P. Maurel et al. [87], who used a model-based approach to calculate the variation of model parameters by fitting a 3D active appearance model. The main scope of this work was to test the fitting method, which was based on energy minimization. An energy was defined, which measures the quality of a given position of the 3D model, based on the cross-correlation between a reference texture, applied to the model, and the image in which the model is to be fitted. P. Maurel reports in his thesis [86] that the fitting was initially performed on manually selected images in order to remove large movements and occlusions. Finally the method was applied a selected video of epileptic seizures, in which the facial expressions were visible during a large portion of the seizure. The aim was to measure the relation between Stereoencephalography and dynamic facial expressions represented in terms of moving vertexes of the fitted model. In this case the epileptic seizure was clinically characterized by a deviation of the eyes, followed by a deviation of the head. The results showed a frequency component on a specific electrode called “SA” (bipolar signals number 22 or 23), which best correlates with the eye facial parameters (opening and position).

1.8 Research question

The previous sections have provided an extensive introduction into the field of study and the final step is to formulate the research question that will guide the upcoming work. The question is:

- Which are the measurable facial characteristics of absence seizures, delivered by a computerised analysis of a patient's facial expression from video sequences and is it possible to use them for detecting at least two seizures for each patient?

The term "measurable" represents the quantitative aspect of the study, while the methodological boundaries are set by the terms "computerised", "facial expression" and "video". Finally the diagnostic aspect is covered by investigating the possibility to detect at least two seizures per patient, as defined by the ILAE (cf. Section 1.3).

CHAPTER 2

Methods

Parts of the contents of this chapter have been published in [108, 109].

2.1 Video-EEG acquisition

The video-EEG system, which was used to record the data, utilizes two SONY® EVI-D70P, PAL color cameras with a resolution of 752 x 582 pixels at 25 fps interlaced. The two cameras are connected to a video mixing device which is set at "picture in picture" mode. In this mode the image of one camera is placed with a reduced resolution (smaller size) on top of the image of the other camera at full resolution. The smaller image covers 1/4 of the area of the underlying image and is placed at the bottom right corner. The "mixed" video is then sent to a frame grabber, which converts the video to a digital format. The final video is then stored with MPEG-2 compression at a given bit-rate. Since each video EEG recording may last up to several hours, a single resulting video file would be too large to be handled by the file system and any analysis software. Therefore, multiple video- and sometimes even multiple EEG files are stored. The synchronization between the EEG and the video files functions on a millisecond basis and is handled by the video EEG system.

The cameras are positioned at the corner where the ceiling meets the wall facing the bed. They are set so that the visible area of the underlying image covers the whole patient (i.e. the whole bed) and the smaller image is zoomed in on the face to provide a better resolution for this area. This image is the one that was taken for analysis for this work. Figure 2.1 shows an example of the recording scenario. Prior to each recording, directions were given to the caring persons and nurses to try to keep the patient within the field of view of the cameras and even readjust the horizontal and vertical tilt if necessary. During

the night two IR lights turn on and the IR filter on the cameras is activated automatically. Unfortunately due to various light sources, mainly TV and night lamp, which were active during the night the IR activation did not function properly.

In synchronization to the video, 19-channel EEG based on the 10-20 positioning standard was recorded at a sampling rate of 256 Hz. All patients were admitted for a first-time diagnosis, while an informed consent was obtained from the parents to use the data for research purposes.

Figure 2.1: An example of the video captured during video-EEG recordings at the University Hospital in Heraklion, Crete.

2.2 Video pre-processing

As mentioned in the previous section, each recording is split into multiple video files. Since the epileptic seizures take up a minimal amount of time compared to all other activities in the video, only those video files were selected that contain a seizure. The fact that the recoded videos are interlaced denotes that they will contain noise, which is heavily connected with motion[56] and would make any attempt of subtle motion analysis, as in the case of absence seizures, impossible. Therefore, each video is deinterlaced prior to any further analysis or processing. For deinterlacing the the FFmpeg [http://www.ffmpeg.org/] filter "yadif" is used. The options are set such that the filter outputs one frame for each input frame, assumes the bottom field first, and deinterlaces all frames. Since variations in the bitrate of the input video files were observed, all videos were stored at the same bitrate of 4096 kbit/s using the MPEG-2 codec. Other parameters that guaranteed continuity within all video files included setting the frame rate at 25 fps as in the original

files, setting the pixel color format to yuv420p and removing the audio. The final command was the following: `ffmpeg -i INPUT.AVI -filter:v yadif=0:1:0 -an -vcodec mpeg2video -pix_fmt yuv420p -threads 4 -r 25 -vb 4096k OUTPUT_D.avi`.

2.3 Video annotation

Video annotation is the process where the regions of interest, which will be used for further analysis are defined. The regions of interest in this case are four and were selected as a result of the description of the clinical image during absence seizures in Section 1.4. These regions are: The region of the eye-pair, includes both eyes and eyebrows. The region of the left eye, which includes the left eye and the left eyebrow. The region of the right eye, which includes the right eye and the right eyebrow. And finally the region of the mouth, which includes both lips. These regions are at first selected in a semi-automatic manner for data analysis. This provides the only way to ensure that the correct regions are analysed. For the final evaluation of the seizure detection capability of the developed methods, automatic ROI detection algorithms are employed.

2.3.1 Semi-automatic annotation

The semi-automatc annotation was performed by using a software tool that was developed specifically for this task, the "Simple Video Annotation Tool" (SVAT). It allows to annotate five different objects inside each frame and the assignment of four identical attributes for each of the objects. The annotation is assisted by using a KLT tracker in conjunction with a function that searches for good features to track. An initially selected ROI can be tracked and automatically annotated in subsequent frames, although corrective measures and re-initialization might me necessary. Using this tool, five regions of interest (i.e. face, eye-pair, left eye, right eye, mouth) were annotated for each seizure period. Seizure-free periods before and after each seizure were annotated as well, the duration of which ranged from seconds to a few minutes, depending on head pose and occlusions. Occluded objects were not annotated. An object was regarded as being occluded if was partly covered by any moving foreign object. Such foreign objects causing occlusions usually were arms, hands, books, electronic devices, blankets, other persons etc. The five aforementioned regions of interest were annotated by taking related definitions in the literature [33, 124] (related to detection benchmarking), as well as the clinical image of the seizures under investigation (Section 1.4) into account. The regions were defined as follows:

The region of the face is defined as a rectangle with sides in parallel to the image borders. It includes both eyes and eyebrows, the nose and mouth. For this region to be valid, all aforementioned elements must be visible. As a result of variations in head pose, it may include parts of the head bondage holding EEG electrodes in place, the pillow, blanket and shirt.

The region of the eye-pair is defined as a rectangle with sides in parallel to the image borders. It includes both eyes and eyebrows. For this region to be valid, all aforementioned elements must be visible. As a result of variations in head pose, it may include

parts of the nose, the head bondage holding EEG electrodes in place, the pillow and blanket.

The region of the left eye is defined as a rectangle with sides in parallel to the image borders. It includes the left eye and the left eyebrow (at least most part of the left eyebrow). For this region to be valid, all aforementioned elements must be visible. As a result of variations in head pose, it may include parts of the nose, the head bondage holding EEG electrodes in place, the pillow and blanket.

The region of the right eye is defined as a rectangle with sides in parallel to the image borders. It includes the right eye and the right eyebrow (at least most part of the right eyebrow). For this region to be valid, all aforementioned elements must be visible. As a result of variations in head pose, it may include parts of the nose, the head bondage holding EEG electrodes in place, the pillow and blanket.

The region of the mouth is defined as a rectangle with sides in parallel to the image borders. It includes both lips. For this region to be valid, all aforementioned elements must be visible. As a result of variations in head pose, it may include parts of the nose, the pillow, blanket and shirt.

An overview of the annotated seizures for patients P01–P08 is given in Tables 5.1–5.8 in the Annex, with comments regarding occlusions and capturing conditions for each seizure.

2.3.2 Automatic annotation

The automatic video annotation is based on the Viola-Jones detection algorithm [141], as implemented in OpenCV 2.4.8 [10], which uses a rejection cascade of boosted classifiers - in this case decision trees - working with an extended haar-like feature set [77, 78] For face and eye-pair detection, the trained cascades "haarcascade_frontalface_alt2.xml" [10] and "frontalEyes35x16.xml" [1] respectively, are used. Both have received the highest rating in their category [12], and performed reasonably well in the application at hand. For the detection of the left and right eyes the trained cascades "haarcascade_lefteye_2splits.xml" and "haarcascade_righteye_2splits.xml" [10], and for the mouth the cascade "haarcascade_mcs_mouth.xml" [12].

The detection method assumes that only one face exists in the video sequence and that it is in frontal position with only slight out-of-plane rotations. The method subsequently takes the largest among multiple positives to be the ROI. Within the detected area of a face, a second scan is performed for the detection of the eye-pair, the left eye, the right and the mouth. Assuming again that the largest positive is the correct region of interest with additional constraints: a) the mouth must be located within the lower third of the detected face, b) the eye-pair must be located within the upper third of the detected face c) the left eye must be located within the upper left square (one third of width and height) of the detected face and d) the right eye must be located within the upper right square (one third of width and height) of the detected face. If a face is not detected, then a scan for the eye-pair, left eye, right eye, and mouth is performed on the whole image.

In order to ensure that the eyebrow is inside the ROIs for the left and right eye, these are enlarged in each direction by 1/4 of their width and height respectively. It was further on noticed that the mouth detector was producing many false positives, widely spread over the image. In order to reduce these false positives, detected mouth regions that were jumping in any horizontal or vertical direction by more than the width or height of the previous detected mouth regions were filtered out. Furthermore, since the eye detectors were more reliable, only mouth ROIs were chosen form frames where at least one eye was also detected.

2.4 Signal extraction

As defined in [101], a signal is something that conveys information, generally about the state or behavior of a physical system. The information is contained in some pattern of variations. Signals are mathematically represented as functions of one or more independent variables. Most commonly, the independent variable is time. For the purpose of this work, signals that represent motion within specific areas of the face - the regions mentioned above - are used as a primary source of information, similar to the work of Karayiannis et al. [69, 73], who extract signals from moving extremities during epileptic seizures. The signals are extracted for each ROI using two techniques, background-foreground segmentation and optical flow.

Background-foreground segmentation (or frame differencing) is the process, where moving objects are segmented from a rather static background. The simplest way of motion segmentation in a video sequences is frame differencing, hence the difference between consecutive frames provides information on moving objects. Usually a reference image is calculated as an average background, from which each new frame is then subtracted. The difference is then thresholded in order to obtain a foreground mask. This work uses a background-foreground segmentation algorithm based on Gaussian mixture models, as implemented in OpenCV, based on the work of KadewTraKuPong and Bowden [57]. It uses a multiple-colour background model for each pixel in order to produce the reference image. This model is an adaptive non-parametric Gaussian mixture model. Each background pixel is modelled by a mixture of Gaussian distributions. Different Gaussians are assumed to represent different colours. The model is fitted and updated as time passes with an on-line Expectation Maximisation algorithm. The applied method uses the default values of OpenCV and the resulting signal is the area (in pixels) of the foreground mask, normalized to the area of the ROI. The signal is abbreviated with "PBFS".

Optical flow is a velocity field that transforms one image to the next image in a sequence. In other words, it describes the relative motion between the camera and the scene. It works under two assumptions. The motion must be smooth in relation to the frame rate, and the brightness of moving pixels must be constant. In this work, the velocity vector for each pixel is calculated within each ROI by using dense optical flow as described by Farnebäck [38]. In order to account for variations in illumination throughout a recording session, the histogram of the whole image is equalized prior to optical flow calculation.

From the resulting velocity field eight time- varying signals are calculated for each ROI: the maximum magnitude (MXM) and the angle in radians of the corresponding vector (AMXM), as well as the maximum magnitude weighted by that angle minus π (MXMW); The mean vector angle in radians (MA), the mean magnitude weighted by the mean vector angle minus π (MMW), the normalized sum of all magnitudes (SM), the normalized area of thresholded (threshold=1) magnitudes (THP) and finally the the normalized area of thresholded magnitudes, using an adaptive threshold (ATHP). Normalization of the three last signals concerns the area of the ROI from which they are extracted. The adaptive thresholding method is a binary method:

$$dst(x,y) = \begin{cases} 255 & \text{if } src(x,y) > T(x,y) \\ 0 & \text{otherwise} \end{cases}$$

The threshold value $T(x,y)$ is a mean of the `blockSize` $\times$ `blockSize` neighborhood of (x,y). The `blockSize` is calculated as nearest odd integer of $\sqrt{\text{ROI\_Area}/8}$.

2.5 Feature extraction

All features are calculated in a C++ environment, using OpenCV 2.4.8 [10] [21], the GNU Scientific Library 1.15 [45] and the Boost C++ Libraries 1.55.0 [127].

Features for vision-based human motion analysis are usually physical quantities such as displacement, velocity, area, angle, angular speed and duration. Some of these features are represented by the extracted signals mentioned in the previous Section. Since a seizure is an event, the signals must be broken up in pieces that represent instances in time. For the shortest possible instance, which is a single frame, the actual value of the signal at that frame constitutes the feature that describes the instance. For instances with a larger duration a window is set over the signal. Features are then extracted from the part of the signal that lies within the window, such as e.g. the mean value of the signal inside the window. This process may be connected with loss of information but it may also help to minimize noise. Beyond that, it enables the extraction of new features that describe characteristic properties of the signal itself, such as e.g. the frequency content. This method is used for the extraction of the features.

It is often the case that not all ROIs are always visible at once, usually when the head is rotated towards a side or when a ROI is occluded by an object, which results in the existence of missing values within the signal in each window. In order to filter out poor data, only those windows, which contain more than 75% of the signal, are further processed. Any remaining missing values in these windows are interpolated by a cubic spline interpolation (GNU Scientific Library 1.15 [45]). In the cases where the window is rejected, all features are set with the flag of a "missing value".

The extracted features from each window are presented in the following two subsections. The first describes the time domain features and the second describes those from the frequency domain. The selection of the features is based on the analysis of the literature in Section 1.6. Beyond that, features used for motion analysis with accelerometer signals [32, 139, 148], as well as features used for sound description [113] were selected.

2.5.1 Time domain features

- Minimum (Minimum): The minimum value of the signal inside the window. It was calculated using the `std::min_element` function of the standard c++ library.
- Maximum (Maximum): The maximum value of the signal inside the window. It was calculated using the `std::max_element` function of the standard c++ library.
- Difference between the minimum and the maximum (MaximumMinusMinimum): The minimum value of the signal inside the window subtracted from the maximum value of the signal inside the window.
- Mean (Mean_Boost): The mean value of the of the signal inside the window. It was calculated using the `boost::accumulators::impl::mean_impl` template from the accumulators framework of the Boost C++ Libraries 1.55.0 [127].
- Median (Median_Boost): The median of the of the signal inside the window. It was calculated using the median estimation based on the P^2 algorithm [54] with a quantile probability of 0.5. The median is implemented with the `boost::accumulators::impl::median_impl` template from the accumulators framework of the Boost C++ Libraries 1.55.0 [127].
- Variance (Variance_Boost): The variance of the of the signal inside the window. It was calculated iteratively based on the `boost::accumulators::impl::variance_impl` template from the accumulators framework of the Boost C++ Libraries 1.55.0 [127].
- Standard deviation (StandardDeviation_Boost): The standard deviation of the of the signal inside the window. It is the square root of the Variance_Boost.
- Root mean square (RootMeanSquare): It is the square root of the sum of squares of the signal values inside the window.
- Interquartile range (InterquartileRange_Boost): The difference of the 0.75 quantile minus the 0.25 quantile. The quantile estimation is based on the the P^2 algorithm [54] as implemented with the `boost::accumulators::impl::p_square_quantile_impl` template from the accumulators framework of the Boost C++ Libraries 1.55.0 [127].
- Skewness (Skewness_Boost): The skewness of a sample distribution is defined as the ratio of the 3rd central moment to the 3/2-th power of the 2nd central moment (the variance) of the samples. It is calculated using the `boost::accumulators::impl::skewness_impl` template from the accumulators framework of the Boost C++ Libraries 1.55.0 [127].
- Kurtosos (Kurtosis_Boost): The kurtosis of a sample distribution is defined as the ratio of the 4th central moment and the square of the 2nd central moment (the variance) of the samples, minus 3. The term -3 is added in order to ensure that the normal distribution has zero kurtosis. It is calculated using the `boost::accumulators::impl::kurtosis_impl` template from the accumulators framework of the Boost C++ Libraries 1.55.0 [127].

- Variance of time intervals between adjacent spikes (VTI): The variance of the time intervals between any two subsequent spikes or transients. This feature is used for estimating the periodicity of the movements based on the observation that rhythmic movements would produce variances close to zero. It is one of the features used by the group of Karayiannis et al. [69] for epileptic seizure recognition.
- Energy ratio (ENR): The energy ratio of the autocorrelation sequence which is calculated as the ratio of the energy contained by the last 75% of the samples of the autocorrelation sequence to the energy contained by the first 25%. It is a measure for the motion manifested as quasiperiodic spikes (randomness). It is one of the features used by the group of Karayiannis et al. [69] for epileptic seizure recognition.
- Zero crossing rate (ZeroCrossingRate): Zero crossing rate is the rate of sign-changes along the signal.
- Mean crossing rate (MeanCrossingRate): Mean crossing rate is the rate of mean crossings along the signal.
- Normalized energy (NormalizedEnergy): The normalized energy is the sum of squares of the signal values, divided by the signal length.
- Entropy of the energy in bins (EntropyEnergyBins): The entropy of the energy in bins is the Shannon entropy $H(x_i)$ calculated from the normalized energy of 10 equally sized consecutive bins, taken from signal.

$$H(x_i) = -\sum_{i=1}^{N} x_i \log_2 x_i$$

2.5.2 Frequency domain features

The frequency domain features are derived from the power spectral density, which is calculated with the discrete Fourier transform as implemented in OpenCV [10]. For this purpose the signal is windowed using a Hamming window in order to reduce DFT leakage.

- 25% spectral power frequency (25SPF): It is the upper bound of the frequency band starting at 0 Hz that contains 25% of the total spectral power. Seizures containing isolated sharp spikes would generate a broader band while seizures with many (near periodic) spikes produce a narrower one. It is one of the features used by the group of Karayiannis et al. [69] for epileptic seizure recognition with the difference that a value of 10% is used instead of 25%.
- Total spectral power from 0 to 3 Hz (PW0-3)
- Total spectral power from 3 to 6 Hz (PW3-6)
- Dominant frequency (DominantFrequency): The frequency with the highest power.
- Entropy of power spectrum in bins (EntropySpectralBins): The Shannon entropy $H(x_i)$ calculated from the normalized power of 10 equally sized consecutive bins,

taken from power spectrum.

$$H(x_i) = -\sum_{i=1}^{N} x_i \log_2 x_i$$

- Spectral roll off (SpectralRollOff): The frequency value at which 80 percent of the spectral power is below that point.
- Spectra centroid (SpectralCentroid): The average frequency of the spectrum.

$$SpectralCentroid = \frac{\sum_{i=1}^{N} f_i p_i}{\sum_{i=1}^{N} p_i}$$

where p_i is the power at frequency f_i.

2.6 Data analysis

2.6.1 Performance measures

Classification tasks are typically evaluated with the help of a confusion matrix (Figure 2.2). The columns represent the classification outcome and the rows the actual condition or class.

	Classified as negative	Classified as positive
Actual negative	True negatives (TN)	False positives (FP)
Actual positive	False negatives (FN)	True positives (TP)

Figure 2.2: The confusion matrix.

Accuracy is the percentage of correctly classified instances (true positives and true negatives) with respect to all instances.

$$\text{Accuracy} = \frac{TP + TN}{TP + FP + TN + FN} \tag{2.1}$$

Recall (also sensitivity or true positive rate) is the ratio of the number of true positives to the total number of actual positives, expressed as a percentage. Recall is a measure of completeness or quantity.

$$\text{Recall} = \frac{TP}{TP + FN} \tag{2.2}$$

Precision (also positive predicted value) is the ratio of the number of true positives to the total number of classified positives (true and false). Precision can be seen as a measure of exactness or quality.

$$\text{Precision} = \frac{TP}{TP + FP} \tag{2.3}$$

Specificity (also true negative rate) is the ratio of the number of true negatives to the total number of negatives. It measures the proportion of negatives which are correctly identified as negatives.

$$\text{Specificity} = \frac{TN}{TN + FP} \tag{2.4}$$

F-measure can be interpreted as a weighted average of the Precision and Recall. The F-measure reaches its best value at 1 and worst at 0.

$$\text{F-measure} = (1 + \beta^2) \cdot \frac{\text{Recall} \cdot \text{Precision}}{\beta^2 \cdot \text{Recall} + \text{Precision}} \tag{2.5}$$

β corresponds to the relative importance of Precision against Recall. It is usually set to 1, so that the F-measure represents the harmonic mean of Precision and Recall.

2.6.2 Window size and step

As mentioned in Section 2.5, a running window of given size and overlap is applied on each signal for the extraction of the features. The actual values for size and overlap play a crucial role in defining the quality of the extracted features. It can be assumed that window size and overlap is related to the duration of the event under examination, i.e. the seizure, as well as to the sampling rate of the signal and the method of feature extraction. In the case of spectral analysis an overlap of 50% to 75% is usually chosen in order to achieve good temporal continuity in the frequency domain. Moreover, the overlap, which defines the window step, should be set such that there is at least one instance associated with the event under examination. The size of the window on the other hand should be large enough to contain an adequate number of samples so that the feature extraction technique does not suffer in quality, especially the spectral analysis. Table 2.1 shows an overview of the mean seizure duration for each of the patients under analysis. It ranges from 2.98 s to 19.33 s with an overall mean of 8.28 s. As a result of the above considerations, window sizes of 2 s, 3 s and 8 s with an overlap of 50% and 75% will be used as a starting point. The 2 and 3 s window cover the patients with the shortest seizure durations, while the 8 s window lies near the overall average. Larger windows are impractical since they would completely miss a large number of seizures.

2.6.3 Standardization

A high difference in the variance of different feature vectors may cause a classifier to behave incorrectly. One feature may lie in the interval of $[0, 1]$ and the other in $[-30000, 30000]$. This difference in variance may make a classifier such as the K-nearest neighbours to see

Table 2.1: Overview of mean seizure duration and standard deviation of the 12 patients under analysis

Patient ID	Number of seizures	Mean seizure duration [s]	Standard deviation
01	4	17.53	4.57
02	8	10.17	3.46
03	21	3.97	1.69
04	65	2.98	0.69
05	25	7.41	3.55
06	14	8.22	1.61
07	16	10.64	4.83
08	26	19.33	7.56
09	25	4.9	1.57
10	68	4.2	0.59
11	38	6.27	1.29
12	25	3.72	1.29

the first feature as more or less constant, thus not being able to learn from it [11]. This problem is addressed by normalizing all feature vectors to unit variance.

Since the variance differences in the current dataset are not extreme and targeted normalization is also taking place during signal and feature extraction, the features were not standardized for the following analysis. In addition to that, standardization is always performed with respect to a given dataset, and since the tests performed for this work are made with multiple training and test sets (e.g. per patient, for all patients, leave-one-out validation), standardization would pose a burden in the process. Finally a simple test, performed with- and without standardization did neither show a positive nor a negative effect on the performance of the classifiers.

2.6.4 Feature selection

The feature selection was performed with the data mining software Weka [49]. The "CfsSubsetEval" evaluation method was used in conjunction with the "BestFirst" search method. This approach has the tendency to return small numbers of selected features, which is desired for the work at hand in order to provide a focus on a few essential features. The "BestFirst" search method searches the space of attribute subsets by greedy hillclimbing augmented with a backtracking facility. An exhaustive search in the feature space is impossible due to the large amount of features. The worth of a subset of attributes is evaluated by considering the individual predictive ability of each feature along with the degree of redundancy between them. Subsets of features that are highly correlated with the class while having low inter-correlation are preferred [50].

2.6.5 Classification

All classification tasks were performed with the data mining software Weka [49]. All classifiers were selected based on initial tests with a subset of the data. A further consideration on the selection of the classifier is the aim to represent a wide range of different classifier types (Bayes, SVM, decision tree etc.). The FFNN was included because it was used by Karayiannis et al. [69, 73] in the classification of myoclonic and focal clonic seizures.

Bayes Network

A Bayes network over a set of variables is a network structure in form of directed acyclic graph over the set of variables an a set of probability tables of a variable, given its parent (conditional distribution) [9]. The algorithm implemented in Weka assumes that the data set has discrete finite variables and no instances have missing values. If there are missing values in the data set, values are filled in using `weka.filters.unsupervised.attribute.ReplaceMissingValues`. The learning of a the network structure is performed as an optimization problem where a quality measure of a network structure given the training data is maximized. For this work, the widely used K2 [21] local scoring method chosen.

Naive Bayes

The Naive Bayes classifier can be seen as a specialized form of a Bayes network, where two simplifying assumptions are made. It assumes that the predictive attributes are conditionally independent, given the class, and that no hidden or latent attributes influence the predictive process [55].

SMO - Sequential minimal optimization

This classifier implements J. Platt's [115] sequential minimal optimization algorithm for training a support vector classifier. This implementation globally replaces all missing values and transforms nominal attributes into binary ones. It also normalizes all attributes by default.

Nearest neighbours classifier

Nearest-neighbour classifier. Uses normalized Euclidean distance to find the training instance closest to the given test instance, and predicts the same class as this training instance. If multiple instances have the same (smallest) distance to the test instance, the first one found is used [3].

AdaBoost

AdaBoost is a meta classifier for boosting a nominal class classifier using the Adaboost M1 method [44]. It often improves performance dramatically, but is prone to overfitting. The classifier, which was used for boosting is decision stump, i.e. a on-level decision tree. Classification is based on entropy and missing values are treated as a separate values.

Feed-Forward Neural Network

The Feed-Forward Neural Network is provided through a Weka plugin called "WEKA Classification Algorithms"[1] provided by Jason Brownlee under the GPLv2 licence. It uses the Back Propagation learning rule with one hidden layer with 20 nodes. The node transfer function is Sigmoid. This classifier was chosen to come as close as possible to the classifier used by Karayiannis et al. [69, 73].

Decision Tree - J48

The decision tree is generated with the C4.5 algorithm by R. Quinlan [119]. At each node of the tree, C4.5 chooses one attribute of the data that most effectively splits its set of samples into subsets enriched in one class or the other.

2.7 Study procedure

The study is performed in terms of 21 experiments and divided in four phases. The first three phases use the semi-automatic annotated ROIs, for patients P01–P08. Based on the results of these phases, a final evaluation with automatic ROI detection is performed in the last phase for P09–P12. The results are presented in Chapter 3 and a comparison and contribution to the state of the art is given in Chapter 4. Finally a thorough discussion is given in Chapter 5.

The four phases, described in more detail:

The first phase (Section 3.1) uses a subset of the annotated seizures in order to limit the capturing conditions and isolate interfering factors including noise from bad illumination, heavy occlusions etc. The main aim of this phase is to select the window size and step for the feature extraction, to test the different classifiers and to perform feature selection.

The second phase (Section 3.2) uses all annotated seizures, including those captured under varying conditions and tests the performance of the selected classifier in phase 1.

[1] http://wekaclassalgos.sourceforge.net/ and http://sourceforge.net/projects/wekaclassalgos/, accessed online: 2014.

It also performs tests with various sub sampling ratios for the training set and finally maps the classified instances to seizure events as a whole.

The third phase (Section 3.3) analyses the influence of the different ROIs in the seizure detection performance. It tests the selected classifier with single separated ROI data (e.g only one eye) and with combinations of all ROIs.

The final phase (Section 3.4) applies the gained information from the previous phases on a new set of patients (P09–P12) in addition to automatic ROI detection as described in Subsection 2.3.2, and tests the performance.

CHAPTER 3

Results

3.1 Phase 1 - Seizure analysis under ideal conditions

One of the major challenges in the area of computer vision is that the video capturing and scene conditions are not constant over time. For the case at hand the greatest deviations are observed with respect to illumination, pose and occlusion. Illumination varies from natural daylight, over artificial room light to low light conditions during the night, with or without the IR acquisition mode being enabled. Although the patient is mainly lying on the bed, it is impossible to force him/her to always face the cameras. Patients are often lying on either side, sitting on the bed to the side or with a steep angle towards the cameras, or even being out of the cameras field of view. Finally, occlusions covering part of the face occur mainly by the hands, hair, game devices and books, blankets and other persons. For these reasons it is inevitable for any initial data analysis to isolate any interfering factors and analyse the data under conditions with limited variations. These "ideal conditions" are the following:

- The face is visible and in a frontal position with only very slight out of plane rotations
- All ROIs are visible during the seizure (not necessary simultaneously)
- Daylight, good illumination
- No photostimulation or other flickering lights such as TV

Based on the above limitations, the following seizures (seizure ID) were selected for patients P01-P08 according to visual inspection and by following comments in Tables 5.1–5.8 in the Annex: 101, 102, 103, 104, 201, 204, 205, 301, 302, 303, 309, 401, 402, 403, 404, 411, 412, 414, 415, 416, 418, 419, 420, 421, 423, 426, 427, 428, 429, 430, 431, 440,

441, 442, 443, 444, 445, 446, 447, 448, 449, 450, 452, 453, 454, 455, 456, 457, 458, 459, 460, 465, 601, 602, 605, 606, 607, 611, 701, 702, 709, 801, 802, 803, 806, 807, 809, 810, 811, 812, 813, 814, 815, 816, 819. No seizures from P05 met the criteria to be included. For the instances describing the seizure-free condition, periods with the same number of instances (i.e. length) of the each seizure, immediately before and after the respective seizure were taken.

The aim of this phase is to persevere the highest possible seizure detection performance. This is achieved through a series of experiments which lead to selecting an appropriate window size and step, selecting the necessary or best features and ROIs, as well as the most suitable/best performing classifier. The following, mainly default, classifier parameters in Weka were used for all experiments:

BayesNet, (1): `bayes.BayesNet '-D -Q bayes.net.search.local.K2 -- -P 1 -S BAYES -E bayes.net.estimate.SimpleEstimator -- -A 0.5' 7460374432587 75954`

Naive Bayes, (2): `bayes.NaiveBayes '' 5995231201785697655`

SMO, (3): `functions.SMO '-C 1.0 -L 0.001 -P 1.0E-12 -N 0 -V -1 -W 1 -K \ "functions.supportVector.PolyKernel -C 250007 -E 1.0\"' -65858836363 78691736`

K nearest neighbours, (4): `lazy.IBk '-K 1 -W 0 -A \"weka.core.neighboursea rch.LinearNNSearch -A \\\"weka.core.EuclideanDistance -R first-last\ \\"\"' -3080186098777067172`

AdaBoost, (5): `meta.AdaBoostM1 '-P 100 -S 1 -I 10 -W trees.DecisionStump' -7378107808933117974`

FFNN, (6): `neural.multilayerperceptron.BackPropagation '-I 500 -L 0.1 -B 1.0 -R 0 -F 1 -N 1 -A 0.2 -D 0.0 -X 20 -Y 0 -Z 0 -M 3' -635536715768 257224`

Decistion Tree, (7): `trees.J48 '-C 0.25 -M2' -217733168393644444`

3.1.1 Experiment 1 - Determination of suitable window size and step

The aim of this experiment is to determine the most suitable window size and step for the windowing process. For this purpose the F-measure has been chosen as a basis for comparison, since it describes the overall performance of the classifiers. All features for all four ROIs were used. All seven classifiers have been tested with each one of the six combinations of window size and step for each patient. The results from a 10-fold cross validation, repeated 10 times, are shown in Table 3.1 for each of the 7 classifiers. The case for P03 with an 8 s window size at a step of 4 s (50% overlap) could not be tested because the number of instances was less than 10. It is observable that patients with seizure durations shorter than 8s (P03, P04 and P06) show lower values for the 8 s window. The other patients (seizure duration above 10 s) show a certain robustness against varying window sizes and step. Although this also depends on the selected classifier, e.g. the weaker classifiers in average (FFNN and decision tree) show higher variabilities. In order

to draw a conclusion of which window size and step should be selected, a ranking of the results from the paired two tailed corrected t-test is shown in Table 3.2 (Significance 0.05). Highlighted is the first rank for each patient. It reveals that a window size of 3 s with 0.75 s step yields the best overall difference (difference = 397) of wins against losses followed by window size of 2 s with 0.5 s step (difference = 304). This ranking is obviously influenced by all classifiers, especially weak classifiers may distort the overall image. Nevertheless, a window size of 3 s with a step of 0.75 s can be seen as the best selection for the given (sub-)dataset. This combination is used for all following experiments and phases.

Table 3.1: Experiment 1: F-measure for the seven classifiers (1)–(7) for the combinations of window size and step per patient. The highest average values for each patient are highlighted in grey.

Dataset	(1)	(2)	(3)	(4)	(5)	(6)	(7)	Average
P01-W2-ST0.5	0.77	0.74	0.89	0.79	0.75	0.05	0.76	0.68
P01-W2-ST1	0.77	0.74	0.77	0.72	0.76	0.57	0.68	0.72
P01-W3-ST0.75	0.78	0.76	0.93	0.82	0.8	0.62	0.79	0.79
P01-W3-ST1.5	0.75	0.75	0.85	0.62	0.70	0.61	0.76	0.72
P01-W8-ST2	0.76	0.75	0.81	0.81	0.75	0.56	0.74	0.74
P01-W8-ST4	0.75	0.74	0.53	0.51	0.62	0.50	0.74	0.63
P02-W2-ST0.5	0.65	0.52	0.87	0.64	0.62	0.16	0.59	0.58
P02-W2-ST1	0.50	0.51	0.60	0.52	0.54	0.29	0.42	0.48
P02-W3-ST0.75	0.65	0.54	0.81	0.60	0.73	0.4	0.64	0.62
P02-W3-ST1.5	0.38	0.46	0.54	0.38	0.54	0.36	0.31	0.42
P02-W8-ST2	0.59	0.51	0.72	0.52	0.70	0.34	0.61	0.57
P02-W8-ST4	0.21	0.29	0.40	0.44	0.19	0.27	0.14	0.28
P03-W2-ST0.5	0.63	0.61	0.90	0.84	0.73	0.43	0.73	0.70
P03-W2-ST1	0.46	0.43	0.54	0.62	0.41	0.34	0.44	0.46
P03-W3-ST0.75	0.69	0.68	0.73	0.78	0.70	0.46	0.80	0.69
P03-W3-ST1.5	0.62	0.27	0.41	0.31	0.56	0.50	0.54	0.46
P03-W8-ST2	0.39	0.16	0.39	0.54	0.40	0.37	0.48	0.39
P04-W2-ST0.5	0.55	0.52	0.60	0.68	0.49	0.00	0.56	0.49
P04-W2-ST1	0.56	0.50	0.46	0.43	0.48	0.00	0.45	0.41
P04-W3-ST0.75	0.56	0.52	0.58	0.57	0.52	0.00	0.50	0.46
P04-W3-ST1.5	0.59	0.48	0.42	0.34	0.54	0.08	0.42	0.41
P04-W8-ST2	0.20	0.33	0.39	0.33	0.34	0.03	0.36	0.28
P04-W8-ST4	0.17	0.29	0.30	0.06	0.29	0.28	0.33	0.25
P06-W2-ST0.5	0.70	0.72	0.84	0.75	0.81	0.73	0.73	0.75
P06-W2-ST1	0.67	0.70	0.76	0.73	0.76	0.73	0.68	0.72
P06-W3-ST0.75	0.71	0.72	0.85	0.79	0.85	0.73	0.75	0.77
P06-W3-ST1.5	0.68	0.66	0.76	0.71	0.77	0.63	0.61	0.69
P06-W8-ST2	0.53	0.75	0.75	0.73	0.73	0.68	0.66	0.69
P06-W8-ST4	0.39	0.63	0.54	0.7	0.43	0.66	0.47	0.55
P07-W2-ST0.5	0.78	0.78	0.92	0.84	0.91	0.75	0.77	0.82
P07-W2-ST1	0.61	0.8	0.86	0.63	0.78	0.78	0.79	0.75
P07-W3-ST0.75	0.81	0.82	0.96	0.91	0.88	0.75	0.74	0.84
P07-W3-ST1.5	0.64	0.79	0.84	0.72	0.68	0.63	0.63	0.70
P07-W8-ST2	0.75	0.72	0.73	0.56	0.62	0.83	0.65	0.69
P07-W8-ST4	0.40	0.40	0.30	0.10	0.20	0.30	0.20	0.27
P08-W2-ST0.5	0.75	0.80	0.85	0.87	0.79	0.70	0.79	0.79
P08-W2-ST1	0.76	0.79	0.77	0.78	0.79	0.70	0.75	0.76
P08-W3-ST0.75	0.78	0.79	0.85	0.85	0.82	0.71	0.80	0.80
P08-W3-ST1.5	0.78	0.79	0.73	0.76	0.79	0.70	0.75	0.76
P08-W8-ST2	0.80	0.79	0.85	0.85	0.86	0.73	0.83	0.82
P08-W8-ST4	0.78	0.77	0.76	0.75	0.82	0.68	0.76	0.76

Table 3.2: Experiment 1: Ranking of the combinations of window size and step per patient, based on F-measure. The highest rank for each patient is highlighted in grey.

Dataset	Wins− Losses	Wins	Losses
P07-W2-ST0.5	151	151	0
P07-W3-ST0.75	143	143	0
P08-W8-ST2	140	142	2
P08-W2-ST0.5	130	135	5
P08-W3-ST0.75	127	132	5
P01-W3-ST0.75	126	127	1
P06-W3-ST0.75	101	106	5
P08-W2-ST1	92	109	17
P06-W2-ST0.5	89	101	12
P08-W8-ST4	87	100	13
P08-W3-ST1.5	83	103	20
P07-W2-ST1	81	88	7
P01-W8-ST2	77	89	12
P01-W3-ST1.5	68	85	17
P06-W2-ST1	64	83	19
P01-W2-ST1	63	88	25
P01-W2-ST0.5	56	96	40
P07-W3-ST1.5	53	54	1
P06-W3-ST1.5	52	65	13
P06-W8-ST2	50	67	17
P03-W2-ST0.5	47	77	30
P03-W3-ST0.75	43	57	14
P07-W8-ST2	38	41	3
P01-W8-ST4	2	46	44
P02-W3-ST0.75	-12	56	68
P02-W8-ST2	-23	27	50
P06-W8-ST4	-42	24	66
P02-W2-ST0.5	-54	47	101
P03-W3-ST1.5	-61	11	72
P03-W2-ST1	-95	12	107
P03-W8-ST2	-105	6	111
P02-W2-ST1	-113	22	135
P04-W2-ST0.5	-115	30	145
P04-W3-ST0.75	-131	22	153
P02-W3-ST1.5	-138	8	146
P04-W3-ST1.5	-156	12	168
P07-W8-ST4	-160	0	160
P04-W2-ST1	-160	11	171
P02-W8-ST4	-180	2	182
P04-W8-ST4	-209	5	214
P04-W8-ST2	-209	2	211

3.1.2 Experiment 2 - Classifier selection per patient with all features

The aim of this experiment is to select the most suitable classifier when using all 864 features for all four ROIs. The evaluation is performed per patient in terms of a 10-fold cross validation, repeated 10 times. The results are shown below for four performance measures (Tables 3.3–3.6). Ranking of the classifiers, based on the corrected two-sided t-test (Significance 0.05) for the four comparison fields is given in Tables 3.7–3.10. The performance evaluation results that classifier (3) performs better than the others, followed by classifiers (5) and (4). Classifier (2) has only a good recall.

Table 3.3: Experiment 2: Accuracy for each classifier and patient. The highest average value is highlighted in grey.

Dataset	(1)	(2)	(3)	(4)	(5)	(6)	(7)
P01-W3-ST0.75	78.79	75.97	94.66	86.28	84.32	71.61	83.64
P02-W3-ST0.75	78.98	52.47	87.92	67.05	83.81	71.52	76.74
P03-W3-ST0.75	75.23	76.77	80.83	80.63	81.57	66.77	85.80
P04-W3-ST0.75	62.68	52.44	71.91	72.41	70.79	65.83	66.44
P06-W3-ST0.75	74.19	66.84	83.88	76.16	84.64	70.01	72.85
P07-W3-ST0.75	82.76	82.93	95.71	89.81	86.74	76.29	72.29
P08-W3-ST0.75	77.02	74.59	82.90	82.82	79.78	55.55	77.98
Average	75.66	68.86	85.40	79.31	81.66	68.22	76.53

Table 3.4: Experiment 2: Recall for each classifier and patient. The highest average value is highlighted in grey.

Dataset	(1)	(2)	(3)	(4)	(5)	(6)	(7)
P01-W3-ST0.75	0.94	0.96	0.93	0.83	0.83	0.70	0.80
P02-W3-ST0.75	0.62	0.85	0.81	0.73	0.68	0.32	0.63
P03-W3-ST0.75	0.76	0.73	0.78	0.90	0.69	0.51	0.84
P04-W3-ST0.75	0.69	0.76	0.58	0.54	0.47	0.00	0.49
P06-W3-ST0.75	0.62	0.81	0.86	0.82	0.85	0.77	0.77
P07-W3-ST0.75	0.74	0.76	0.94	0.90	0.88	0.70	0.74
P08-W3-ST0.75	0.73	0.87	0.85	0.88	0.81	0.99	0.79
Average	0.73	0.82	0.82	0.80	0.74	0.57	0.72

Table 3.5: Experiment 2: Precision for each classifier and patient. The highest average value is highlighted in grey.

Dataset	(1)	(2)	(3)	(4)	(5)	(6)	(7)
P01-W3-ST0.75	0.67	0.63	0.94	0.83	0.80	0.64	0.79
P02-W3-ST0.75	0.75	0.40	0.84	0.52	0.82	0.61	0.70
P03-W3-ST0.75	0.69	0.69	0.73	0.72	0.78	0.48	0.82
P04-W3-ST0.75	0.47	0.40	0.60	0.62	0.61	0.01	0.51
P06-W3-ST0.75	0.87	0.66	0.85	0.76	0.88	0.71	0.74
P07-W3-ST0.75	0.94	0.93	0.99	0.93	0.91	0.85	0.79
P08-W3-ST0.75	0.84	0.73	0.85	0.82	0.83	0.55	0.81
Average	0.75	0.63	0.83	0.74	0.80	0.55	0.74

Table 3.6: Experiment 2: F-measure for each classifier and patient. The highest average value is highlighted in grey.

Dataset	(1)	(2)	(3)	(4)	(5)	(6)	(7)
P01-W3-ST0.75	0.78	0.76	0.93	0.82	0.80	0.62	0.79
P02-W3-ST0.75	0.65	0.54	0.81	0.60	0.73	0.40	0.64
P03-W3-ST0.75	0.69	0.68	0.73	0.78	0.70	0.46	0.80
P04-W3-ST0.75	0.56	0.52	0.58	0.57	0.52	0.00	0.50
P06-W3-ST0.75	0.71	0.72	0.85	0.79	0.85	0.73	0.75
P07-W3-ST0.75	0.81	0.82	0.96	0.91	0.88	0.75	0.74
P08-W3-ST0.75	0.78	0.79	0.85	0.85	0.82	0.71	0.80
Average	0.71	0.69	0.81	0.76	0.76	0.52	0.72

Table 3.7: Experiment 2: Classifier ranking based on accuracy. The highest rank is highlighted in grey.

Resultset	Wins−Losses	Wins	Losses
(3)	27	27	0
(5)	13	15	2
(4)	9	14	5
(7)	-1	7	8
(1)	-6	6	12
(6)	-19	2	21
(2)	-23	1	24

Table 3.8: Experiment 2: Classifier ranking based on recall. The highest rank is highlighted in grey.

Resultset	Wins−Losses	Wins	Losses
(2)	14	16	2
(3)	12	15	3
(4)	3	9	6
(5)	-5	4	9
(1)	-5	10	15
(7)	-7	5	12
(6)	-12	7	19

Table 3.9: Experiment 2: Classifier ranking based on precision. The highest rank is highlighted in grey.

Resultset	Wins−Losses	Wins	Losses
(3)	17	17	0
(5)	12	13	1
(4)	5	11	6
(7)	4	10	6
(1)	4	11	7
(6)	-20	0	20
(2)	-22	2	24

Table 3.10: Experiment 2: Classifier ranking based on F-measure. The highest rank is highlighted in grey.

Resultset	Wins−Losses	Wins	Losses
(3)	26	26	0
(5)	8	10	2
(4)	7	9	2
(1)	-3	5	8
(7)	-4	5	9
(2)	-5	3	8
(6)	-29	0	29

3.1.3 Experiment 3 - Classifier selection per patient with selected features for each patient separately

The aim of this experiment is to select the most suitable classifier when using selected features for each patient for all four ROIs. The evaluation is performed per patient

in terms of a 10-fold cross validation, repeated 10 times. The results are shown in Tables 3.11–3.14 for four performance measures. Ranking of the classifiers is based on the corrected two-sided t-test for the four comparison fields and is given in Tables 3.15–3.18. The performance evaluation results that classifiers (1),(3) and (4) perform better than the others. Considering the ranking, classifiers (1) and (4) stand out by taking the first place in F-measure and precision respectively. It is noticeable that with the selected features performance in general is slightly better than with all features (cf. experiment 2).

Features were selected with the `weka.attributeSelection.CfsSubsetEval` evaluator using the `weka.attributeSelection.BestFirst -D 1 -N 5` search and the full training set. Total selected features: P01: 57; P02: 36; P03: 21; P04: 30; P06: 30; P07: 32; P08: 67.

Table 3.11: Experiment 3: Accuracy for each classifier after feature selection for each patient. The highest average value is highlighted in grey.

Dataset	(1)	(2)	(3)	(4)	(5)	(6)	(7)
'P01-W3-ST0.75	87.77	78.35	92.68	90.78	83.55	69.16	85.99
'P02-W3-ST0.75	86.68	72.55	86.87	88.23	87.42	74.55	78.90
'P03-W3-ST0.75	89.50	81.23	80.90	88.03	87.87	70.20	88.87
'P04-W3-ST0.75	74.69	68.56	74.28	67.04	71.25	65.87	69.87
'P06-W3-ST0.75	84.19	78.14	80.75	79.66	86.87	74.52	72.88
'P07-W3-ST0.75	95.67	91.88	93.74	90.64	88.81	92.17	76.05
'P08-W3-ST0.75	82.57	79.05	81.08	84.81	79.46	55.22	78.95
Average	85.87	78.54	84.33	84.17	83.60	71.67	78.79

Table 3.12: Experiment 3: Recall for each classifier after feature selection for each patient. The highest average value is highlighted in grey.

Dataset	(1)	(2)	(3)	(4)	(5)	(6)	(7)
'P01-W3-ST0.75	0.94	0.95	0.89	0.94	0.84	0.30	0.83
'P02-W3-ST0.75	0.78	0.92	0.77	0.77	0.78	0.43	0.66
'P03-W3-ST0.75	0.83	0.73	0.68	0.92	0.81	0.66	0.82
'P04-W3-ST0.75	0.69	0.78	0.46	0.56	0.47	0.00	0.50
'P06-W3-ST0.75	0.78	0.80	0.79	0.74	0.87	0.81	0.77
'P07-W3-ST0.75	0.94	0.93	0.93	0.88	0.90	0.94	0.77
'P08-W3-ST0.75	0.81	0.82	0.85	0.86	0.81	0.99	0.81
Average	0.82	0.85	0.77	0.81	0.78	0.59	0.74

Table 3.13: Experiment 3: Precision for each classifier after feature selection for each patient. The highest average value is highlighted in grey.

Dataset	(1)	(2)	(3)	(4)	(5)	(6)	(7)
'P01-W3-ST0.75	0.80	0.66	0.93	0.85	0.78	0.37	0.82
'P02-W3-ST0.75	0.83	0.57	0.85	0.88	0.86	0.67	0.74
'P03-W3-ST0.75	0.91	0.78	0.78	0.83	0.88	0.57	0.90
'P04-W3-ST0.75	0.62	0.53	0.69	0.52	0.62	0.00	0.58
'P06-W3-ST0.75	0.92	0.80	0.85	0.87	0.90	0.75	0.75
'P07-W3-ST0.75	0.99	0.94	0.96	0.96	0.92	0.94	0.82
'P08-W3-ST0.75	0.87	0.81	0.82	0.87	0.82	0.55	0.81
Average	0.85	0.73	0.84	0.82	0.82	0.55	0.77

Table 3.14: Experiment 3: F-measure for each classifier after feature selection for each patient. The highest average value is highlighted in grey.

Dataset	(1)	(2)	(3)	(4)	(5)	(6)	(7)
'P01-W3-ST0.75	0.86	0.77	0.90	0.89	0.80	0.29	0.82
'P02-W3-ST0.75	0.79	0.70	0.79	0.81	0.80	0.47	0.67
'P03-W3-ST0.75	0.84	0.72	0.69	0.85	0.81	0.58	0.83
'P04-W3-ST0.75	0.65	0.63	0.55	0.54	0.52	0.00	0.53
'P06-W3-ST0.75	0.83	0.79	0.81	0.79	0.87	0.77	0.75
'P07-W3-ST0.75	0.96	0.93	0.94	0.91	0.90	0.93	0.77
'P08-W3-ST0.75	0.84	0.81	0.83	0.86	0.81	0.71	0.81
Average	0.82	0.77	0.79	0.81	0.79	0.54	0.74

Table 3.15: Experiment 3: Classifier ranking based on accuracy after feature selection for each patient. The highest rank is highlighted in grey.

Resultset	Wins− Losses	Wins	Losses
(1)	14	15	1
(4)	11	13	2
(3)	11	12	1
(5)	8	12	4
(7)	-9	4	13
(2)	-11	3	14
(6)	-24	1	25

Table 3.16: Experiment 3: Classifier ranking based on recall after feature selection for each patient. The highest rank is highlighted in grey.

Resultset	Wins− Losses	Wins	Losses
(2)	13	14	1
(1)	6	10	4
(4)	2	7	5
(3)	0	5	5
(5)	-2	4	6
(7)	-9	2	11
(6)	-10	7	17

Table 3.17: Experiment 3: Classifier ranking based on precision after feature selection for each patient. The highest rank is highlighted in grey.

Resultset	Wins−Losses	Wins	Losses
(1)	16	17	1
(4)	10	12	2
(3)	8	11	3
(5)	6	9	3
(7)	-2	6	8
(2)	-14	2	16
(6)	-24	0	24

Table 3.18: Experiment 3: Classifier ranking based on F-measure after feature selection for each patient. The highest rank is highlighted in grey.

Resultset	Wins−Losses	Wins	Losses
(1)	14	14	0
(4)	12	14	2
(3)	6	8	2
(5)	3	8	5
(2)	3	9	6
(7)	-12	4	16
(6)	-26	1	27

3.1.4 Experiment 4 - Classifier selection per patient with union of selected features for each patient

The aim of this experiment is to select the most suitable classifier when using the union of selected features for each patient for all four ROIs from the previous experiment. This resulted in a total of 229 features. A full list is given in the Annex, Table 5.20. The evaluation is performed per patient in terms of a 10-fold cross validation, repeated 10 times. The results are shown in Tables 3.19–3.22 for four performance measures. Ranking of the classifiers is based on the corrected two-sided t-test for the four comparison fields and is given in Tables 3.23–3.26. Classifiers (3) and (4) stand out in this experiment. The overall performance is more or less equal to that of experiment 2 (all features), but with a gain of 635 less features.

Table 3.19: Experiment 4: Accuracy for each classifier with union of selected features for each patient. The highest average value is highlighted in grey.

Dataset	(1)	(2)	(3)	(4)	(5)	(6)	(7)
'P01-W3-ST0.75	79.38	74.94	92.56	92.71	85.25	73.44	84.61
'P02-W3-ST0.75	85.28	50.72	86.80	86.73	86.16	70.52	78.63
'P03-W3-ST0.75	77.63	80.70	81.17	80.80	80.77	68.63	82.20
'P04-W3-ST0.75	70.93	58.50	73.01	71.88	71.07	65.87	68.17
'P06-W3-ST0.75	77.01	68.94	85.99	76.44	85.69	74.45	76.56
'P07-W3-ST0.75	86.76	77.81	95.98	91.24	86.98	73.07	75.33
'P08-W3-ST0.75	79.15	76.19	84.20	84.37	78.74	58.69	79.14
Average	79.45	69.68	85.67	83.45	82.10	69.24	77.81

Table 3.20: Experiment 4: Recall for each classifier with union of selected features for each patient. The highest average value is highlighted in grey.

Dataset	(1)	(2)	(3)	(4)	(5)	(6)	(7)
'P01-W3-ST0.75	0.96	0.93	0.90	0.90	0.84	0.66	0.80
'P02-W3-ST0.75	0.72	0.84	0.78	0.74	0.75	0.17	0.65
'P03-W3-ST0.75	0.74	0.80	0.79	0.87	0.69	0.63	0.80
'P04-W3-ST0.75	0.68	0.73	0.51	0.54	0.47	0.00	0.52
'P06-W3-ST0.75	0.65	0.78	0.86	0.87	0.85	0.76	0.80
'P07-W3-ST0.75	0.81	0.70	0.94	0.94	0.86	0.69	0.77
'P08-W3-ST0.75	0.76	0.86	0.88	0.85	0.81	0.80	0.80
Average	0.76	0.81	0.81	0.82	0.75	0.53	0.73

Table 3.21: Experiment 4: Precision for each classifier with union of selected features for each patient. The highest average value is highlighted in grey.

Dataset	(1)	(2)	(3)	(4)	(5)	(6)	(7)
'P01-W3-ST0.75	0.67	0.62	0.91	0.92	0.81	0.51	0.81
'P02-W3-ST0.75	0.84	0.39	0.84	0.86	0.84	0.57	0.71
'P03-W3-ST0.75	0.72	0.73	0.75	0.74	0.76	0.60	0.79
'P04-W3-ST0.75	0.57	0.44	0.64	0.60	0.62	0.00	0.54
'P06-W3-ST0.75	0.90	0.69	0.89	0.75	0.89	0.77	0.79
'P07-W3-ST0.75	0.96	0.89	0.99	0.92	0.91	0.83	0.82
'P08-W3-ST0.75	0.85	0.75	0.84	0.87	0.81	0.63	0.82
Average	0.79	0.65	0.84	0.81	0.80	0.56	0.75

Table 3.22: Experiment 4: F-measure for each classifier with union of selected features for each patient. The highest average value is highlighted in grey.

Dataset	(1)	(2)	(3)	(4)	(5)	(6)	(7)
'P01-W3-ST0.75	0.79	0.74	0.90	0.90	0.81	0.55	0.80
'P02-W3-ST0.75	0.76	0.53	0.79	0.78	0.77	0.24	0.66
'P03-W3-ST0.75	0.70	0.74	0.75	0.78	0.69	0.57	0.76
'P04-W3-ST0.75	0.62	0.55	0.56	0.57	0.52	0.00	0.53
'P06-W3-ST0.75	0.74	0.73	0.87	0.80	0.86	0.76	0.78
'P07-W3-ST0.75	0.85	0.76	0.96	0.92	0.87	0.73	0.77
'P08-W3-ST0.75	0.80	0.80	0.86	0.86	0.81	0.65	0.81
Average	0.75	0.69	0.81	0.80	0.76	0.50	0.73

Table 3.23: Experiment 4: Classifier ranking based on accuracy for the union of selected features for each patient. The highest rank is highlighted in grey.

Resultset	Wins−Losses	Wins	Losses
(3)	22	22	0
(4)	18	18	0
(5)	7	11	4
(1)	-2	6	8
(7)	-3	5	8
(6)	-20	2	22
(2)	-22	1	23

Table 3.24: Experiment 4: Classifier ranking based on recall for the union of selected features for each patient. The highest rank is highlighted in grey.

Resultset	Wins−Losses	Wins	Losses
(2)	11	13	2
(3)	8	10	2
(4)	4	7	3
(1)	0	9	9
(5)	-2	4	6
(7)	-7	3	10
(6)	-14	0	14

Table 3.25: Experiment 4: Classifier ranking based on precision for the union of selected features for each patient. The highest rank is highlighted in grey.

Resultset	Wins−Losses	Wins	Losses
(3)	17	17	0
(4)	10	13	3
(5)	7	11	4
(1)	7	12	5
(7)	0	8	8
(6)	-20	0	20
(2)	-21	2	23

Table 3.26: Experiment 4: Classifier ranking based on F-measure for the union of selected features for each patient. The highest rank is highlighted in grey.

Resultset	Wins−Losses	Wins	Losses
(3)	19	19	0
(4)	18	18	0
(5)	4	9	5
(1)	2	8	6
(7)	-4	4	8
(2)	-13	3	16
(6)	-26	0	26

3.1.5 Remarks for experiments 2–4

So far, the performance of each classifier was tested in terms of a 10-fold cross validation for each patient individually. This allowed to see if there are any peculiarities among patients. Results for P04 e.g. are low in all three experiments, while P01, P07 and P08 show the best overall results. This could expected to certain extend since the latter three patients took high ranking places in experiment 1, with the chosen windows size of 3 s and step of 0.75 s, while P04 generally takes a low ranking place.

A second approach is to form a single dataset with the data from all patients and to perform a 10-fold cross validation with the new dataset. The following three experiments follow this approach with either all features, a subset of features selected from the new dataset, and the union of features, selected individually from each patient as in experiment 4.

3.1.6 Experiment 5 - Classifier selection for all patients at once with all features

The aim of this experiment is to select the most suitable classifier when using a single dataset with all patients and all features. The evaluation is performed in terms of a 10-fold cross validation, repeated 10 times. The results are shown in Table 3.27 for four performance measures. Ranking of the classifiers is based on the corrected two-sided t-test for the four comparison fields and is given in Tables 3.28–3.31. Classifiers (3) and (4) stand out in this experiment. A recall of 1.00 for classifier (6) is extraordinarily good, although counterbalanced by the worst overall precision. Classifier (2) shows the best recall.

Table 3.27: Experiment 5: Performance measures for each classifier with all patients in one dataset and all features. Highest values are highlighted in grey.

Measure	(1)	(2)	(3)	(4)	(5)	(6)	(7)
Accuracy [%]	64.86	56.30	73.14	71.33	68.14	44.75	68.87
Recall	0.65	0.83	0.68	0.65	0.63	1.00	0.63
Precision	0.60	0.51	0.71	0.69	0.65	0.45	0.66
F-measure	0.62	0.63	0.69	0.67	0.64	0.62	0.64

Table 3.28: Experiment 5: Classifier ranking based on accuracy for all patients in one dataset and all features. The highest rank is highlighted in grey.

Resultset	Wins− Losses	Wins	Losses
(3)	5	5	0
(4)	4	4	0
(7)	2	3	1
(5)	1	3	2
(1)	-2	2	4
(2)	-4	1	5
(6)	-6	0	6

Table 3.29: Experiment 5: Classifier ranking based on recall for all patients in one dataset and all features. The highest rank is highlighted in grey.

Resultset	Wins− Losses	Wins	Losses
(6)	6	6	0
(2)	4	5	1
(3)	-1	1	2
(5)	-2	0	2
(4)	-2	0	2
(1)	-2	0	2
(7)	-3	0	3

Table 3.30: Experiment 5: Classifier ranking based on precision for all patients in one dataset and all features. The highest rank is highlighted in grey.

Resultset	Wins− Losses	Wins	Losses
(4)	5	5	0
(3)	5	5	0
(7)	1	3	2
(5)	1	3	2
(1)	-2	2	4
(2)	-4	1	5
(6)	-6	0	6

Table 3.31: Experiment 5: Classifier ranking based on F-measure for all patients in one dataset and all features. The highest rank is highlighted in grey.

Resultset	Wins− Losses	Wins	Losses
(3)	5	5	0
(4)	3	3	0
(7)	-1	0	1
(5)	-1	0	1
(6)	-2	0	2
(2)	-2	0	2
(1)	-2	0	2

3.1.7 Experiment 6 - Classifier selection for all patients at once with selected features from all patients

The aim of this experiment is to select the most suitable classifier when using a single dataset with all patients and a subset of features, 81 in total (Table 5.21, Annex), selected from the same dataset. The evaluation is performed in terms of a 10-fold cross validation, repeated 10 times. The results are shown in Table 3.32 for four performance measures. Ranking of the classifiers is based on the corrected two-sided t-test for the four comparison fields and is given in Tables 3.33–3.36. Classifiers (3) and (4) stand out in this experiment mostly due to the ranking based on precision (classifier (3)), and average F-measure (classifier(4)). It is observable that classifier (6) fails in therms of precision and recall due to zero true positives. Classifier (2) shows the best recall.

Features were selected with the `weka.attributeSelection.CfsSubsetEval` evaluator using the `weka.attributeSelection.BestFirst -D 1 -N 5` search and the full training set.

Table 3.32: Experiment 6: Performance measures for each classifier with all patients in one dataset and selected features from all patients. Highest values are highlighted in grey.

Measure	(1)	(2)	(3)	(4)	(5)	(6)	(7)
Accuracy	68.26	62.99	69.91	69.69	68.29	54.82	69.33
Recall	0.65	0.74	0.60	0.65	0.61	0.00	0.62
Precision	0.64	0.57	0.69	0.66	0.66	0.00	0.67
F-measure	0.65	0.64	0.64	0.66	0.63	0.00	0.65

Table 3.33: Experiment 6: Classifier ranking based on accuracy for all patients in one dataset and selected features from all patients. The highest rank is highlighted in grey.

Resultset	Wins− Losses	Wins	Losses
(7)	2	2	0
(5)	2	2	0
(4)	2	2	0
(3)	2	2	0
(1)	2	2	0
(2)	-4	1	5
(6)	-6	0	6

Table 3.34: Experiment 6: Classifier ranking based on recall for all patients in one dataset and selected features from all patients. The highest rank is highlighted in grey.

Resultset	Wins− Losses	Wins	Losses
(2)	6	6	0
(1)	2	3	1
(4)	1	2	1
(7)	0	1	1
(5)	-1	1	2
(3)	-2	1	3
(6)	-6	0	6

Table 3.35: Experiment 6: Classifier ranking based on precision for all patients in one dataset and selected features from all patients. The highest rank is highlighted in grey.

Resultset	Wins− Losses	Wins	Losses
(3)	3	3	0
(7)	2	2	0
(5)	2	2	0
(4)	2	2	0
(1)	1	2	1
(2)	-4	1	5
(6)	-6	0	6

Table 3.36: Experiment 6: Classifier ranking based on F-measure for all patients in one dataset and selected features from all patients. The highest rank is highlighted in grey.

Resultset	Wins− Losses	Wins	Losses
(7)	1	1	0
(5)	1	1	0
(4)	1	1	0
(3)	1	1	0
(2)	1	1	0
(1)	1	1	0
(6)	-6	0	6

3.1.8 Experiment 7 - Classifier selection for all patients at once with union of selected features from each patient

The aim of this experiment is to select the most suitable classifier when using a single dataset with all patients and a subset of features, consistion of the union of features selected individually for each patient as in experiment 4 (cf. Table 5.20). The evaluation is performed in terms of a 10-fold cross validation, repeated 10 times. The results are shown in Table 3.37 for four performance measures. Ranking of the classifiers is based on the corrected two-sided t-test for the four comparison fields and is given in Tables 3.38–3.41. Classifiers (4) and (7) stand out in this experiment mostly due to the ranking based on precision and F-measure. Classifier (2) shows the best recall.

Table 3.37: Experiment 7: Performance measures for each classifier with all patients in one dataset and union of selected features from each patient. Highest values are highlighted in grey.

Measure	(1)	(2)	(3)	(4)	(5)	(6)	(7)
Accuracy	66.74	57.50	70.56	73.95	68.63	46.79	70.95
Recall	0.65	0.81	0.63	0.65	0.63	0.76	0.65
Precision	0.63	0.52	0.69	0.74	0.66	0.37	0.69
F-measure	0.64	0.63	0.66	0.69	0.64	0.48	0.67

Table 3.38: Experiment 7: Classifier ranking based on accuracy for all patients in one dataset and union of selected features from each patient. The highest rank is highlighted in grey.

Resultset	Wins−Losses	Wins	Losses
(4)	5	5	0
(7)	3	3	0
(3)	2	3	1
(5)	1	2	1
(1)	-1	2	3
(2)	-4	1	5
(6)	-6	0	6

Table 3.39: Experiment 7: Classifier ranking based on recall for all patients in one dataset and union of selected features from each patient. The highest rank is highlighted in grey.

Resultset	Wins−Losses	Wins	Losses
(2)	5	5	0
(6)	0	0	0
(7)	-1	0	1
(5)	-1	0	1
(4)	-1	0	1
(3)	-1	0	1
(1)	-1	0	1

Table 3.40: Experiment 7: Classifier ranking based on precision for all patients in one dataset and union of selected features from each patient. The highest rank is highlighted in grey.

Resultset	Wins−Losses	Wins	Losses
(4)	6	6	0
(7)	2	3	1
(5)	2	3	1
(3)	2	3	1
(1)	-2	2	4
(2)	-4	1	5
(6)	-6	0	6

Table 3.41: Experiment 7: Classifier ranking based on F-measure for all patients in one dataset and union of selected features from each patient. The highest rank is highlighted in grey.

Resultset	Wins−Losses	Wins	Losses
(4)	5	5	0
(7)	2	2	0
(3)	0	1	1
(5)	-1	0	1
(1)	-1	0	1
(2)	-2	0	2
(6)	-3	0	3

3.1.9 Remarks for experiments 2–7

Classifier (1) achieves the best overall accuracy (85.87 %), precision (0.85) and F-measure (0.82) in experiment 3. in the same experiment, classifier (2) achieves the best overall

recall. Classifier (3) wins in the most ranking tests, especially in experiments 2 and 4. Classifier (4) stands out in experiment 7 with the highest rank in accuracy, precision and F-measure. It is also always clos behind classifier (3) in the remaining experiments. Concluding, classifiers (1), (3) and (4) should be closer examined in the the next experiments.

All previous experiments have been performed on the basis of a 10-fold cross validation. This method limits problems like overfitting and is useful for simulating the classifier performance on an unknown dataset. Each fold is produced by randomly sampling instances from the whole dataset. Since one seizure usually consists of multiple instances, it could happen that the same seizure is represented through neighbouring instances of itself in both the training and the test set. An approach which is closer to reality is to use one patient's complete data set for testing, while training on the datasets of the remaining patients. This "per patient leave-one-out cross validation" is performed in the next experiments in order to test the classifiers generalization ability.

Feature selection does not seem to have a major impact on the performance. Therefore, a smaller feature set can be taken for further experiments. The next three experiments study the impact of the three different feature sets.

3.1.10 Experiment 8 - Classifier selection, per patient leave-one-out cross validation with all features

The aim of this experiment is to test the performance of the three selected classifiers from the previous experiments through a per patient leave-one-out cross validation. This experiment uses all features. The results are shown in Tables 3.42–3.44. Cells highlighted in grey serve the comparison of the results of experiments 8 to 10.

Table 3.42: Experiment 8: Per patient leave-one-out cross validation using the Bayesian Network classifier (1) with all features.

Test set	Accuracy [%]	Recall	Precision	F-measure
P01	69.92	0.97	0.56	0.71
P02	45.28	0.79	0.36	0.49
P03	32.20	0.18	0.15	0.17
P04	58.21	0.64	0.43	0.51
P06	70.31	0.62	0.78	0.69
P07	53.03	0.35	0.65	0.46
P08	68.65	0.51	0.87	0.64
Average	56.80	0.58	0.54	0.52
Standard deviation	14.43	0.26	0.25	0.19

Table 3.43: Experiment 8: Per patient leave-one-out cross validation using the SMO classifier (3) with all features.

Test set	Accuracy [%]	Recall	Precision	F-measure
P01	66.53	0.76	0.55	0.64
P02	42.14	0.68	0.32	0.44
P03	33.90	0.14	0.13	0.13
P04	55.14	0.49	0.38	0.43
P06	55.47	0.38	0.63	0.48
P07	53.03	0.32	0.67	0.44
P08	55.02	0.59	0.59	0.59
Average	51.60	0.48	0.47	0.45
Standard deviation	10.54	0.22	0.20	0.16

Table 3.44: Experiment 8: Per patient leave-one-out cross validation using the Nearest Neighbours classifier (4) with all features.

Test set	Accuracy [%]	Recall	Precision	F-measure
P01	61.02	0.70	0.50	0.58
P02	38.36	0.57	0.29	0.38
P03	40.68	0.23	0.22	0.22
P04	55.80	0.25	0.32	0.28
P06	49.22	0.27	0.55	0.36
P07	37.88	0.22	0.40	0.28
P08	54.08	0.34	0.67	0.45
Average	48.15	0.37	0.42	0.36
Standard deviation	09.29	0.19	0.16	0.12

3.1.11 Experiment 9 - Classifier selection, per patient leave-one-out cross validation with 81 selected features from all patients.

The aim of this experiment is to test the performance of the four selected classifiers from the previous experiments through a per patient leave-one-out cross validation. This experiment uses the 81 features, selected from all patients at once. The results are shown in Tables 3.45–3.47. Cells highlighted in grey serve the comparison of the results of experiments 8 to 10.

Table 3.45: Experiment 9: Per patient leave-one-out cross validation using the Bayesian Network classifier (1) with selected features from all patients.

Test set	Accuracy [%]	Recall	Precision	F-measure
P01	69.92	0.97	0.56	0.71
P02	45.28	0.77	0.35	0.49
P03	42.37	0.14	0.17	0.15
P04	65.21	0.49	0.49	0.49
P06	71.88	0.66	0.78	0.71
P07	63.64	0.38	0.93	0.54
P08	72.26	0.58	0.88	0.70
Average	61.51	0.57	0.59	0.54
Standard deviation	12.53	0.27	0.28	0.20

Table 3.46: Experiment 9: Per patient leave-one-out cross validation using the SMO classifier (3) with selected features from all patients.

Test set	Accuracy [%]	Recall	Precision	F-measure
P01	72.88	0.87	0.60	0.71
P02	41.51	0.79	0.34	0.48
P03	55.93	0.32	0.39	0.35
P04	58.21	0.42	0.39	0.41
P06	57.03	0.29	0.74	0.42
P07	56.06	0.32	0.75	0.45
P08	54.70	0.34	0.68	0.46
Average	56.62	0.48	0.56	0.47
Standard deviation	09.13	0.24	0.18	0.12

Table 3.47: Experiment 9: Per patient leave-one-out cross validation using the Nearest Neighbours classifier (4) with selected features from all patients.

Test set	Accuracy [%]	Recall	Precision	F-measure
P01	60.59	0.82	0.49	0.62
P02	40.88	0.76	0.33	0.46
P03	52.54	0.41	0.38	0.39
P04	58.21	0.30	0.36	0.33
P06	55.47	0.37	0.64	0.47
P07	50.00	0.19	0.70	0.30
P08	64.26	0.52	0.76	0.62
Average	54.56	0.48	0.52	0.45
Standard deviation	07.71	0.24	0.18	0.13

3.1.12 Experiment 10 - Classifier selection, per patient leave-one-out cross validation with union of selected features from each patient.

The aim of this experiment is to test the performance of the four selected classifiers from the previous experiments through a per patient leave-one-out cross validation. This experiment uses the union of features, selected from each patient separately. The results are shown in Tables 3.48–3.50. Cells highlighted in grey serve the comparison of the results of experiments 8 to 10.

Table 3.48: Experiment 10: Per patient leave-one-out cross validation using the Bayesian Network classifier (1) with union of selected features from each patient.

Test set	Accuracy [%]	Recall	Precision	F-measure
P01	69.92	0.97	0.56	0.71
P02	44.65	0.79	0.35	0.49
P03	37.29	0.18	0.17	0.18
P04	60.18	0.59	0.44	0.50
P06	70.31	0.57	0.81	0.67
P07	53.03	0.32	0.67	0.44
P08	69.28	0.51	0.89	0.65
Average	57.81	0.56	0.56	0.52
Standard deviation	13.27	0.27	0.25	0.18

Table 3.49: Experiment 10: Per patient leave-one-out cross validation using the SMO classifier (3) with union of selected features from each patient.

Test set	Accuracy [%]	Recall	Precision	F-measure
P01	71.19	0.85	0.59	0.69
P02	41.51	0.76	0.33	0.46
P03	33.90	0.23	0.19	0.20
P04	54.92	0.43	0.36	0.39
P06	47.66	0.19	0.52	0.28
P07	48.48	0.24	0.60	0.35
P08	51.25	0.47	0.57	0.52
Average	49.84	0.45	0.45	0.41
Standard deviation	11.65	0.26	0.16	0.16

Table 3.50: Experiment 10: Per patient leave-one-out cross validation using the Nearest Neighbours classifier (4) with union of selected features from each patient.

Test set	Accuracy [%]	Recall	Precision	F-measure
P01	61.44	0.77	0.50	0.61
P02	45.91	0.66	0.34	0.45
P03	45.76	0.27	0.27	0.27
P04	52.52	0.22	0.26	0.24
P06	51.56	0.21	0.64	0.31
P07	48.48	0.24	0.60	0.35
P08	55.96	0.35	0.71	0.47
Average	51.66	0.39	0.47	0.38
Standard deviation	05.67	0.23	0.18	0.13

3.1.13 Remarks for experiments 8–10

The best overall performance, especially in terms of precision and F-measure, is achieved by the Bayesian Network classifier (1) in experiment 9, where the selected features from all patients are used. In general, the results of experiment 9 are better than those of experiment 8 (all features) and experiment 10 (union of features), which shows similar results to experiment 8. The most problematic case is patient P03, which is not performing well because of the limited number of instances. There are only 4 seizures with a small seizure duration (average: 3.97 s). For this patient only, the Nearest Neighbours classifier (4) performs better than the Bayesian Network. While generally performing worse than the other two, the Nearest Neighbours classifier shows lower standard deviation in the results with respect to each patient.

Concluding, since the most important goal is to achieve a high precision for the majority of the patients, the Bayesian Network classifier is selected for further experiments. Moreover the settings of experiment 9, utilizing the subset of 81 features will be used for the subsequent evaluation.

3.1.14 Analysis of the selected features

The 81 features, which were selected in experiment 6 and subsequently confirmed in experiment 9, are shown in Figure 3.1 grouped according to the ROI and signal, from which they were extracted. The distribution of the number of features between the ROIs does not show an extreme tendency towards a specific region. More or less all signals are used for feature extraction, with the exception of the mouth region, where the sum of magnitudes (SM), adaptive thresholded pixels (ATHP), mean magnitude weighted (MMW) and maximum magnitude weighted (MXMW) are not used. The signal, from which the most features (21 features) are extracted is the mean angle (MA) resulting from the optical flow, followed by the pixel area from background-foreground segmentation (14 features) and the angle at maximum magnitude (9 features), again resulting from the optical flow. The remaining signals are used for an average of 6 features each. Within the selected features, the most prominent are the variance of time intervals between adjacent

spikes (VTI), the median and the minimum. VTI is generally closely connected with signals related to the angle (MA, MMW and MXMW) for the left and right eye. The probability distribution table of the Bayes Network on the whole training set, e.g. for the VTI (MA, right eye) shows a higher probability (0.725) for it to be above 0.8 for the "NoSeizure" class, while the probability for VTI to be within $(0.26 - 0.8]$ is higher for the "AbsenceSeizure" class. The median has a slightly higher probability ($+0.1$) for the "AbsenceSeizure" class to be within a certain range. The same applies to the minimum of the MA with a higher probability of about 0.2 for the "AbsenceSeizure" class. Regarding the frequency domain features, the power in the band between 3 an 6 Hz is the most often used feature (6 times) followed by the dominant frequency (5 times features), mainly from signals related to the angle (AMXM, MA, MMW) and the pixel area from background-foreground segmentation (PBFS). The power between 3 and 6 Hz from the MA signal (left eye) shows a higher probability (0.759) to be below 6.24 during an absence seizure. The dominant frequency of the MMW in the area of both eyes shows a higher probability (0.772) to be below 2.4 for the seizure free period, while for the absence seizures the frequency is more wide spread.

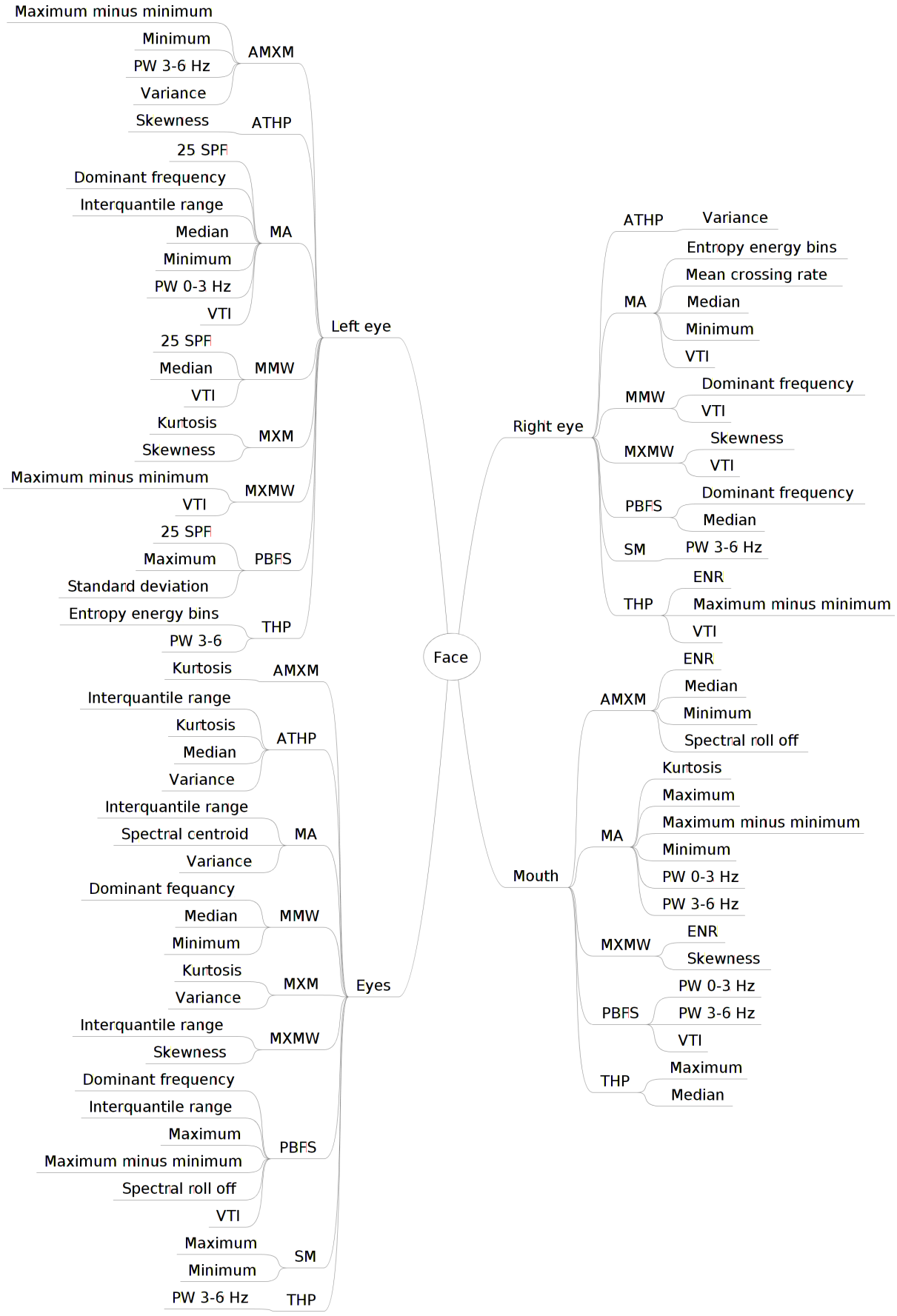

Figure 3.1: Overview of the feature dependencies for each ROI for the 81 selected features.

3.2 Phase 2 - Introduction of non ideal conditions: all annotated seizures

The previous phase provided valuable information regarding the most suitable classifier, feature selection, window size and step for seizure events captured under ideal conditions. The aim of the second phase is to examine the influence of adding all annotated seizures and their related seizure-free periods to the dataset. Since the classifier performance is calculated based on correctly, or not, classified instances, while a seizure may consist of multiple instances, in this phase a mapping of the instances to whole seizure events is also performed (experiment 14).

3.2.1 Experiment 11 - Classifier performance per patient for all annotated seizures with the 81 selected features from all patients

The aim of this experiment is to closely evaluate the performance of the Bayesian Network classifier, which was selected as the most suitable in the previous phase, with the addition of all annotated seizures that were not included in phase 1, introducing patient P05. For this purpose the same 81 selected features were chosen as in experiment 9, which showed the best performance under the given criteria. The results of this experiment are shown in Table 3.51 and were gained by a 10-fold cross validation, repeated 10 times for each patient. The additional performance measure true negative rate (TN-rate, specificity) was added to the result table, in order to give a better image of the performance. The accuracy is rather high as a result of the dataset's imbalanced towards the negative class ("NoSeizure") in conjunction to high TN-rate. This means that the classifier is very good in classifying ictal-free behavior. An overview of the dataset balance is shown in Table 3.52. The balance issue is examined in the next experiment.

Table 3.51: Experiment 11: Performance of the Bayesian Network classifier (1) for each patient for all annotated seizures with selected features from all patients.

Dataset	Accuracy	TN-rate	Recall	Precision	F-measure
P01	83.65	0.81	0.94	0.57	0.70
P02	82.71	0.90	0.47	0.53	0.49
P03	89.35	0.93	0.66	0.57	0.59
P04	86.43	0.90	0.50	0.34	0.40
P05	75.27	0.87	0.44	0.58	0.49
P06	66.31	0.75	0.54	0.62	0.56
P07	82.91	0.90	0.73	0.85	0.78
P08	77.63	0.76	0.79	0.81	0.80
Average	80.53	0.85	0.63	0.61	0.60

Table 3.52: Dataset balance in terms of numbers of instances for patients P01–P08..

Dataset	"AbsenceSeizure"	"NoSeizure"	"NoSeizure" to "Absence-Seizure" ratio	Represented seizures	Annotated seizures (semi-automatically)
P01	91	370	4.1	4	4
P02	90	416	4.6	7	7
P03	51	380	7.5	10	16
P04	236	2341	9.9	64	64
P05	197	511	2.6	23	23
P06	114	165	1.4	11	11
P07	86	116	1.3	8	8
P08	475	378	0.8	21	21
Total	1340	4677	-	148	194

3.2.2 Experiment 12 - Classifier performance for all annotated seizures, 81 selected features with various sub-sampling rations

The previous experiment showed that the classifier is very good in classifying instances that describe behaviour other than that of the seizures. This could be the result of the high imbalance between the number of instances between the two classes. The aim of this experiment is to find the minimum balance ratio at which the classifier performs best in term of precision, TN-rate and F-measure. The main thought behind this optimization is to reduce chances of over fitting and to reduce the size of dataset, since it is expected that in phase 4, where automatic ROI detection is introduced, the number of instances for the "NoSeizure" class will be very high.

The experiment is performed per patient at "NoSeizure" to "AbsenceSeizure" ratios of 1 to 10 (maximum imbalance, P04, Table 3.52) in increments of 1. To achieve this, random subsampling is performed on the "NoSeizure"class. The results are based on a 10 fold cross-validation, performed 10 times.

Figures 3.2–3.6 show the results of the experiment. The accuracy (Fig. 3.2), which is connected to the TN-rate at larger ratios (Fig. 3.3) rises to reach its limit at a ratio of 3. Similarly, the precision (Fig. 3.5) and F-measure (Fig. 3.6) reach their limit at the same ratio. It can be deduced that at this ratio, the number of instances of the "NoSeizure" class is enough for the classifier to distinguish it form the "AbsenceSeizure" class.

The recall has its maximum value at a ratio of 1 (perfect balance). At this ratio, the measures of TN-rate and precision show their minimum. This means that the classifier correctly classifies the positive class ("AbsenceSeizure") but misses the negative class ("NoSeizure"), in terms of more false positives. This is probably the case because the amount of instances for the negative class is not enough to truly represent it, since it is randomly taken from a set of many various conditions and behaviours.

Finally the recall, the precision and the F-measure reach their average limit at a ratio of

3. This ratio will be used for further experiments. It has to be noted that some patients (i.e. P02 and P03) would reach the maximum precision at higher ratios as can be seen in Fig. 3.5.

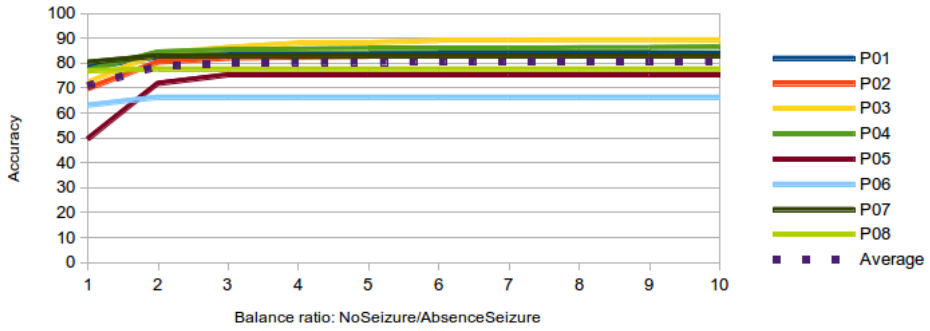

Figure 3.2: Accuracy of the Bayesian Network classifier over various balance ratios of the number of instances of the "NoSeizure" to the AbsenceSeizure class. Average values and values per patient are shown.

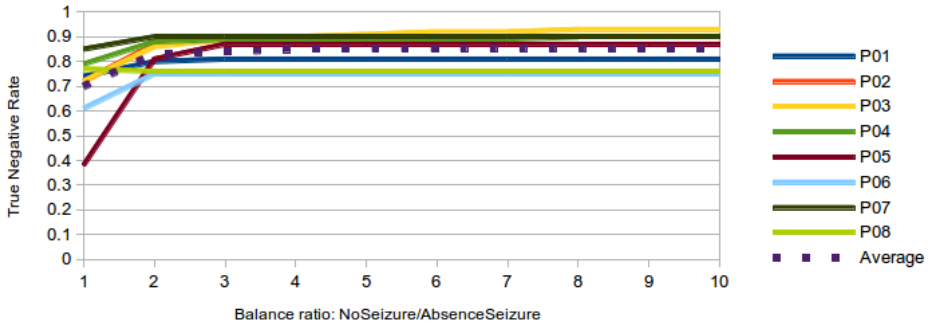

Figure 3.3: True negative rate of the Bayesian Network classifier over various balance ratios of the number of instances of the "NoSeizure" to the "AbsenceSeizure" class. Average values and values per patient are shown.

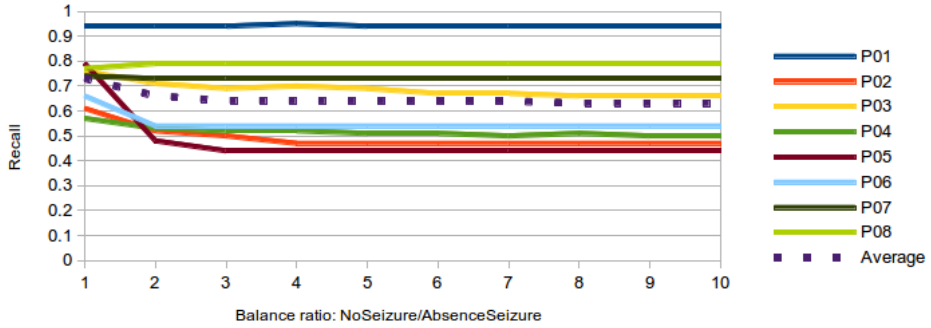

Figure 3.4: Recall of the Bayesian Network classifier over various balance ratios of the number of instances of the "NoSeizure" to the "AbsenceSeizure" class. Average values and values per patient are shown.

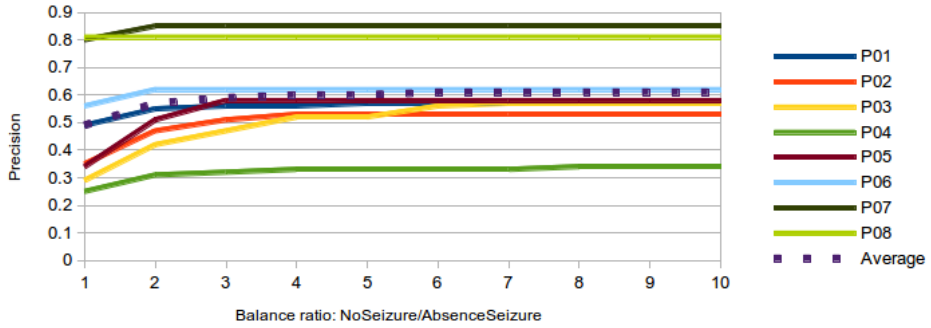

Figure 3.5: Precision of the Bayesian Network classifier over various balance ratios of the number of instances of the "NoSeizure" to the "AbsenceSeizure" class. Average values and values per patient are shown.

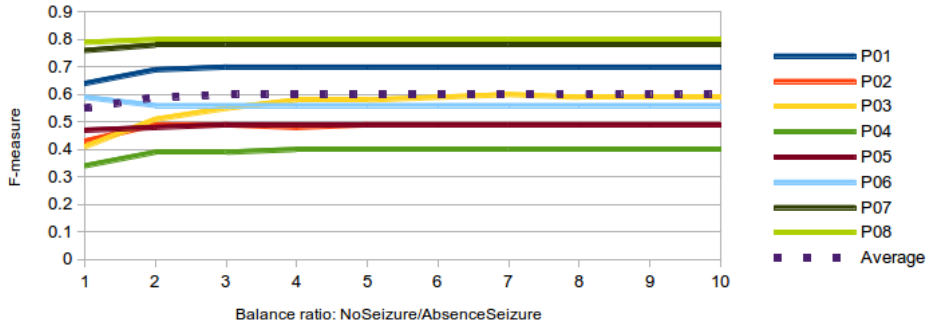

Figure 3.6: F-measure of the Bayesian Network classifier over various balance ratios of the number of instances of the "NoSeizure" to the "AbsenceSeizure" class. Average values and values per patient are shown.

3.2.3 Experiment 13 - Classifier performance, per patient leave-one-out cross validation

The aim of this experiment is to evaluate the performance of the Bayesian Network classifier through a per patient leave-one-out cross validation. As mentioned earlier this approach is closer to reality since it uses one patient's complete data set for testing, while training is done using the datasets of the remaining patients. This experiment uses the 81 selected features, which were chosen in experiment 9 and a "NoSeizure" to "AbsenceSeizure" ratio of 3, as elaborated in the previous experiment, for the training set. The results are shown in Table 3.53.

The overall precision is notably low. precision is the ratio of the number of true positives to the total number of positives (true and false). The number of false positives is influenced by the total number of actual negatives, which are many more than the actual positives due to the class imbalance in the test set[1]. This means that it is likely to have many more false positives than true positives. This results to low numbers for precision, although the higher values for recall and true negative rate are promising. Seizures could be filtered based on the fact that they are dense periods of small duration in contrast to the ictal-free period, which is spread over time.

Table 3.53: Experiment 13: Performance of the Bayesian Network classifier (1), per patient leave-one-out cross validation.

Dataset	Accuracy	TN-rate	Recall	Precision	F-measure
P01	49.67	0.38	0.98	0.28	0.43
P02	73.12	0.78	0.49	0.33	0.39
P03	70.30	0.76	0.28	0.13	0.18
P04	84.48	0.90	0.27	0.22	0.24
P05	58.62	0.63	0.48	0.33	0.39
P06	62.72	0.70	0.53	0.55	0.54
P07	40.59	0.43	0.37	0.33	0.35
P08	69.75	0.79	0.62	0.79	0.70
Average	63.66	0.67	0.50	0.37	0.40

3.2.4 Experiment 14 - Classifier performance, per patient leave-one-out cross validation and mapping to seizures as whole events

All performance metrics so far have been based on instances. Since one seizure is usually represented by more than one instance it is worthwhile to analyse the results of experiment 13 in terms of actual seizures. This requires a mapping of the instances to the actual seizures and their ID. For this purpose, continuous regions of the "AbsenceSeizure" class have been treated as individual seizure events. They are kept apart through continuous regions of the "NoSeizure" class. The evaluation is performed under the assumption that if

[1]Note that that no subsampling is performed on the test set

a continuous region classified as "AbsenceSeizure" overlaps with an actual absence seizure event, then a true positive is counted. It has to be noted that one continuous region of a classified seizure may overlap with multiple actual seizures. This case counts as one true positive. Further on, it is not practical to calculate a value for true negatives, since the "NoSeizure" period cannot be partitioned. The results are shown in Table 3.54. The precision is still quite low. By taking advantage of the fact that seizures are short dense events, filtering can be applied on the classifier results. It includes a running average with a window length of 8 instances, followed by thresholding with a threshold set at 0.3 times the maximum average value. The results after filtering are shown in Table 3.55. It is noticeable that the false positives are reduced effectively.

Table 3.54: Experiment 14: Per patient leave-one-out cross validation and projection to seizures as whole events

Patient	TP	FP	FN	Recall	Precision	F-measure
P01	4	29	0	1.00	0.12	0.22
P02	4	1	3	0.57	0.80	0.67
P03	3	17	5	0.38	0.15	0.21
P04	20	82	32	0.38	0.20	0.26
P05	17	19	7	0.71	0.47	0.57
P06	10	6	1	0.91	0.63	0.74
P07	6	11	1	0.86	0.35	0.50
P08	23	18	2	0.92	0.56	0.70
Average	-	-	-	0.72	0.41	0.48

Table 3.55: Experiment 14: Per patient leave-one-out cross validation and projection to seizures as whole events. Filtered classifier output.

Patient	TP	FP	FN	Recall	Precision	F-measure
P01	4	3	0	1.00	0.57	0.73
P02	4	1	3	0.57	0.80	0.67
P03	5	3	5	0.50	0.63	0.56
P04	22	14	41	0.35	0.61	0.44
P05	12	2	8	0.60	0.86	0.71
P06	9	0	1	0.90	1.00	0.95
P07	4	1	2	0.67	0.80	0.73
P08	15	1	4	0.79	0.94	0.86
Average	-	-	-	0.67	0.78	0.70

3.3 Phase 3 - Tests with single and multiple regions of interest

The semi-automatic ROI annotation of the videos for patients P01–P09 showed that very often, not all ROIs are concurrently visible. Having this in mind and trying to answer the question if one facial region plays a particular role in analysing absence seizures, it

is important to test the detection performance with individual and all combinations of ROIs.

3.3.1 Experiment 15 - Classifier performance with respect to various regions of interest

This experiment is based on experiment 13, performing a per patient leave-one-out cross validation. It uses one patient's complete data set for testing, while training is done using the datasets of the remaining patients. This experiment uses the 81 selected features, which were chosen in experiment 9 and a "NoSeizure" to "AbsenceSeizure" ratio of 3 as elaborated in experiment 12. The cross validation is performed for the following cases: Eye-pair; left eye; right eye; mouth; left eye and right eye; left eye, right eye and mouth; eye-pair and mouth; all ROIs.

The performance measures, averaged over the patients, are shown in Figure 3.7. The accuracy and TN-rate show little variation due to the high number of negative instances, as already commented in experiment 11. In the first four cases, where one ROI alone is used, the recall is lower than in the cases that include combinations of multiple ROIs, while the case with all ROIs is slightly surpassed by the two cases with either the eyes or the eyes and the mouth missing. It is observable that the case with all ROIs shows the worst overall precision. Figures 3.8 and 3.9 show the recall and precision for each patient for each case. Both measures show different variabilities for each patient. Some patients, such as P05 and P06 show a high varying recall. The low value for the mouth ROI in P05 may be explained by the exceptionally low number of instances (the mouth was obviously not visible), which lies at 72% below the average for the other ROIs of the same patient. Although the precision does not seem to suffer much.

One might conclude that using more ROIs is advantageous for detecting more positive instances. The reason for this most probably resides in the fact that occlusions of one ROI are handled by the existence of the other ROI. The cases where the left eye, the right eye, and/or the mouth are included seem to be the best choices. When the mouth is included, a marginally higher average recall (+0.01) and precision (+0.01).

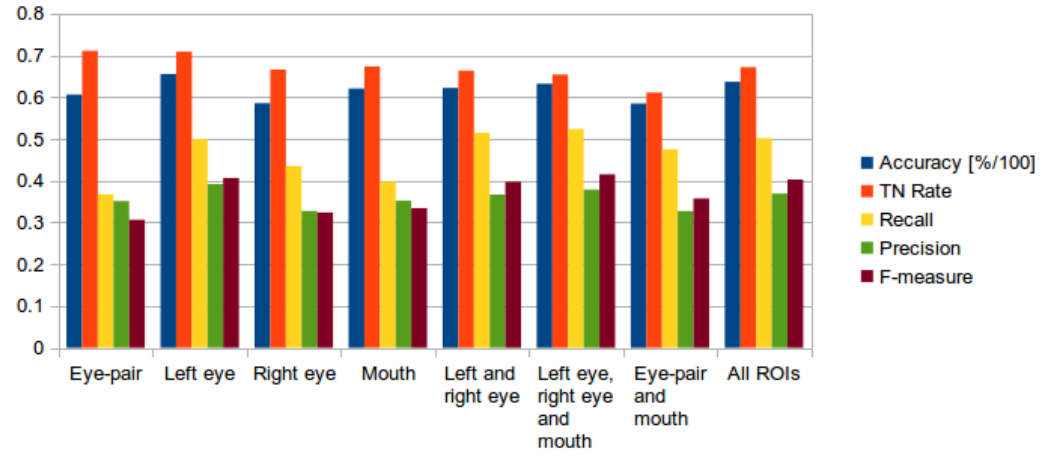

Figure 3.7: Average performance measures for various ROIs.

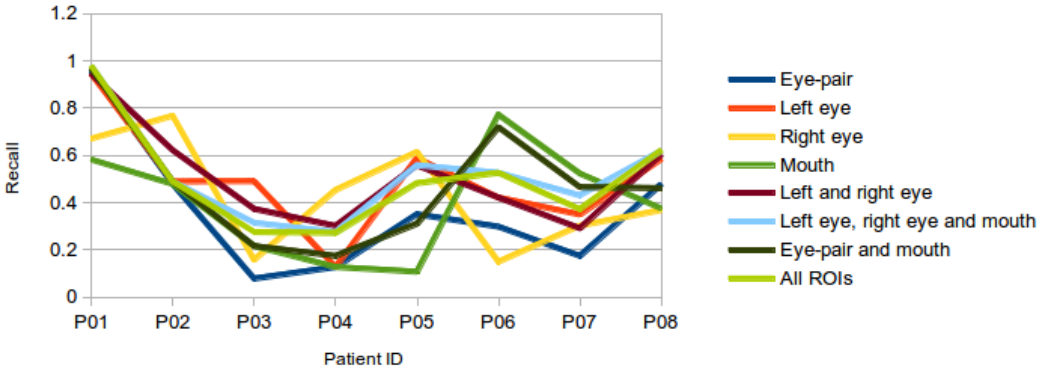

Figure 3.8: Recall for each patient for various ROIs.

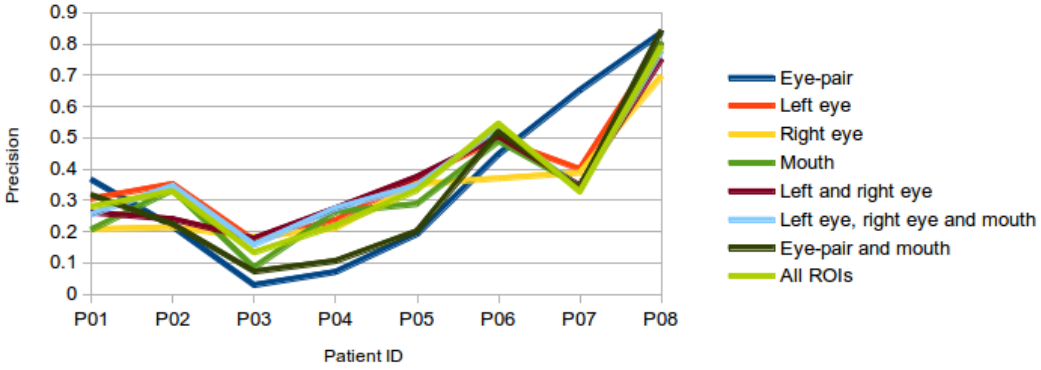

Figure 3.9: Precision for each patient for various ROIs.

3.3.2 Experiment 16 - Classifier performance, per patient leave-one-out cross validation and projection to seizures as whole events (repetition of experiment 14 with left eye and right eye only)

Given the results of the previous experiment, it is worthwhile to repeat experiment 14 with the left and the right eye. The experiment performs a mapping of the instances to the actual seizures and their ID. For this purpose, continuous regions of the "AbsenceSeizure" class have been treated as individual seizure events. Table 3.56 shows the results prior to filtering and Table 3.57 shows the results after filtering. In both cases the performance is slightly worse than experiment 14.

Table 3.56: Experiment 16: Per patient leave-one-out cross validation and projection to seizures as whole events

Patient	TP	FP	FN	Recall	Precision	F-measure
P01	7	31	0	1.00	0.18	0.31
P02	6	26	0	1.00	0.19	0.32
P03	4	28	4	0.50	0.13	0.20
P04	23	81	27	0.46	0.22	0.30
P05	16	6	7	0.70	0.73	0.71
P06	11	4	2	0.85	0.73	0.79
P07	3	13	3	0.50	0.19	0.27
P08	32	30	3	0.91	0.52	0.66
Average	-	-	-	0.74	0.36	0.44

Table 3.57: Experiment 16: Per patient leave-one-out cross validation and projection to seizures as whole events. Filtered classifier output.

Patient	TP	FP	FN	Recall	Precision	F-measure
P01	4	3	0	1.00	0.57	0.73
P02	5	6	2	0.71	0.45	0.56
P03	5	6	5	0.50	0.45	0.48
P04	24	8	40	0.38	0.75	0.50
P05	11	0	8	0.58	1.00	0.73
P06	8	0	2	0.80	1.00	0.89
P07	4	3	4	0.50	0.57	0.53
P08	15	2	8	0.65	0.88	0.75
Average	-	-	-	0.64	0.71	0.65

3.3.3 Experiment 17 - Classifier performance, per patient leave-one-out cross validation and projection to seizures as whole events (repetition of experiment 14 with left eye, right eye and mouth)

Given the results of the previous experiment, it is worthwhile to repeat experiment 14 with the left and the right eye. The experiment performs a mapping of the instances to the actual seizures and their ID. For this purpose, continuous regions of the "AbsenceSeizure" class have been treated as individual seizure events. Table 3.58 shows the results prior to filtering and Table 3.59 shows the results after filtering. In the first case, the performance is comparable to that of all ROIs, while in the second case with the filtered classifier output the performance is better than that of all ROIs.

Table 3.58: Experiment 17: Per patient leave-one-out cross validation and projection to seizures as whole events

Patient	TP	FP	FN	Recall	Precision	F-measure
P01	4	32	0	1.00	0.11	0.20
P02	4	3	3	0.57	0.57	0.57
P03	5	20	4	0.56	0.20	0.29
P04	21	72	31	0.40	0.23	0.29
P05	18	10	7	0.72	0.64	0.68
P06	9	7	1	0.90	0.56	0.69
P07	6	11	0	1.00	0.35	0.52
P08	27	25	2	0.93	0.52	0.67
Average	-	-	-	0.76	0.40	0.49

Table 3.59: Experiment 17: Per patient leave-one-out cross validation and projection to seizures as whole events. Filtered classifier output.

Patient	TP	FP	FN	Recall	Precision	F-measure
P01	4	1	0	1.00	0.80	0.89
P02	4	1	3	0.57	0.80	0.67
P03	5	1	5	0.50	0.83	0.63
P04	22	6	42	0.34	0.79	0.48
P05	13	0	7	0.65	1.00	0.79
P06	8	0	2	0.80	1.00	0.89
P07	4	1	2	0.67	0.80	0.73
P08	17	2	3	0.85	0.89	0.87
Average	-	-	-	0.67	0.86	0.74

3.3.4 Remarks for experiments 14, 16 and 17

In experiments 14, 16 and 17 the mapping of instances to whole seizure events has been performed for a) all ROIs, b) the left eye and right eye, and c) the left eye, right eye and mouth. Figures 3.10 and 3.11 show the non-filtered and filtered average results

respectively. The filtered results with both eyes and the mouth show the best overall precision (0.86) and F-measure (0.74). The recall is the highest in the non-filtered case for the same three ROIs (0.76). Its drop to 0.67 for the filtered case can be accepted, given the high increase of the precision (+ 117%) and F-measure (+ 52%).

Concluding, the eye-pair, which is missing in case c) with the best results, obviously introduces noise that diminishes the classifier's performance. When using only the left and right eye, the performance is slightly worse than in the other two cases. This suggests, that motion in the eyes reveals most of the necessary information to correctly detect the seizures. Of course on the other hand one can argue that an eye as such is the most often visible element and was most often annotated. The addition of information of the mouth enhanced the classifier performance. This can be related to additional information coming from mouth automatisms that usually occur during a seizure.

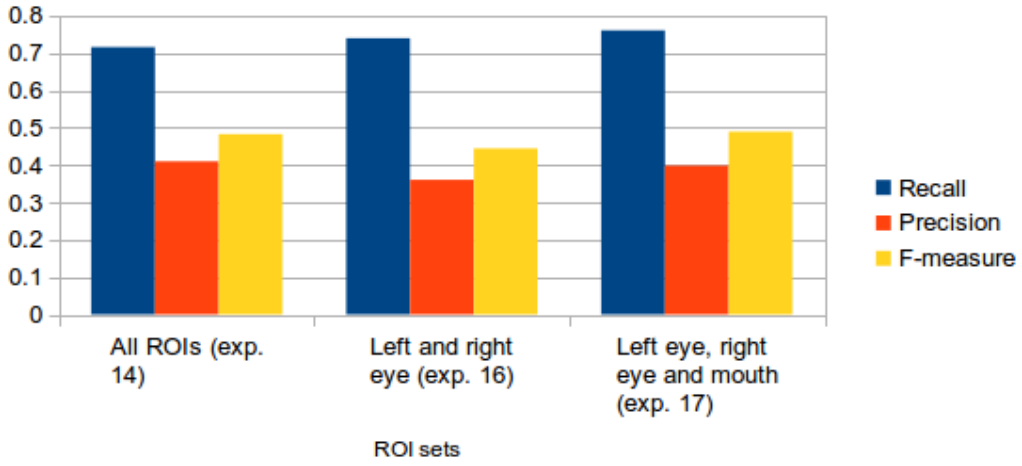

Figure 3.10: Average performance measures for three different ROI sets.

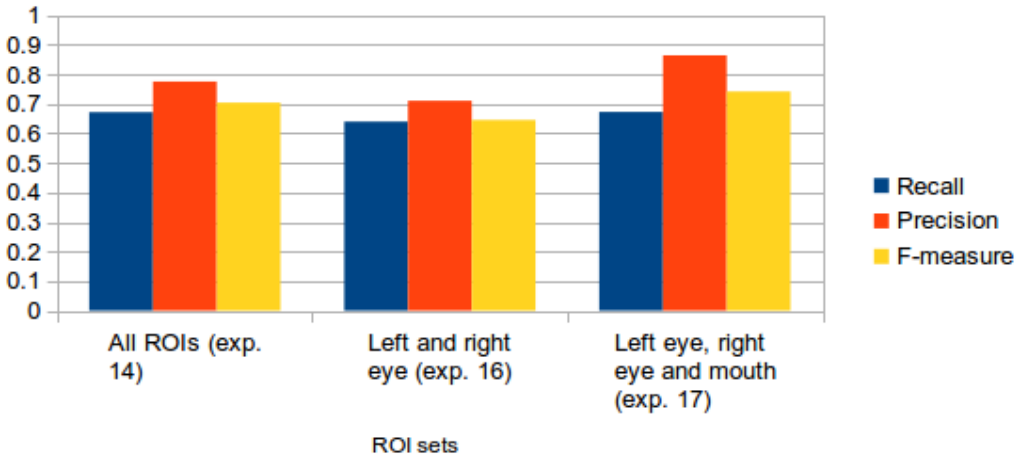

Figure 3.11: Average performance measures for three different ROI sets. Filtered classifier output.

3.4 Phase 4 - Introduction of automatic ROI detection

The aim of this phase is to investigate the feasibility of a fully automatic seizure detection scenario. As elaborated in the previous phase, the ROIs of the left eye, the right eye and mouth are used, following the detection scheme described in Section 2.3.2. In addition to that, the features, which were selected from patients P01–P08 as a whole dataset are used. Concerning the three aforementioned ROIs, this results in 57 features out of the initial 81. The training set is sub sampled to a "AbsenceSeizure" to "NoSeizure" ratio of 3 as elaborated in experiment 12. These parameters are applied at first on P01–P08. They are tested with the classifier trained on the features, extracted from the automatically detected ROIs (exp. 18), as well as on the semi-automatically extracted features already used in the previous three phases (exp. 19). Finally, the same tests are applied on a new test set, consisting of four new patients (P09–P12). It can be expected that automatic ROI detection may not detect any ROI during some seizures. Table 3.60 shows the detailed class distributions for all patients after the automatic ROI detection. The heavy dataset imbalance, as well as the fact that more than half of the annotated seizures are not represented in the dataset is cognizable.

Table 3.60: Dataset balance in terms of numbers of instances for patients P01–P12. Automatic ROI detection.

Dataset	"AbsenceSeizure" instances	"NoSeizure" instances	"NoSeizure" to "Absence-Seizure" ratio	Represented seizures	Annotated seizures by neurologist
P01	86	846	9.8	4	4
P02	68	6462	95.0	7	7
P03	27	5672	210.1	5	16
P04	52	6238	120.0	18	64
P05	40	3109	77.7	7	23
P06	40	6072	151.8	5	11
P07	40	9518	238.0	6	8
P08	343	25838	75.3	19	21
P09	30	5340	178.0	6	25
P10	10	1323	132.3	4	68
P11	164	16703	101.8	22	38
P12	79	17440	220.8	18	25
Total	979	104561	106.8	121	310

3.4.1 Experiment 18 - Classifier performance, patients P01–P08, automatic ROI detection for training and testing

This experiment uses for training and testing the 57 selected features (cf. experiment 9), which are extracted from the automatically detected ROIs of the left eye, the right eye and the mouth. It performs a per patient leave-one-out cross validation for P01–P08 and the results are mapped to actual seizure events as in experiment 14. The non-filtered results are shown in Table 3.61, while the filtered results are shown in Table 3.62. It is immediately visible that the number of false positives is very high, compared to the true positives. Although the false positives are reduced effectively with filtering (Table 3.62), the overall difference is still high.

Table 3.61: Experiment 18: Performance of the Bayesian Network classifier. Per patient leave-one-out cross validation and projection to seizures as whole events

Patient	TP	FP	FN	Recall	Precision	F-measure
P01	5	70	0	1.00	0.07	0.13
P02	9	581	2	0.82	0.02	0.03
P03	0	530	5	0.00	0.00	-
P04	3	396	11	0.21	0.01	0.01
P05	6	245	1	0.86	0.02	0.05
P06	3	188	2	0.60	0.02	0.03
P07	3	568	3	0.50	0.01	0.01
P08	10	1064	10	0.50	0.01	0.02
Average	-	-	-	0.56	0.02	0.04

Table 3.62: Experiment 18: Performance of the Bayesian Network classifier. Per patient leave-one-out cross validation and projection to seizures as whole events. Filtered classifier output.

Patient	TP	FP	FN	Recall	Precision	F-measure
P01	4	19	0	1.00	0.17	0.30
P02	5	175	2	0.71	0.03	0.05
P03	2	128	3	0.40	0.02	0.03
P04	6	117	12	0.33	0.05	0.09
P05	4	42	0	1.00	0.09	0.16
P06	1	49	4	0.20	0.02	0.04
P07	5	153	1	0.83	0.03	0.06
P08	11	228	12	0.48	0.05	0.08
Average	-	-	-	0.62	0.06	0.10

3.4.2 Experiment 19 - Classifier performance, patients P01–P08, semi-automatic ROI detection for training, automatic ROI detection for testing

The relatively poor results of the previous experiment may be due to the fact that the training data can be corrupted with noise, since the ROI detection is unsupervised. This experiment is performed under the same conditions as the previous experiment, except that the classifier is trained with the features, extracted from the semi-automatically annotated ROIs, as in phases 1–3. The testing is carried out with the features from the automatic ROI detection. The classifier results are mapped to seizure events. The non-filtered results are shown in Table 3.63, while the filtered results are shown in Table 3.64. This approach does not seem to have a positive impact on the false positive rate, except for patient P01, which can be considered a special case, since the recording duration is short and the class imbalance for this patient is very low (cf. Table 3.60).

Table 3.63: Experiment 19: Performance of the Bayesian Network classifier. Per patient leave-one-out cross validation and projection to seizures as whole events

Patient	TP	FP	FN	Recall	Precision	F-measure
P01	4	44	0	1.00	0.08	0.15
P02	7	429	1	0.88	0.02	0.03
P03	1	445	2	0.33	0.00	0.00
P04	0	352	14	0.00	0.00	-
P05	6	206	2	0.75	0.03	0.05
P06	1	243	3	0.25	0.00	0.01
P07	5	622	2	0.71	0.01	0.02
P08	24	1796	6	0.80	0.01	0.03
Average	-	-	-	0.59	0.02	0.04

Table 3.64: Experiment 19: Performance of the Bayesian Network classifier. Per patient leave-one-out cross validation and projection to seizures as whole events. Filtered classifier output.

Patient	TP	FP	FN	Recall	Precision	F-measure
P01	4	6	0	1.00	0.40	0.57
P02	5	115	1	0.83	0.04	0.08
P03	1	145	3	0.25	0.01	0.01
P04	1	98	16	0.06	0.01	0.02
P05	4	54	0	1.00	0.07	0.13
P06	1	64	4	0.20	0.02	0.03
P07	4	146	1	0.80	0.03	0.05
P08	12	522	7	0.63	0.02	0.04
Average	-	-	-	0.60	0.07	0.12

3.4.3 Experiment 20 - Classifier performance for patients P09–P12, with training set from P01–P08 (automatic ROI detection)

This experiments uses the training set from patients P01–P08 as gained from the automatic ROI detection (left eye, right eye and mouth). Patients P09–P12 are used for testing (automatic ROI detection). The results are shown in Table 3.65. The accuracy and the TN-rate are within relatively acceptable limits and the low recall could be tolerated if the precision would be high, which is actually dramatically low. The main reason for this is the imbalance in the test sets. Since the total duration of the recording for each of the new patients spans several hours, the amount of "NoSeizure" instances is considerably higher. This means that even with a high TN-rate, the false positives are immensely more than the true positives. They are even more than the "AbsenceSeizure" instances in total. Since the false positives appear in the denominator of the fraction for the precision calculation, the latter takes very small values. As shown in Table 3.60 (detailed class distributions), it is furthermore noticeable that the automatic ROI detection does not provide the needed ROIs for the majority of seizures for patients P09 and P10, therefore only a fraction of the actual seizures is represented in the dataset, especially for the last four patients.

Considering the mapping of the instances to the actual seizures and their ID, where continuous regions of the "AbsenceSeizure" class have been treated as individual seizure events, Table 3.66 shows the results prior to filtering and Table 3.67 shows the results after filtering. Although filtering reduces the false positives, the overall results in terms of precision are rather poor.

Table 3.65: Experiment 20: Performance of the Bayesian Network classifier for patients P09–P12, using P01–P08 for training (57 selected features, automatic ROI detection).

Dataset	Accuracy	TN-rate	Recall	Precision	F-measure
P09	55.62	0.56	0.23	0.00	0.01
P10	61.82	0.62	0.30	0.01	0.01
P11	61.58	0.62	0.30	0.01	0.02
P12	48.94	0.49	0.68	0.01	0.01
Average	56.99	0.57	0.38	0.01	0.01

Table 3.66: Experiment 20: Performance of the Bayesian Network classifier for each patient (P09–P12), using P01-P08 for training (57 selected features). Projection to seizures as whole events

Patient	TP	FP	FN	Recall	Precision	F-measure
P09	3	553	3	0.50	0.01	0.01
P10	1	155	3	0.25	0.01	0.01
P11	11	1234	9	0.55	0.01	0.02
P12	15	1349	3	0.83	0.01	0.02
Average	-	-	-	0.53	0.01	0.02

Table 3.67: Experiment 20: Performance of the Bayesian Network classifier for each patient (P09–P12), using P01-P08 for training (57 selected features, automatic ROI detection). Projection to seizures as whole events. Filtered classifier output

Patient	TP	FP	FN	Recall	Precision	F-measure
P09	2	120	4	0.33	0.02	0.03
P10	3	37	1	0.75	0.08	0.14
P11	12	374	10	0.55	0.03	0.06
P12	12	369	3	0.80	0.03	0.06
Average	-	-	-	0.61	0.04	0.07

3.4.4 Experiment 21 - Classifier performance for patients P09–P12, with training set from P01–P08 (semi-automatic ROI detection)

This experiment is performed under the same conditions as the previous experiment, except that the classifier is trained with the features, extracted from the semi-automatically annotated ROIs, in a simmilar manner to experiment 19. The testing is carried out with the features from the automatic ROI detection for the four new patients. The classifier results are shown in Table 3.68, while the results in terms of mapping to seizure events are shown in Table 3.69 prior to filtering and in Table 3.70 after filtering.

Although the TN-rate is higher in this experiment (0.71) than in the previous (0.57), the results of mapping to actual seizure events are not generally better, although differences

within some patients exist. Considering the filtered results, these include P10 who shows a slightly higher precision from 0.08 to 0.12, and P12 who shows a lower precision from 0.03 to 0.01. It is noticeable that the number of false negatives for P12 is also higher, reducing the recall from 0.80 to 0.17.

Table 3.68: Experiment 21: Performance of the Bayesian Network classifier for patients P09–P12, using P01–P08 for training (57 selected features, semi-automatic ROI detection).

Dataset	Accuracy	TN-rate	Recall	Precision	F-measure
P09	47.67	0.48	0.30	0.00	0.01
P10	79.28	0.80	0.20	0.01	0.01
P11	70.05	0.70	0.42	0.01	0.03
P12	87.36	0.88	0.13	0.01	0.01
Average	71.09	0.71	0.26	0.01	0.01

Table 3.69: Experiment 21: Performance of the Bayesian Network classifier for each patient (P09–P12), using P01-P08 for training (57 selected features, semi-automatic ROI detection). Projection to seizures as whole events

Patient	TP	FP	FN	Recall	Precision	F-measure
P09	4	569	3	0.57	0.01	0.01
P10	0	119	2	0.00	0.00	-
P11	14	1123	7	0.67	0.01	0.02
P12	3	827	13	0.19	0.00	0.01
Average	-	-	-	0.36	0.01	0.02

Table 3.70: Experiment 21: Performance of the Bayesian Network classifier for each patient (P09–P12), using P01-P08 for training (57 selected features, semi-automatic ROI detection). Projection to seizures as whole events. Filtered classifier output.

Patient	TP	FP	FN	Recall	Precision	F-measure
P09	2	116	4	0.33	0.02	0.03
P10	3	23	1	0.75	0.12	0.20
P11	11	325	10	0.52	0.03	0.06
P12	3	246	15	0.17	0.01	0.02
Average	-	-	-	0.44	0.04	0.08

3.4.5 Experiment 22 - Classifier performance, per patient leave-one-out cross validation for P09–P12

In this final experiment, the data from patients P09–P12 (automatic ROI detection) are used for training in terms of a per patient leave-one-out cross validation as already performed in experiment 13. The results in Table 3.71 show a satisfactory values for the accuracy (90%) and the TN-rate (0.91). Unfortunately these are bundled with a low

recall (0.17), the lowest overall value. Especially for patient P11, a recall of 0.00 and TN-rate of 1.00 shows that all instances were classified as "NoSeizure", an indication that this scenario suffers in modelling the "AbsenceSeizure" class. The mapping of instances to actual seizures and their ID is also performed in. Table 3.72 shows the results prior to filtering and Table 3.73 shows the results after filtering. The results are slightly inferior to those of experiment 18, where the same scenario is tested with patients P01–P08.

Table 3.71: Experiment 22: Performance of the Bayesian Network classifier (1), per patient leave-one-out cross validation for P09–P12 (57 selected features).

Dataset	Accuracy	TN-rate	Recall	Precision	F-measure
P09	84.02	0.84	0.23	0.01	0.02
P10	89.94	0.90	0.30	0.02	0.04
P11	99.02	1.00	0.00	0.00	0.00
P12	87.19	0.88	0.15	0.01	0.01
Average	90.04	0.91	0.17	0.01	0.02

Table 3.72: Experiment 22: Per patient leave-one-out cross validation for P09–P12 (57 selected features) and projection to seizures as whole events

Patient	TP	FP	FN	Recall	Precision	F-measure
P09	3	459	3	0.50	0.01	0.01
P10	1	80	2	0.33	0.01	0.02
P11	0	0	22	0.00	-	-
P12	3	1237	10	0.23	0.00	0.00
Average	-	-	-	0.27	0.01	0.01

Table 3.73: Experiment 22: Per patient leave-one-out cross validation for P09–P12 (57 selected features) and projection to seizures as whole events. Filtered classifier output.

Patient	TP	FP	FN	Recall	Precision	F-measure
P09	2	131	4	0.33	0.02	0.03
P10	1	21	3	0.25	0.05	0.08
P11	0	0	22	0.00	-	-
P12	5	347	13	0.28	0.01	0.03
Average	-	-	-	0.29	0.02	0.04

CHAPTER 4

Comparison and contribution to the state of the art

4.1 Comparison to the state of the art

The comparison to the state of the art can be performed on three levels: The dataset, the methods, and the results. An overview of the comparison to the latest related studies is given in Table 4.1.

With respect to the dataset, the main difference lies within the fact the all reports focus essentially on clonic and myoclonic convolutions, mainly of neonatal seizures, while this study has analysed absence seizures. Clonic and myoclonic convolutions are characterized by sudden fast motion of the affected body parts (usually the extremities), which means that a ROI detection can be simply achieved by filtering fast motion in the image. Additionally, motion of the extremities is more severe than the subtle motion in the face during absence seizures, thus distinguishable even if a patient is lying on the side or if he/she is covered by a sheet. Moreover, in the case of neonatal seizures, the patient rarely moves out of the field of view of the camera. The number of patients and seizures studied in the related reports varies from 9 to 50 patients and 11 to 80 seizures. This study has analysed 12 patients and 350 seizures in total.

Considering the methods, similarities of this work to the state of the art can be seen. The usage of frame differencing and optical flow is common in many relates articles. This study introduces the application of a more advanced method for frame differencing, which is based on mixture of Gaussians. Respectively, dense optical flow is used herein in contrast to the more common sparse approach. Finally the major methodological difference to other related studies lies within the large amount of analysed features and the fact that multiple regions of interest were analysed simultaneously. This qualities, in conjunction with the investigation of multiple signals relate this thesis closely data mining and knowledge discovery approaches.

With respect to obtained results, the published reports can be compared to phase 3 (experiment 17) of this thesis, since ROI detection does not pose a significant burden in the published literature and phase 3 uses manually annotated data. As can be seen in Table 4.1, in this case, the precision (0.86) and sensitivity (0.67) is acceptably close to the reported values in the literature. With regard to automatic ROI detection (phase 4), the same metrics are considerably lower, but cannot actually be compared to other publications since they report the solely usage of segments of videos with a limited duration, a fact that greatly reduces the class imbalance an the chances of false positives, as well as noise from false ROI detections. In contrast to that, phase 4 has analysed several hours of video for each patient.

4.2 Contribution to the state of the art

As described in the introductory chapter (Sections 1.6 and 1.7), examples of quantification of motion during epileptic seizures already exist and seizure recognition approaches have been successful for specific seizure types [29, 58, 69, 73, 114]. Nevertheless, a global methodology for vision-based clinical image analysis in epilepsy has not been reported yet. Motion of the body, extremities and the head has been analysed but very little attention has been given to more detailed motion characteristics such as eye or finger motion. In connection to a thorough examination of the clinical manifestations of all known epileptic syndromes, which was performed by the author and published in [108], the strong belief emerges that face-related motion analysis, as well as precise human posture recognition, are essential parts of an integrated vision-based clinical image analysis system in epilepsy. Moreover, these two elements have not yet received significant attention. This work contributes primarily to motion analysis in the area of the face of epileptic patients. As discussed in Section 1.7, the face and its expressions have been analysed in the context of epilepsy only for a correlation study to the EEG. This work approached this problem in order to extract motion patterns that are characteristic of epileptic motion and has shown that it is possible to detect and characterise such patterns through a selection of specific features.

A further contribution point relates to the selected type of epileptic seizure that has been studied. While all other reports in this field analyse clonic and myoclonic seizures, which can be detected through their intense motion nature, this work has analysed absence seizures, which are characterised by subtle motion patterns and facial expressions. This by itself poses a challenge that has been only indirectly studied by the research community dealing with facial emotion recognition, but not explicitly in relation to epilepsy.

Finally, one of the challenges that is strongly related to health monitoring and surveillance is the problem of analysing data with a duration of several hours, which are bundled with non-controlled acquisition conditions. This work has performed this study, although with relatively poor results. It is nevertheless the first to report on an attempt to face this problem and propose possible solutions (cf. Chapter 5).

Table 4.1: Overview and comparison of related publication to this study (values with an asterisk are derived from other supplied values).

Author	Year	Total patients	Age	Seizure type	ROI	Testing conditions	Classifier	False positive rate	Precision (PPV)	Sensitivity	True positive rate (Specificity)	Video	Comments
Karayiannis et al. [69]	2005	43	Neonatal	80 myoclonic seizures, 80 focal clonic seizures, 80 random infant movement	Extremities	50% percentage split	FFNN	0.03*	n.a.	89.5	0.97	Video segments	Automatically selected body parts for tracking, otherwise unknown body part, results averaged for two seizure classes, result-pair with best Specificity, subject is well positioned into the camera field of vision
Karayiannis et al. [73]	2006	54	Neonatal	80 myoclonic seizures, 80 focal clonic seizures, 80 random infant movement	Extremities	50% percentage split	FFNN	0.08*	n.a.	86.5	0.92	Video segments	ROI probably manually selected, result-pair with best Specificity, subject is well positioned into the camera field of vision and other forms of interference with the video signal are minimal

Cuppens et al. [29]	2010	9	Up to 18 a	11 convolutions, 62 movements	Extremities	3-fold cross validation with groups of patients	Variable threshold based on standard deviation, using a movement vs. non-movement ratio	n.a.	0.95	1	n.a.	Video segments	Main aim is to distinguish convulsive movement from non-movement, infrared camera and nocturnal recording only, clustering of events
Kalitzin et al. [58]	2012	50	Unknown	72 major motor seizures (clonic movements)	Extremities	Comparison to a random detector and one 37h video of one patient with no seizure activity	Thresholding	<1	n.a.	0.95	>0.9*	Video segments from 12 to 56 minutes	major convulsive seizures are long lasting, towards real-time
Pisani et al. [114]	2014	12	Neonatal	78 clonic seizures	Extremities	Unknown	Thresholding	0.31*	0.12*	0.71	0.69	Video segments	No ROI detection, towards real-time
This study (phase 3)	2014	8	Pediatric (2-13 a)	194 absence seizures	Face (left eye, right eye, mouth)	Per patient cross validation	Bayesian network	n.a.	0.86	0.67	n.a.	Video segments	Manually annotated ROIs, experiment 17, filtered classifier output mapped to seizures represented in the dataset
This study (phase 4)	2014	12	Pediatric (2-13 a)	350 absence seizures	Face (left eye, right eye, mouth)	Per patient percentage split: 8 patients for training, 4 for testing	Bayesian network	0.29	0.01	0.26	0.71	Long term video recording	Automatically detected ROIs for test set, classifier results with respect to seizures represented in the dataset

CHAPTER 5

Discussion and future work

5.1 Discussion

This monograph documents the work performed in order to analyse dynamic facial expressions of epileptic absence seizures, using computer vision. 12 patients with a total of 350 seizures, annotated by an experienced neurologist, were included in the analysis. While all related studies target on focal epileptic seizures with distinct clinical characteristics (focal clonic, myoclonic, cf. Table 1.1, p. 36), this is the first attempt to analyse generalised seizures with only subtle clinical manifestations. Moreover, it is the first attempt to analyse the facial expressions of epileptic seizures on an extended dataset with a high seizure count.

The results demonstrate the existence of several features that differentiate motion patterns of the eyes and the mouth from seizure and seizure-free epochs, although the number and type of features is influenced by noise introduced as a result of the high variance in capturing conditions (illumination, pose, occlusion), as well as the inter-person variability of the seizure manifestation by itself. This is underlined by experiment 3 (Subsection 3.1.3), which shows the highest seizure detection performance for all metrics, for feature sets that have been selected for each patient individually. These feature sets did not have the same elements. Moreover, for the feature set that works best for all patients, as elaborated in experiment 6 (Subsection 3.1.7), it is noticeable that the feature spaces of the three eye ROIs do not overlap much, as should be expected.

A further factor is the duration of the seizures, which varies between patients. The seizure detection in patients P01, P03, P09, P10 and P12 with small mean seizure durations (2.98 s to 4.9 s) generally performed worse than in the other patients with higher mean durations (7.41 s to 19.33). The duration of a seizure is closely connected to the amount of instances that can be extracted from it using the windowing technique. Shorter seizures

inevitably are represented with less instances than longer ones. In this case a shorter window could be used, although this would reduce the available signal length necessary for the useful extraction of some features, especially in the frequency domain.

The biggest challenge when it comes to detecting individual seizures in a video sequence with a duration of several hours is the dataset imbalance (many negatives and few positives). As shown in phase 4 (Section 3.4) even a few percentage of false positives may easily exceed the total number of actual positives. In order to account for that, an extremely high true negative rate would be necessary. This problem, known as anomaly detection, is an important problem within diverse research areas and application domains such as fraud detection for credit cards, insurance, health care etc. It refers to the problem of finding patterns in data that do not conform the expected behaviour (i.e. anomalies, outliers, aberrations etc.) [15]. In cases where abnormalities are rare or the data describing the conditions under investigation might not be enough, traditional classification methods might be less successful due to imbalanced class distributions. In such cases methods that statistically model normal data/behaviour such as semi-supervised anomaly detection (e.g. that only uses the normal labels) might prove useful [146]. In addition to that, the negative class may include various other subclasses. For the case at hand such subclasses would be "sleeping", "eating", "talking", "reading" and others, all of which have to be modelled under a single class label, a fact that deteriorates the classifier performance. For this reason, breaking up the negative class into multiple classes can be a possible solution. A further solution includes a multimodal approach that includes the EEG as a second channel of information. Both channels would act complementary to each other, since the video analysis can help in rejecting artefacts in the EEG and the EEG would help in dealing periods with missing ROI detections, as well as rejecting many false positives in the video analysis. Of course the main drawback of the EEG is that it needs electrodes attached to a patient's skull and is therefore an obtrusive technique.

Regarding the selected features, Subsection 3.1.14 concludes in a set of most prominent characteristics that differentiate the absence seizure from the seizure-free periods. These are related to the angle and magnitude of the vectors in the velocity field in the eye and especially in the mouth area as shown in Figure 3.1. One of the most relevant features is the variance of time intervals between adjacent spikes in the eye regions, while other statistical features such as the minimum, maximum and median dominate in the mouth region for the above signals. Considering the frequency domain, the dominant frequency, as well as the power in the band between 3 and 6 Hz, from signals related to the angle, the magnitude, and the pixel area from background-foreground segmentation are the features most often used.

The dissection of the ROIs showed that information form the left and right eye is necessary for a precise seizure detection, while the addition of the mouth provides slightly better results. The reason for this most probably resides in the fact that occlusions of one ROI are handled by the existence of the other ROI, particularly in cases where the head is rotated to one side. Moreover, the information delivered from motion patterns in the mouth area might include a primitive description of automatisms, which often occur in absence seizures.

The comparison to the state of the art is not straight forward. Section 4.1 has shown that the related reports face less challenges than the current work, within the analysis domain. They focus on large and fast movements, mainly of the body extremities, that can be extracted from the video based on their extreme characteristic, without the need of special ROI detectors. In contrast to that, this work relies on subtle motion of the facial musculature, which may also occur in non extreme situations, e.g. while the patient is sleeping or reeding a book. Nevertheless the results are not far behind, when the ROI detection parameter is left out. Moreover a scenario including automatic seizure (and ROI) detection for long-term video recordings lasting over several hours has not been reported yet.

Finally, the following answer can be given to the research question: Based on the analysed data, the most relevant measurable characteristics that differentiate the facial expression of absence seizures from other (unknown) expressions include the variance of time intervals between adjacent spikes, derived from the mean angle, the mean magnitude weighted by the mean angle and the maximum magnitude weighted by the angle for the left and right eye. The minimum, maximum and median of the same signals is mainly relevant for the mouth region. Additional characteristics include the power in the band between 3 an 6 Hz and the dominant frequency derived from signals measuring the angle at maximum magnitude, the mean angle, the mean magnitude weighted by the mean angle, and the pixel area from background-foreground segmentation for the left eye, right eye and mouth.

Considering the detection of at least two seizures for each patient, the results showed that under the conditions of a robust detection of the left eye, the right eye and the mouth (whenever visible), and given an initial position of an assumed existence of a seizure with a duration of approximately 3 times the seizure duration, at least 2 seizures can be detected with an average precision of 0.86 (experiment 17, Table 3.59, p. 105).

5.2 Future work

By analysing the clinical image of absence seizures, this thesis has added a new seizure type to the group of seizures studied with computer vision and has demonstrated that epileptic motion patterns in the area of the face are measurable. This process has revealed several problems, one of which is the robust ROI detection. The method should be highly specific and sensitive enough in detecting the correct ROI. A possible approach could be the usage of a skin detector in connection with a sensitive object detector and additional heuristics concerning the face anatomy and head movement. As discussed in the previous section, the major challenge is the variability in capturing conditions and patient behaviour as a result of the long duration of the recordings, in connection with an observed inter-patient variability in seizure manifestation (duration and motion characteristics). The first problem could be solved with image processing methods, especially designed for surveillance and monitoring, while the second is more likely to be solved with classification techniques that include multiple classes, supported by features that describe these classes. The issue regarding the differences in the seizures between patients demands for a closer investigation with a potentially larger set of subjects.

Annex

5.2.1 Annotation data for patient P01

Gender: Male
Age at time of Video-EEG recording: 5 a
Total duration of Video-EEG: 14 m
Total number of seizures: 4
Mean seizure duration: 17.53 s
Standard deviation: 4.57 s
Comments: -

Table 5.1: Overview of the recorded seizures of patient P01

Seizure ID	Video file name	Starting frame	Ending frame	Duration [s]	Comments
0101	VID_389_D	4145	4746	24.08	Day; awake; lying; during hyperventilation; face, eye-pair, left eye, right eye and mouth visible and annotated during seizure
0102	VID_389_D	5380	5730	14.04	Day; awake; lying; during hyperventilation; face, eye-pair, left eye, right eye and mouth visible and annotated during seizure
0103	VID_389_D	7175	7544	14.76	Day; awake; lying; during hyperventilation; face, eye-pair, left eye, right eye and mouth visible and annotated during seizure

0104	VID_389_D	20143	20572	17.02	Day; awake; lying; seizure starts immediately after photic stimulation; face, eye-pair, left eye, right eye and mouth visible and annotated during seizure

5.2.2 Annotation data for patient P02

Gender: Female
Age at time of Video-EEG recording: 9 a
Total duration of Video-EEG: 14 h and 48 m
Total number of seizures: 8
Mean seizure duration: 10.17 s
Standard deviation: 3.46 s
Comments: -

Table 5.2: Overview of the recorded seizures of patient P02

Seizure ID	**Video file name**	**Starting frame**	**Ending frame**	**Duration [s]**	**Comments**
0201	VID_4_D	3541	3890	14.00	Day; awake; lying; during hyperventilation; rubs left eye at the end of seizure; face, eye-pair, left eye, right eye and mouth visible and annotated during most part of seizure
0202	VID_6_D	49014	49254	9.64	Day; awake; sitting; profile face; only left eye hardly visible; nothing annotated
0203	VID_8_D	37531	37751	8.84	Night; awake; lying; IR switched on; face, eye-pair, right eye and mouth visible and annotated during most part of seizure; left eye annotated during remaining part of seizure; light is being switched on at the last second of seizure
0204	VID_14_D	56862	57179	12.72	Day; awake; lying; face, eye-pair, left eye, right eye and mouth visible and annotated during seizure
0205	VID_17_D	14140	14496	14.28	Day; sleeping; lying; face, eye-pair, left eye, right eye and mouth visible and annotated during seizure
0206	VID_17_D	24079	24322	9.76	Day; sleeping; lying; profile face; only right eye visible and annotated during seizure
0207	VID_17_D	28453	28658	8.24	Day; sleeping; lying; profile face; only right eye visible and annotated during seizure

0208	VID_17_D	31189	31285	3.84	Day; sleeping; lying; profile face; only right eye visible and annotated during seizure

5.2.3 Annotation data for patient P03

Gender: Male
Age at time of Video-EEG recording: 10 a
Total duration of Video-EEG: 16 h and 13 m
Total number of seizures: 21
Mean seizure duration: 3.97 s
Standard deviation: 1.69 s
Comments: The seizures of this patient usually exhibit a myoclonic jerk in the musculature of the whole body.

Table 5.3: Overview of the recorded seizures of patient P03

Seizure ID	Video file name	Starting frame	Ending frame	Duration [s]	Comments
0301	VID_52_D	3011	3180	6.80	Day; awake; lying; during hyperventilation; face, eye-pair, left eye, right eye and mouth visible and annotated during seizure
0302	VID_52_D	9701	9842	5.68	Day; awake; lying; during hyperventilation; face, eye-pair, left eye, right eye and mouth visible and annotated during seizure
0303	VID_52_D	54116	54172	2.28	Day; awake; leaning with back on bed pillow; face, eye-pair, left eye, right eye and mouth visible and annotated during seizure
0304	VID_53_D	55365	55477.	4.52	Day; awake; lying; playing portable video-game; mouth is hidden by game device; eye-pair, left eye and right eye visible and annotated during seizure
0305	VID_54_D	26230	26308	3.16	Day; awake; lying on the side; playing portable video-game; mouth is hidden by game device; only right eye visible and annotated during seizure
0306	VID_59_D	23615	23738	4.96	Day; awake; lying on the side; profile face; only left eye visible and annotated during seizure; mouth annotated during last part of seizure

0307	VID_59_D	47829	47881	2.12	Day; awake; lying; playing portable video-game; mouth is hidden by game device; eye-pair, left eye and right eye visible and annotated during seizure
0308	VID_60_D	5036	5133	3.92	Day; sleeping; lying on the side; only right eye visible and annotated during seizure; profile mouth also annotated
0309	VID_60_D	32033	32080	1.92	Day; awake; sitting on bed; face, eye-pair, left eye, right eye and mouth visible and annotated during seizure
0310	VID_61_D	55493	55551	2.36	Day; awake; sitting on bed; only left eye and mouth visible and annotated during seizure
0311	VID_62_D	21012	21098	3.48	Day; awake; lying on the side; reading book; only right eye visible and annotated during parts of seizure
0312	VID_62_D	38032	38159	5.12	Day; awake; lying; reading book; face completely hidden behind book; rejected
0313	VID_63_D	31861	31972	4.48	Night; sleeping; lying on the side; IR not switched on; noise; profile face hardly visible; rejected
0314	VID_63_D	39829	39893	2.60	Night; sleeping; lying on the side; IR not switched on; noise; face not visible; rejected
0315	VID_63_D	54911	55014	4.16	Night; sleeping; lying; IR not switched on; noise; face, left eye, mouth and eye-pair visible and annotated during seizure
0316	VID_63_D	57553	57600	1.92	Night; sleeping; lying on the side; IR not switched on; noise; face not visible; Rejected
0317	VID_63_D	58288	58353	2.64	Night; sleeping; lying on the side; IR not switched on; noise; face not visible; Rejected
0318	VID_66_D	11338	11528	7.64	Night; sleeping; lying on the side; IR not switched on; noise; right eye slightly visible and annotated during seizure
0319	VID_70_D	48332	48499	6.72	Night; sleeping; lying on the side; IR not switched on; noise; right eye slightly visible and annotated during seizure
0320	VID_75_D	21645	21726	3.28	Night; sleeping; lying on the side; IR not switched on; noise; right eye slightly visible and annotated during seizure

0321	VID_75_D	28994	29084	3.64	Night; sleeping; lying on the side; IR not switched on; noise; right eye slightly visible and annotated during seizure

5.2.4 Annotation data for patient P04

Gender: Male
Age at time of Video-EEG recording: 7 a
Total duration of Video-EEG: 15 h and 1 m
Total number of seizures: 65
Mean seizure duration: 2.98 s
Standard deviation: 0.69 s
Comments: Patient often puts fingers in mouth. Usually exhibits a clonic jerk during the seizure.

Table 5.4: Overview of the recorded seizures of patient P04

Seizure ID	Video file name	Starting frame	Ending frame	Duration [s]	Comments
0401	VID_101_D	2507	2632	5.04	Day; awake; lying; during hyperventilation; head looking slightly to the side; face, left eye, right eye, mouth and eye-pair visible and annotated during seizure
0402	VID_101_D	12393	12494	4.08	Day; awake; lying; face, eye-pair, left eye, right eye and mouth visible and annotated during seizure
0403	VID_101_D	14310	14370	2.44	Day; awake; lying; head looking slightly to the side; face, eye-pair, left eye and right eye, visible and annotated during seizure
0404	VID_101_D	20822	20918	3.88	Day; awake; lying; face, eye-pair, left eye, right eye and mouth visible and annotated during most part of seizure
0405	VID_101_D	22195	22254	2.40	Day; awake; lying; eating; face partly occluded (hands over mouth); eye-pair, left eye and right eye visible and annotated during seizure
0406	VID_101_D	28743	28817	3.00	Day; awake; lying; face partly occluded (hands over mouth); eye-pair, left eye and right eye visible and annotated during seizure

0407	VID_101_D	30170	30227	2.32	Day; awake; lying; face partly occluded by hands; eye-pair, left eye and right eye visible and annotated during most part of seizure
0408	VID_101_D	34698	34799	4.08	Day; awake; lying; face partly occluded by hands; eye-pair, left eye and mouth visible and annotated during most part of seizure; right eye annotated during whole seizure
0409	VID_101_D	39677	39749	2.92	Day; awake; lying; looking to the side; face, eye-pair, left eye, right eye and mouth visible and annotated during seizure
0410	VID_101_D	42376	42437	2.48	Day; awake; lying; face partly occluded by hands; eye-pair, left eye and right eye visible and annotated during seizure; mouth annotated during parts of seizure
0411	VID_101_D	46202	46262	2.44	Day; awake; lying; looking to the side; face, eye-pair, left eye, right eye and mouth visible and annotated during seizure
0412	VID_101_D	46744	46822	3.16	Day; awake; lying; looking to the side; face, eye-pair, left eye, right eye and mouth visible and annotated during seizure
0413	VID_101_D	55450	55563	4.56	Day; awake; lying; looking to the side; face partly occluded by hands over mouth; eye-pair, left eye and right eye visible and annotated during seizure
0414	VID_101_D	57615	57670	2.24	Day; awake; lying; looking to the side; face, eye-pair, left eye and right visible and annotated during seizure; mouth annotated during most parts of seizure
0415	VID_102_D	13014	13110	3.88	Day; awake; lying; face partly occluded by hands; face, eye-pair, left eye, right eye and mouth visible and annotated during most part of seizure
0416	VID_102_D	46570	46661	3.68	Day; awake; lying; face minimally occluded by finger; face, eye-pair, left eye and right eye visible and annotated during seizure; mouth annotated during last part of seizure

0417	VID_102_D	52676	52753	3.12	Day; awake; lying; looking to the side; face minimally occluded by finger; face, eye-pair, left eye and right eye visible and annotated during seizure
0418	VID_102_D	53539	53588	2.00	Day; awake; lying; looking to the side; face, eye-pair, left eye, right eye and mouth visible and annotated during seizure
0419	VID_103_D	3441	3524	2.00	Day; awake; lying; looking slightly to the side; face, eye-pair, left eye, right eye and mouth visible and annotated during seizure
0420	VID_103_D	12335	12439	4.20	Day; awake; lying; face, eye-pair, left eye, right eye and mouth visible and annotated during seizure
0421	VID_103_D	14293	14360	2.72	Day; awake; lying; face, eye-pair, left eye, right eye and mouth visible and annotated during seizure
0422	VID_103_D	19146	19214	2.76	Day; awake; lying; looking to the side; face occluded by hand on beginning of seizure; eye-pair, left eye and right eye visible and annotated during most part of seizure
0423	VID_103_D	21877	21957	3.24	Day; awake; lying; face, eye-pair, left eye and mouth visible and annotated during seizure; right eye annotated during most part of seizure
0424	VID_103_D	23375	23452	3.12	Day; awake; lying; looking slightly to the side; face occluded by hand over mouth; eye-pair, left eye and right eye visible and annotated during seizure
0425	VID_103_D	24376	24429	2.16	Day; awake; lying; looking slightly to the side; Mouth occluded by finger; face, eye-pair, left eye and right eye visible and annotated during seizure; mouth annotated during very last part of seizure
0426	VID_103_D	28124	28189	2.64	Day; awake; lying; face, eye-pair, left eye, right eye and mouth visible and annotated during seizure

0427	VID_103_D	29784	29862	3.16	Day; awake; lying; looking slightly to the side; face, eye-pair, left eye, right eye and mouth visible and annotated during seizure
0428	VID_103_D	32107	32164	2.32	Day; awake; lying; looking slightly to the side; face, eye-pair, left eye, right eye and mouth visible and annotated during seizure
0429	VID_103_D	35699	35782	3.36	Day; awake; lying; face, eye-pair, left eye, right eye and mouth visible and annotated during seizure
0430	VID_103_D	43761	43833	2.92	Day; awake; lying; face, eye-pair, left eye, right eye and mouth visible and annotated during seizure
0431	VID_105_D	1746	1827	3.28	Day; awake; lying; face, eye-pair, left eye, right eye and mouth visible and annotated during seizure
0432	VID_105_D	24587	24669	3.32	Day; awake; sitting; eating; face occluded (hand over mouth); eye-pair, left eye and right eye visible and annotated during seizure; face and mouth annotated during most part of seizure
0433	VID_105_D	29294	29365	2.88	Day; awake; sitting; eating; face, eye-pair, left eye, right eye and mouth visible and annotated during seizure
0434	VID_105_D	30555	30619	2.60	Day; awake; sitting; eating; face, eye-pair, left eye, right eye and mouth visible and annotated during seizure
0435	VID_105_D	43112	43194	3.32	Day; awake; lying; eating; face, eye-pair, left eye, right eye and mouth visible and annotated during seizure
0436	VID_106_D	11842	11900	2.36	Day; awake; lying; face occluded (hand over mouth); eye-pair, left eye and right eye visible and annotated during seizure
0437	VID_106_D	14434	14491	2.32	Day; awake; lying; face slightly occluded (finger over mouth); face, eye-pair, left eye and right eye visible and annotated during seizure

0438	VID_106_D	17933	18006	2.96	Day; awake; lying; face slightly occluded (finger over mouth); face, eye-pair, left eye and right eye visible and annotated during seizure
0439	VID_106_D	24308	24376	2.76	Day; awake; lying; face occluded (hand over mouth); eye-pair, left eye and right eye visible and annotated during seizure
0440	VID_106_D	46096	46186	3.64	Day; awake; lying; looking to the side; face, eye-pair, left eye, right eye and mouth visible and annotated during seizure
0441	VID_106_D	52181	52248	2.72	Day; awake; lying; looking slightly to the side; face, eye-pair, left eye, right eye and mouth visible and annotated during seizure
0442	VID_106_D	59704	59764	2.44	Day; awake; lying; face, eye-pair, left eye, right eye and mouth visible and annotated during seizure
0443	VID_107_D	496	567	2.88	Day; awake; lying; looking slightly to the side; face, eye-pair, left eye, right eye and mouth visible and annotated during seizure
0444	VID_107_D	13204	13282	3.16	Day; awake; lying; looking slightly to the side; face, eye-pair, left eye, right eye and mouth visible and annotated during seizure
0445	VID_107_D	19892	19961	2.80	Day; awake; lying; face, eye-pair, left eye, right eye and mouth visible and annotated during seizure
0446	VID_107_D	34710	34771	2.48	Day; awake; lying; looking slightly to the side; head slightly rotated; face, eye-pair, left eye, right eye and mouth visible and annotated during seizure
0447	VID_107_D	38398	38459	2.48	Day; awake; lying; looking slightly to the side; head slightly rotated; face, eye-pair, left eye, right eye and mouth visible and annotated during seizure
0448	VID_107_D	53085	53146	2.48	Day; awake; lying; face, eye-pair, left eye, right eye and mouth visible and annotated during seizure

0449	VID_107_D	55797	55861	2.60	Day; awake; lying; face, eye-pair, left eye, right eye and mouth visible and annotated during seizure
0450	VID_109_D	4076	4143	2.72	Day; awake; lying; face, eye-pair, left eye, right eye and mouth visible and annotated during seizure
0451	VID_109_D	7549	7598	2.00	Day; awake; lying; face slightly occluded (finger over mouth); face, eye-pair, left eye and right eye visible and annotated during seizure
0452	VID_109_D	11078	11124	1.88	Day; awake; lying; face, eye-pair, left eye, right eye and mouth visible and annotated during seizure
0453	VID_109_D	20354	20402	1.96	Day; awake; lying; face, eye-pair, left eye, right eye and mouth visible and annotated during seizure
0454	VID_109_D	27266	27339	2.96	Day; awake; lying; looking slightly to the side; face occluded by arm during some parts of seizure; face, eye-pair, left eye, right eye and mouth visible and annotated during most part of seizure
0455	VID_109_D	39086	39158	2.92	Day; awake; lying; face, eye-pair, left eye, right eye and mouth visible and annotated during seizure
0456	VID_109_D	56641	56714	2.96	Day; awake; lying; looking to the side; face, eye-pair, left eye, right eye and mouth visible and annotated during seizure
0457	VID_110_D	1523	1603	3.24	Day; awake; lying; looking to the side; face, eye-pair, left eye, right eye and mouth visible and annotated during seizure
0458	VID_110_D	14587	14653	2.68	Day; awake; lying; looking to the side; face occluded at the end of seizure; face, eye-pair, right eye and mouth visible and annotated during most part of seizure; left eye visible and annotated during seizure
0459	VID_110_D	33939	33986	1.92	Day; awake; lying; looking slightly to the side; face, eye-pair, left eye, right eye and mouth visible and annotated during seizure

0460	VID_111_D	16748	16803	2.24	Day; awake; lying; face, eye-pair, left eye, right eye and mouth visible and annotated during seizure
0461	VID_113_D	40740	40824	3.40	Day; awake; sitting on bed; profile face; left eye hardly visible and annotated during seizure
0462	VID_113_D	46279	46359	3.24	Day; awake; sitting on bed; profile face; left eye and mouth hardly visible and annotated during seizure
0463	VID_114_D	24305	24396	3.68	Day; awake; sitting on bed; profile face; left eye hardly visible and annotated during parts of seizure
0464	VID_115_D	46	155	4.40	Night; sleeping; no IR; noise; face not visible; rejected
0465	VID_130_D	28204	28309	4.24	Daylight; sleeping; face, eye-pair, left eye, right eye and mouth visible and annotated during seizure

5.2.5 Annotation data for patient P05

Gender: Male
Age at time of Video-EEG recording: 2 a
Total duration of Video-EEG: 15 h and 27 m
Total number of seizures: 25
Mean seizure duration: 7.41 s
Standard deviation: 3.55 s
Comments: -

Table 5.5: Overview of the recorded seizures of patient P05

Seizure ID	**Video file name**	**Starting frame**	**Ending frame**	**Duration [s]**	**Comments**
0501	VID_183_D	2472	2589	4.72	Day; lying on the front; face not visible; rejected
0502	VID_183_D	5920	6145	9.04	Day; lying; sleeping; face occluded (dummy in the mouth); left eye visible and annotated during seizure; eye-pair and right eye annotated during most part of seizure
0503	VID_183_D	8206	8367	6.48	Day; lying; sleeping; face occluded (dummy in the mouth); eye-pair, left eye and right eye visible and annotated during seizure

0504	VID_183_D	9145	9268	4.96	Day; lying; sleeping; face occluded (dummy in the mouth); eye-pair, left eye and right eye visible and annotated during seizure
0505	VID_184_D	39238	39461	8.96	Day; awake; sitting on bed; face heavily occluded; rejected
0506	VID_184_D	45352	45542	7.64	Day; awake; sitting on bed; eating; face occluded; eye-pair (rotated), left eye and right eye visible and annotated during seizure
0507	VID_184_D	45765	45869	4.20	Day; awake; sitting on bed; eating; face occluded; eye-pair (rotated), left eye and right eye visible and annotated during seizure
0508	VID_187_D	34439	34659	8.84	Day; awake; sitting on bed; looking down; eye-pair, left eye and right eye hardly visible and annotated during last part of seizure
0509	VID_189_D	13060	13251	7.68	Low light conditions; awake; sitting on bed; looking to the side; left eye hardly visible and annotated during seizure
0510	VID_189_D	21647	21866	8.80	Low light conditions; awake; sitting on bed; looking to the side; left eye, right eye and eye-pair hardly visible and annotated during parts of seizure
0511	VID_189_D	22315	22408	3.76	Low light conditions; awake; sitting on bed; looking to the side; left eye hardly visible and annotated during seizure
0512	VID_190_D	3643	3837	7.80	Day; awake; sitting on bed; looking slightly to the side; right eye visible and annotated during seizure; mouth, eye-pair and left eye annotated during small parts of seizure
0513	VID_190_D	9452	9601	6.00	Day; awake; sitting on bed; looking slightly to the side; left eye visible and annotated during seizure
0514	VID_192_D	46614	47096	19.32	Day; awake; lying on bed; face partially occluded by hand; right eye visible and annotated during seizure; left eye annotated during parts of seizure

0515	VID_192_D	47300	47693	15.76	Day; awake; lying on bed; face partially occluded by hand; left eye visible and annotated during last part of seizure; right eye annotated during parts of seizure
0516	VID_192_D	48721	48879	6.36	Day; awake; lying on bed; face partially occluded by hand and dummy; eye-pair, left eye and right eye visible and annotated during seizure
0517	VID_192_D	64256	64470	8.60	Night; lying on bed; no IR; noise; face partially occluded by mother's arm; left eye visible and annotated during small last part of seizure
0518	VID_192_D	100907	101084	7.12	Night; awake; lying on bed; no IR; noise; face occluded (dummy in the mouth); eye-pair, left eye and right eye visible and annotated during seizure
0519	VID_192_D	101350	101427	3.12	Night; awake; lying on bed; no IR; noise; face occluded (dummy in the mouth); eye-pair left eye and right eye visible and annotated during seizure
0520	VID_192_D	101975	102181	8.28	Night; awake; lying on bed; no IR; noise; face occluded (dummy in the mouth); eye-pair, left eye and right eye visible and annotated during seizure
0521	VID_192_D	109248	109402	6.20	Night; awake; lying on bed; no IR; noise; face occluded (dummy in the mouth); eye-pair, left eye and right eye visible and annotated during seizure
0522	VID_192_D	114321	114482	6.48	Night; sleeping; lying on bed; no IR; noise; face occluded at the beginning (dummy in the mouth); eye-pair and right eye visible and annotated during most part of seizure; left eye annotated during seizure; face and mouth annotated during the last part of seizure
0523	VID_198_D	83282	83419	5.52	Night; sleeping; lying on bed; face rotated to the side; no IR; right eye and mouth visible and annotated during seizure

0524	VID_201_D	61342	61448	4.28	Night; sleeping; lying on bed; face rotated to the side; no IR; right eye and mouth visible and annotated during seizure
0525	VID_201_D	89164	89298	5.40	Night; sleeping; lying on bed; face rotated to the side; no IR; left eye and mouth hardly visible and annotated during seizure

5.2.6 Annotation data for patient P06

Gender: Female
Age at time of Video-EEG recording: 5 a
Total duration of Video-EEG: 15 h and 15 m
Total number of seizures: 14
Mean seizure duration: 8.22 s
Standard deviation: 1.61 s
Comments: Stops ongoing activity (arrest); eyes usually opening; looking up; frequent, maybe periodic eye blinks; mouth activity usually stops during seizure.

Table 5.6: Overview of the recorded seizures of patient P06

Seizure ID	**Video file name**	**Starting frame**	**Ending frame**	**Duration [s]**	**Comments**
0601	VID_241_D	42	276	9.40	Day; awake; lying; head slightly rotated within plane; face, eye-pair, left eye, right eye and mouth visible and annotated during seizure
0602	VID_241_D	3049	3282	9.36	Day; awake; lying; during hyperventilation; face occluded by third person's hand at the beginning of the seizure; face, eye-pair, left eye and right eye visible and annotated during remaining part of seizure; mouth annotated during whole seizure
0603	VID_241_D	11599	11826	9.12	Day; awake; lying; during photostimulation; face, eye-pair, left eye, right eye and mouth visible and annotated during seizure
0604	VID_243_D	28668	28783	4.64	Day; low light conditions; sleeping; lying; face, eye-pair, left eye, right eye and mouth visible and annotated during seizure

0605	VID_246_D	45394	45588	7.80	Day; awake; sitting on bed; face, eye-pair, left eye, right eye and mouth visible and annotated during seizure
0606	VID_250_D	51296	51514	8.76	Day; awake; lying; face occluded by an object; right eye visible and annotated during seizure; face, eye-pair, left eye and mouth annotated during parts of seizure
0607	VID_250_D	54913	55131	8.76	Day; awake; lying; face, eye-pair, right eye and mouth annotated during seizure
0608	VID_251_D	8978	9190	8.52	Patient not visible; rejected
0609	VID_251_D	27004	27251	9.92	Night; awake; noise; no IR; face occluded by moving arms; face, eye-pair, left eye and right-eye annotated during parts of seizure; mouth annotated during whole seizure
0610	VID_251_D	53939	54161	8.92	Day; awake; lying on the side; part of face is outside of camera view; left eye and mouth annotated during most part of seizure
0611	VID_251_D	57345	57554	8.40	Day; awake; sitting on bed; face, eye-pair and left eye annotated during most part of seizure; right eye and mouth annotated during whole seizure
0612	VID_251_D	59209	59413	8.20	Lights on; awake; lying; eating; face, eye-pair. left eye, right eye and mouth visible and annotated during most parts of seizure
0613	VID_252_D	42505	42720	8.64	Night; sleeping; lying on the side; no IR; noise; right eye hardly visible; rejected
0614	VID_261_D	40854	40969	4.64	Night; sleeping; lying on the side; no IR; noise; face not visible; rejected

5.2.7 Annotation data for patient P07

Gender: Female
Age at time of Video-EEG recording: 2 a
Total duration of Video-EEG: 15 h and 50 m
Total number of seizures: 16
Mean seizure duration: 10.64 s
Standard deviation: 4.83 s
Comments: Stops ongoing activity; blinking; mouth automatisms, lip smacking, fast clonic component.

Table 5.7: Overview of the recorded seizures of patient P07

Seizure ID	Video file name	Starting frame	Ending frame	Duration [s]	Comments
0701	VID_281_D	6279	6560	11.28	Day; lying; during hyperventilation; face, eye-pair, left eye, right eye and mouth visible and annotated during most part of seizure
0702	VID_281_D	6762	6891	5.20	Day; lying; during hyperventilation; face, eye-pair, left eye, right eye and mouth visible and annotated during seizure
0703	VID_281_D	45442	45847	16.24	Low light conditions; lying on the front; face not visible; rejected
0704	VID_281_D	71358	71790	17.32	Patient out of camera view; rejected
0705	VID_281_D	89253	89639	15.48	Low light conditions; awake; lying on the side; profile face; left eye and mouth annotated during most part of seizure
0706	VID_284_D	38131	38471	13.64	Low light conditions; awake; sitting on bed; eating; right eye annotated during most part of seizure; eye-pair, left eye and mouth annotated during some parts of seizure
0707	VID_284_D	55235	55481	9.88	Patient out of camera view; rejected
0708	VID_285_D	26811	27187	15.08	Patient out of camera view; rejected
0709	VID_287_D	2558	2992	17.40	Day; awake; lying on the side; patient moves alot eye-pair, right eye, left eye and mouth annotated during parts of seizure
0710	VID_290_D	2267	2531	10.60	Night; sleeping; no IR; noise; lying on the side; face not visible; rejected
0711	VID_296_D	21616	21775	6.40	Night; sleeping; no IR; noise; lying on the front; face not visible; rejected
0712	VID_297_D	1939	2129	7.64	Night; sleeping; lying on the back; noise; no IR; Face, eye-pair and right eye annotated during first part of seizure; Mouth and left eye annotated during whole seizure
0713	VID_299_D	107024	107296	10.92	Night; sleeping; no IR; noise; lying on the front; face not visible; rejected
0714	VID_299_D	114302	114428	5.08	Night; sleeping; no IR; noise; lying on the front; face not visible; rejected

0715	VID_302_D	53682	53787	4.24	Low light condition; sleeping; lying on the side; profile face; right eye and mouth annotated during seizure
0716	VID_303_D	6999	7093	3.80	Day; low light; sleeping; lying on the back; face partially out of camera view; left eye and mouth annotated during seizure

5.2.8 Annotation data for patient P08

Gender: Female
Age at time of Video-EEG recording: 7 a
Total duration of Video-EEG: 15 h and 49 m
Total number of seizures: 26
Mean seizure duration: 19.33 s
Standard deviation: 7.56 s
Comments: Usually opens eyes if closed during seizure; mouth automatisms; lip smacking; eye blinking; gaze fixation; may not always stop ongoing activity such as eating (e.g. Seizure ID 0815).

Table 5.8: Overview of the recorded seizures of patient P08

Seizure ID	**Video file name**	**Starting frame**	**Ending frame**	**Duration [s]**	**Comments**
0801	VID_331_D	2581	3151	22.84	Day; awake; lying on bed; during hyperventilation; face annotated during most part of seizure; eye-pair, left eye, right eye and mouth annotated during whole seizure
0802	VID_331_D	4417	5129	28.48	Day; awake; lying on bed; during hyperventilation; face, eye-pair, left eye, right eye and mouth annotated during seizure
0803	VID_331_D	5944	6547	24.12	Day; low light condition; awake; lying on bed; during hyperventilation; face, eye-pair, left eye, right eye and mouth annotated during seizure
0804	VID_331_D	13170	13611	17.64	Day; low light condition; awake; lying on bed; during photic stimulation; camera looses focus at the end of seizure; face and mouth occluded by photic stimulation device, eye-pair, left eye and right eye annotated during seizure

0805	VID_331_D	16578	16958	15.20	Day; low light condition; awake; lying on bed; during photic stimulation; face and mouth occluded by photic stimulation device, eye-pair, left eye and right eye annotated during seizure
0806	VID_331_D	25503	26015	20.48	Day; low light condition; awake; lying on bed; eye-pair annotated during whole seizure; face and mouth annotated during parts of seizure; eye-pair, left eye and right eye annotated during whole seizure
0807	VID_331_D	31052	31326	10.96	Day; low light condition; awake; lying on bed; face partly out of camera view; eye-pair, left eye and mouth annotated during parts of seizure; right eye annotated during whole seizure
0808	VID_331_D	44961	45348	15.48	Day; low light condition; awake; lying on bed; face partly out of camera view; only right eye visible and annotated during seizure
0809	VID_331_D	90384	90876	19.68	Day; low light condition; awake; lying on bed; face, eye-pair, left eye and mouth annotated during most parts of seizure; right eye annotated during whole seizure
0810	VID_332_D	17878	18324	17.84	Day; lying on bed; awake; using tablet; face, eye-pair, right eye, left eye and mouth annotated during whole seizure
0811	VID_332_D	29369	29888	20.76	Day; lying on bed; awake; using tablet; face, left eye and mouth annotated during most part of seizure; right eye annotated during whole seizure
0812	VID_332_D	42846	43273	17.08	Day; lying on bed; awake; using tablet; face annotated during most part of seizure; eye-pair left eye, right eye and mouth annotated during whole seizure
0813	VID_334_D	17669	18032	14.52	Day; lying on bed; awake; using tablet; face and mouth annotated during most part of seizure; eye-pair left eye and right eye annotated during whole seizure

0814	VID_334_D	111866	112309	17.72	Day; lying on bed; awake; looking down; face eye-pair left eye, right eye and mouth annotated during whole seizure
0815	VID_335_D	9937	10491	22.16	Day; lying on bed; awake; eating; face partially out of camera view; eye pair, left eye and right eye annotated during whole seizure; mouth annotated during most part of seizure
0816	VID_337_D	77261	77660	15.96	Day; lying on bed; awake; looking down; head being moved by clinician; face, eye-pair, left eye and mouth annotated during most part of seizure; right eye annotated during whole seizure
0817	VID_340_D	15519	15859	13.60	Day; lying on bed; awake; using tablet pc; eating lollipop; face partially out of camera view; eye pair, left eye and right eye annotated during whole seizure; mouth and face not annotated
0818	VID_340_D	20193	20650	18.28	Day; lying on bed; awake; using tablet pc; eating lollipop; face partially out of camera view; eye pair, left eye and right eye annotated during whole seizure; mouth and face not annotated
0819	VID_341_D	3168	3505	13.48	Day; leaning on pillow; awake; face looking down and to the side; face, eye-pair right eye and mouth annotated during parts of seizure; left eye annotated during whole seizure
0820	VID_343_D	72605	72942	13.48	Day; lying on the front; awake; camera moves; face not visible; rejected
0821	VID_343_D	81329	82432	44.12	Night; lying on the front; sleeping; no IR; noise; face not visible; only eyelashes visible; rejected
0822	VID_343_D	86689	87417	29.12	Night; lying on the front; probably sleeping; no IR; noise; face not visible; only eyelashes visible; rejected
0823	VID_343_D	90000	90774	30.96	Night; lying on the front; probably sleeping; no IR; noise; face not visible; only eyelashes visible; rejected

0824	VID_343_D	92122	92613	19.64	Night; lying on the front; probably sleeping; no IR; noise; face not visible; only eyelashes visible; rejected
0825	VID_349_D	38390	38575	7.40	Night; lying; probably sleeping; no IR; noise; face, eye-pair, left eye, right eye and mouth visible and annotated during a small first part of seizure
0826	VID_352_D	57223	57513	11.60	Low light conditions; lying on the side; sleeping; only right eye visible and annotated during most part of seizure

5.2.9 Annotation data for patient P09

Gender: Female
Age at time of Video-EEG recording: 8 a
Total duration of Video-EEG: 15 h and 51 m
Total number of seizures: 25
Mean seizure duration: 4.90 s
Standard deviation: 1.57 s
Comments: -

Table 5.9: Overview of the recorded seizures of patient P09

Seizure ID	Video file name	Starting frame	Ending frame	Duration [s]	Comments
0901	VID_379_D	5207	5329	4.92	-
0902	VID_400_D	12996	13115	4.80	-
0903	VID_400_D	18688	18789	4.08	-
0904	VID_400_D	24407	24472	2.64	-
0905	VID_400_D	60311	60459	5.96	-
0906	VID_400_D	104215	104334	4.80	-
0907	VID_400_D	111344	111489	5.84	-
0908	VID_400_D	119664	119771	4.32	-
0909	VID_401_D	3089	3191	4.12	-
0910	VID_403_D	20580	20728	5.96	-
0911	VID_403_D	29713	29821	4.36	-
0912	VID_403_D	76245	76484	9.60	-
0913	VID_403_D	113256	113420	6.60	-
0914	VID_404_D	25039	25230	7.68	-
0915	VID_404_D	34700	34789	3.60	-
0916	VID_407_D	10951	11084	5.36	-
0917	VID_407_D	40484	40617	5.36	-
0918	VID_407_D	45531	45644	4.56	-
0919	VID_407_D	70214	70371	6.32	-
0920	VID_407_D	82565	82667	4.12	-
0921	VID_410_D	7543	7641	3.96	-
0922	VID_410_D	11126	11191	2.64	-
0923	VID_410_D	14946	15036	3.64	-

0924	VID_410_D	111251	111351	4.04	-
0925	VID_410_D	119865	119942	3.12	-

5.2.10 Annotation data for patient P10

Gender: Male
Age at time of Video-EEG recording: 5 a
Total duration of Video-EEG: 15 h and 9 m
Total number of seizures: 68
Mean seizure duration: 4.20 s
Standard deviation: 0.59 s
Comments: -

Table 5.10: Overview of the recorded seizures of patient P10

Seizure ID	Video file name	Starting frame	Ending frame	Duration [s]	Comments
1001	VID_453_D	14143	14263	4.84	-
1002	VID_454_D	15663	15861	7.96	-
1003	VID_454_D	28953	29076	4.96	-
1004	VID_454_D	43219	43310	3.68	-
1005	VID_454_D	49652	49811	6.40	-
1006	VID_454_D	55005	55108	4.16	-
1007	VID_455_D	1044	1137	3.76	-
1008	VID_455_D	5532	5622	3.64	-
1009	VID_455_D	7965	8051	3.48	-
1010	VID_455_D	13969	14063	3.80	-
1011	VID_455_D	21714	21818	4.20	-
1012	VID_455_D	28213	28308	3.84	-
1013	VID_455_D	49307	49412	4.24	-
1014	VID_455_D	54292	54399	4.32	-
1015	VID_455_D	56182	56283	4.08	-
1016	VID_455_D	59420	59512	3.72	-
1017	VID_456_D	16681	16786	4.24	-
1018	VID_456_D	33404	33505	4.08	-
1019	VID_456_D	43430	43534	4.20	-
1020	VID_456_D	47919	48039	4.84	-
1021	VID_457_D	28389	28489	4.04	-
1022	VID_457_D	46754	46854	4.04	-
1023	VID_457_D	50152	50270	4.76	-
1024	VID_458_D	10522	10624	4.12	-
1025	VID_458_D	28449	28533	3.40	-
1026	VID_459_D	10522	10624	4.12	-
1027	VID_459_D	15500	15609	4.40	-
1028	VID_459_D	40742	40828	3.48	-
1029	VID_460_D	5421	5532	4.48	-
1030	VID_460_D	33462	33573	4.48	-
1031	VID_462_D	55821	55914	3.76	-
1032	VID_466_D	8614	8655	1.68	-
1033	VID_466_D	36536	36647	4.48	-
1034	VID_466_D	37660	37746	3.48	-

1035	VID_466_D	45181	45292	4.48	-
1036	VID_466_D	53566	53663	3.92	-
1037	VID_466_D	55930	56021	3.68	-
1038	VID_466_D	57038	57136	3.96	-
1039	VID_470_D	7338	7386	1.96	-
1040	VID_470_D	15998	16059	2.48	-
1041	VID_470_D	24706	24812	4.28	-
1042	VID_470_D	27709	27834	5.04	-
1043	VID_470_D	30197	30301	4.20	-
1044	VID_470_D	33282	33363	3.28	-
1045	VID_470_D	43438	43602	6.60	-
1046	VID_470_D	50971	51110	5.60	-
1047	VID_471_D	9117	9214	3.92	-
1048	VID_471_D	11454	11570	4.68	-
1049	VID_471_D	17423	17535	4.52	-
1050	VID_471_D	18676	18766	3.64	-
1051	VID_471_D	20296	20403	4.32	-
1052	VID_471_D	22848	22936	3.56	-
1053	VID_471_D	26567	26670	4.16	-
1054	VID_471_D	27204	27315	4.48	-
1055	VID_471_D	30415	30537	4.92	-
1056	VID_471_D	42969	43141	6.92	-
1057	VID_471_D	47581	47699	4.76	-
1058	VID_471_D	48135	48209	3.00	-
1059	VID_471_D	49516	49616	4.04	-
1060	VID_471_D	51717	51840	4.96	-
1061	VID_471_D	56280	56351	2.88	-
1062	VID_471_D	56976	57072	3.88	-
1063	VID_471_D	57816	57898	3.32	-
1064	VID_472_D	2753	2882	5.20	-
1065	VID_473_D	53394	53463	2.80	-
1066	VID_473_D	54466	54555	3.60	-
1067	VID_475_D	12266	12406	5.64	-
1068	VID_475_D	27387	27486	4.00	-

5.2.11 Annotation data for patient P11

Gender: Male
Age at time of Video-EEG recording: 13 a
Total duration of Video-EEG: 15 h and 2 m
Total number of seizures: 38
Mean seizure duration: 6.27 s
Standard deviation: 1.29 s
Comments: -

Table 5.11: Overview of the recorded seizures of patient P11

Seizure ID	Video file name	Starting frame	Ending frame	Duration [s]	Comments
1101	VID_506_D	12145	12390	9.84	-
1102	VID_506_D	31437	31604	6.72	-

1103	VID_506_D	52274	52431	6.32	-
1104	VID_507_D	5951	6118	6.72	-
1105	VID_507_D	34026	34176	6.04	-
1106	VID_507_D	40772	40929	6.32	-
1107	VID_507_D	47017	47182	6.64	-
1108	VID_507_D	54327	54488	6.48	-
1109	VID_507_D	58614	58766	6.12	-
1110	VID_508_D	1322	1471	6.00	-
1111	VID_508_D	28184	28328	5.80	-
1112	VID_508_D	32443	32603	6.44	-
1113	VID_509_D	14651	14822	6.88	-
1114	VID_509_D	46811	46955	5.80	-
1115	VID_510_D	24816	24974	6.36	-
1116	VID_510_D	58190	58356	6.68	-
1117	VID_511_D	17646	17773	5.12	-
1118	VID_512_D	30155	30310	6.24	-
1119	VID_512_D	38931	39076	5.84	-
1120	VID_513_D	12453	12629	7.08	-
1121	VID_514_D	30479	30620	5.68	-
1122	VID_514_D	35108	35288	7.24	-
1123	VID_514_D	57117	57275	6.36	-
1124	VID_516_D	960	1031	2.88	-
1125	VID_512_D	44680	44799	4.80	-
1126	VID_512_D	47288	47380	3.72	-
1127	VID_512_D	50678	50783	4.24	-
1128	VID_524_D	49920	50091	6.88	-
1129	VID_525_D	860	1032	6.92	-
1130	VID_525_D	2231	2427	7.88	-
1131	VID_525_D	13874	14073	8.00	-
1132	VID_525_D	45696	45856	6.44	-
1133	VID_526_D	2294	2485	7.68	-
1134	VID_526_D	4949	5114	6.64	-
1135	VID_526_D	23549	23736	7.52	-
1136	VID_526_D	29303	29486	7.36	-
1137	VID_527_D	52820	52919	4.00	-
1138	VID_527_D	57834	57945	4.48	-

5.2.12 Annotation data for patient P12

Gender: Female
Age at time of Video-EEG recording: 10 a
Total duration of Video-EEG: 7 h and 21 m
Total number of seizures: 25
Mean seizure duration: 3.72 s
Standard deviation: 1.29 s
Comments: -

Table 5.12: Overview of the recorded seizures of patient P12

Seizure ID	Video file name	Starting frame	Ending frame	Duration [s]	Comments

1201	VID_532_D	8671	8732	2.48	-
1202	VID_532_D	9353	9488	5.44	-
1203	VID_532_D	11218	11271	2.16	-
1204	VID_532_D	11817	11966	6.00	-
1205	VID_533_D	29106	29202	3.88	-
1206	VID_534_D	9368	9488	4.84	-
1207	VID_534_D	58865	58959	3.80	-
1208	VID_535_D	11216	11360	5.80	-
1209	VID_535_D	51144	51263	4.80	-
1210	VID_536_D	11114	11213	4.00	-
1211	VID_536_D	29322	29397	3.04	-
1212	VID_537_D	27983	28101	4.76	-
1213	VID_539_D	2712	2802	3.64	-
1214	VID_539_D	40152	40217	2.64	-
1215	VID_539_D	46879	46977	3.96	-
1216	VID_539_D	47028	47042	0.60	-
1217	VID_540_D	18946	19023	3.12	-
1218	VID_540_D	23122	23253	5.28	-
1219	VID_540_D	32565	32635	2.84	-
1220	VID_540_D	50996	51042	1.88	-
1221	VID_540_D	64067	64161	3.80	-
1222	VID_553_D	44	132	3.56	-
1223	VID_553_D	902	1011	4.40	-
1224	VID_553_D	33886	33954	2.76	-
1225	VID_553_D	45593	45680	3.52	-

5.2.13 Experiment 3 - Selected features for each patient

Table 5.13: Experiment 3: Selected features for patient P01.

MMW_Eyes_W3_Kurtosis	MXM_Mouth_W3_ENR
MMW_REye_W3_Skewness	MXM_Mouth_W3_InterquartileRange
MMW_Mouth_W3_ENR	MXM_Mouth_W3_PW3-6
MMW_Mouth_W3_Minimum	AMXM_Eyes_W3_Median_Boost
MMW_Mouth_W3_Variance_Boost	AMXM_Eyes_W3_Variance_Boost
MMW_Mouth_W3_StandardDeviation_Boost	AMXM_Eyes_W3_Kurtosis
SM_Eyes_W3_Skewness	AMXM_LEye_W3_VTI
SM_REye_W3_Skewness	AMXM_LEye_W3_MaximumMinusMinimum
THP_LEye_W3_VTI	AMXM_LEye_W3_Skewness
THP_REye_W3_Median_Boost	AMXM_REye_W3_InterquartileRange
THP_REye_W3_DominantFrequency	AMXM_REye_W3_DominantFrequency
THP_Mouth_W3_VTI	AMXM_Mouth_W3_VTI
PBFS_LEye_W3_Maximum	AMXM_Mouth_W3_EntropyEnergyBins
PBFS_REye_W3_DominantFrequency	AMXM_Mouth_W3_PW0-3
ATHP_Eyes_W3_Skewness	MXMW_Eyes_W3_VTI
ATHP_LEye_W3_VTI	MXMW_Eyes_W3_Median_Boost
ATHP_LEye_W3_Minimum	MXMW_Eyes_W3_InterquartileRange
ATHP_LEye_W3_Kurtosis	MXMW_Eyes_W3_Kurtosis
ATHP_REye_W3_ZeroCrossingRate	MXMW_LEye_W3_VTI
ATHP_Mouth_W3_Skewness	MXMW_LEye_W3_Maximum
ATHP_Mouth_W3_ZeroCrossingRate	MXMW_LEye_W3_MaximumMinusMinimum
MA_Eyes_W3_PW3-6	MXMW_LEye_W3_ZeroCrossingRate

MA_LEye_W3_EntropyEnergyBins	MXMW_REye_W3_Maximum
MA_Mouth_W3_Minimum	MXMW_REye_W3_MaximumMinusMinimum
MA_Mouth_W3_Maximum	MXMW_REye_W3_Median_Boost
MA_Mouth_W3_EntropyEnergyBins	MXMW_REye_W3_Skewness
MXM_Eyes_W3_VTI	MXMW_Mouth_W3_VTI
MXM_Eyes_W3_Median_Boost	MXMW_Mouth_W3_PW3-6
MXM_Eyes_W3_Skewness	

Table 5.14: Experiment 3: Selected features for patient P02.

MMW_LEye_W3_VTI	MA_LEye_W3_VTI
MMW_LEye_W3_DominantFrequency	MA_REye_W3_Minimum
MMW_REye_W3_ZeroCrossingRate	MA_REye_W3_Median_Boost
SM_LEye_W3_ENR	MA_REye_W3_InterquartileRange
SM_LEye_W3_EntropySpectralBins	MXM_Eyes_W3_Variance_Boost
SM_REye_W3_VTI	MXM_Eyes_W3_StandardDeviation_Boost
SM_REye_W3_InterquartileRange	MXM_Eyes_W3_MeanCrossingRate
THP_Eyes_W3_Kurtosis	MXM_LEye_W3_Maximum
THP_REye_W3_EntropySpectralBins	MXM_LEye_W3_MaximumMinusMinimum
PBFS_Eyes_W3_Maximum	MXM_Mouth_W3_Skewness
PBFS_Eyes_W3_MaximumMinusMinimum	MXM_Mouth_W3_Kurtosis
ATHP_Eyes_W3_VTI	AMXM_Eyes_W3_Variance_Boost
ATHP_LEye_W3_Median_Boost	AMXM_Eyes_W3_StandardDeviation_Boost
ATHP_REye_W3_Skewness	AMXM_LEye_W3_Variance_Boost
ATHP_REye_W3_SpectralRollOff	AMXM_LEye_W3_PW3-6
ATHP_Mouth_W3_VTI	AMXM_REye_W3_Kurtosis
ATHP_Mouth_W3_Kurtosis	AMXM_Mouth_W3_ZeroCrossingRate
MA_Eyes_W3_25SPF	MXMW_Eyes_W3_Maximum

Table 5.15: Experiment 3: Selected features for patient P03.

MMW_Eyes_W3_DominantFrequency	MA_Eyes_W3_Skewness
MMW_LEye_W3_InterquartileRange	MA_Eyes_W3_PW3-6
MMW_REye_W3_PW3-6	MA_Eyes_W3_DominantFrequency
SM_Eyes_W3_Median_Boost	MA_REye_W3_Skewness
THP_Eyes_W3_Maximum	MXM_Eyes_W3_Skewness
THP_Eyes_W3_PW3-6	AMXM_Eyes_W3_VTI
THP_LEye_W3_Maximum	MXMW_Eyes_W3_Minimum
THP_LEye_W3_ZeroCrossingRate	MXMW_Eyes_W3_MaximumMinusMinimum
ATHP_LEye_W3_ENR	MXMW_LEye_W3_Maximum
ATHP_LEye_W3_Median_Boost	MXMW_REye_W3_PW3-6
ATHP_LEye_W3_Kurtosis	

Table 5.16: Experiment 3: Selected features for patient P04.

MMW_Eyes_W3_25SPF	MA_Eyes_W3_Kurtosis
MMW_REye_W3_25SPF	MA_Eyes_W3_PW0-3
MMW_REye_W3_DominantFrequency	MA_Eyes_W3_DominantFrequency
MMW_Mouth_W3_ENR	MA_LEye_W3_Minimum
MMW_Mouth_W3_DominantFrequency	MA_LEye_W3_MaximumMinusMinimum
SM_LEye_W3_VTI	MA_LEye_W3_Kurtosis
SM_LEye_W3_25SPF	MA_LEye_W3_PW0-3
THP_Eyes_W3_EntropyEnergyBins	MA_LEye_W3_DominantFrequency

THP_REye_W3_PW0-3	MA_Mouth_W3_25SPF
PBFS_REye_W3_Kurtosis	MA_Mouth_W3_PW3-6
PBFS_REye_W3_PW0-3	MXM_LEye_W3_25SPF
PBFS_Mouth_W3_Mean_Boost	MXM_REye_W3_PW3-6
ATHP_LEye_W3_Kurtosis	AMXM_LEye_W3_25SPF
ATHP_Mouth_W3_Minimum	AMXM_LEye_W3_PW0-3
ATHP_Mouth_W3_Skewness	MXMW_Mouth_W3_SpectralCentroid

Table 5.17: Experiment 3: Selected features for patient P06.

MMW_Eyes_W3_PW3-6	PBFS_Mouth_W3_MaximumMinusMinimum
MMW_REye_W3_Maximum	PBFS_Mouth_W3_Kurtosis
MMW_Mouth_W3_InterquartileRange	ATHP_Mouth_W3_MaximumMinusMinimum
MMW_Mouth_W3_Skewness	ATHP_Mouth_W3_InterquartileRange
SM_Eyes_W3_InterquartileRange	ATHP_Mouth_W3_Kurtosis
SM_REye_W3_InterquartileRange	ATHP_Mouth_W3_25SPF
SM_Mouth_W3_VTI	ATHP_Mouth_W3_DominantFrequency
SM_Mouth_W3_Maximum	MA_Eyes_W3_Minimum
SM_Mouth_W3_Skewness	MA_Mouth_W3_MeanCrossingRate
SM_Mouth_W3_EntropyEnergyBins	MXM_Mouth_W3_VTI
THP_Eyes_W3_VTI	AMXM_Mouth_W3_ENR
THP_REye_W3_Maximum	AMXM_Mouth_W3_Minimum
THP_Mouth_W3_VTI	AMXM_Mouth_W3_Median_Boost
THP_Mouth_W3_Median_Boost	MXMW_Eyes_W3_Minimum
PBFS_Eyes_W3_Median_Boost	MXMW_Eyes_W3_Skewness

Table 5.18: Experiment 3: Selected features for patient P07.

MMW_Mouth_W3_Median_Boost	ATHP_Mouth_W3_Kurtosis
SM_REye_W3_Median_Boost	ATHP_Mouth_W3_ZeroCrossingRate
SM_REye_W3_EntropySpectralBins	ATHP_Mouth_W3_PW0-3
THP_Eyes_W3_Median_Boost	ATHP_Mouth_W3_PW3-6
THP_REye_W3_Maximum	MA_LEye_W3_ZeroCrossingRate
THP_REye_W3_Median_Boost	MA_REye_W3_Kurtosis
THP_Mouth_W3_Skewness	MXM_REye_W3_Median_Boost
PBFS_Eyes_W3_PW0-3	MXM_Mouth_W3_Maximum
PBFS_LEye_W3_PW3-6	MXM_Mouth_W3_InterquartileRange
PBFS_REye_W3_Maximum	MXM_Mouth_W3_Skewness
PBFS_Mouth_W3_Kurtosis	MXM_Mouth_W3_EntropyEnergyBins
PBFS_Mouth_W3_PW3-6	AMXM_REye_W3_Variance_Boost
ATHP_Eyes_W3_VTI	AMXM_REye_W3_StandardDeviation_Boost
ATHP_REye_W3_Variance_Boost	AMXM_Mouth_W3_EntropySpectralBins
ATHP_REye_W3_StandardDeviation_Boost	MXMW_LEye_W3_Skewness
ATHP_Mouth_W3_Minimum	MXMW_Mouth_W3_EntropyEnergyBins

Table 5.19: Experiment 3: Selected features for patient P08.

MMW_Eyes_W3_Mean_Boost	MA_LEye_W3_StandardDeviation_Boo
MMW_LEye_W3_VTI	MA_LEye_W3_Kurtosis
MMW_LEye_W3_PW3-6	MA_LEye_W3_PW3-6
MMW_REye_W3_VTI	MA_LEye_W3_SpectralRollOff
MMW_REye_W3_ZeroCrossingRate	MA_REye_W3_VTI
MMW_REye_W3_EntropyEnergyBins	MA_REye_W3_Minimum

SM_LEye_W3_Skewness	MA_REye_W3_Median_Boost
SM_REye_W3_VTI	MA_REye_W3_InterquartileRange
SM_REye_W3_InterquartileRange	MA_REye_W3_PW3-6
SM_REye_W3_EntropyEnergyBins	MA_REye_W3_SpectralRollOff
THP_LEye_W3_Mean_Boost	MA_REye_W3_SpectralCentroid
THP_LEye_W3_Skewness	MA_Mouth_W3_Maximum
THP_LEye_W3_Kurtosis	MA_Mouth_W3_Variance_Boost
THP_LEye_W3_EntropyEnergyBins	MA_Mouth_W3_InterquartileRange
THP_LEye_W3_PW3-6	MXM_LEye_W3_ENR
THP_REye_W3_VTI	MXM_REye_W3_ZeroCrossingRate
THP_REye_W3_ENR	AMXM_Eyes_W3_MeanCrossingRate
THP_REye_W3_MaximumMinusMinimum	AMXM_Eyes_W3_SpectralRollOff
THP_REye_W3_InterquartileRange	AMXM_LEye_W3_VTI
THP_REye_W3_Kurtosis	AMXM_LEye_W3_PW3-6
THP_REye_W3_EntropyEnergyBins	AMXM_REye_W3_VTI
THP_Mouth_W3_MaximumMinusMinimum	AMXM_REye_W3_Minimum
THP_Mouth_W3_Median_Boost	AMXM_REye_W3_Kurtosis
PBFS_LEye_W3_MeanCrossingRate	AMXM_REye_W3_MeanCrossingRate
PBFS_Mouth_W3_VTI	AMXM_Mouth_W3_ENR
ATHP_Eyes_W3_VTI	AMXM_Mouth_W3_MaximumMinusMinimu
ATHP_Eyes_W3_Median_Boost	AMXM_Mouth_W3_SpectralRollOff
ATHP_Eyes_W3_Variance_Boost	MXMW_LEye_W3_VTI
ATHP_REye_W3_Median_Boost	MXMW_LEye_W3_Median_Boost
ATHP_REye_W3_Variance_Boost	MXMW_LEye_W3_EntropySpectralBins
MA_Eyes_W3_PW3-6	MXMW_REye_W3_VTI
MA_LEye_W3_VTI	MXMW_REye_W3_Maximum
MA_LEye_W3_Minimum	MXMW_REye_W3_EntropySpectralBins
MA_LEye_W3_Variance_Boost	

5.2.14 Experiment 4 - Union of selected features for each patient

Table 5.20: Experiment 4: Union of selected features for each patient.

MMW_Eyes_W3_Mean_Boost	MA_Eyes_W3_Skewness
MMW_Eyes_W3_Kurtosis	MA_Eyes_W3_Kurtosis
MMW_Eyes_W3_25SPF	MA_Eyes_W3_25SPF
MMW_Eyes_W3_PW3-6	MA_Eyes_W3_PW0-3
MMW_Eyes_W3_DominantFrequency	MA_Eyes_W3_PW3-6
MMW_LEye_W3_VTI	MA_Eyes_W3_DominantFrequency
MMW_LEye_W3_InterquartileRange	MA_LEye_W3_VTI
MMW_LEye_W3_PW3-6	MA_LEye_W3_Minimum
MMW_LEye_W3_DominantFrequency	MA_LEye_W3_MaximumMinusMinimum
MMW_REye_W3_VTI	MA_LEye_W3_Variance_Boost
MMW_REye_W3_Maximum	MA_LEye_W3_StandardDeviation_Boost
MMW_REye_W3_Skewness	MA_LEye_W3_Kurtosis
MMW_REye_W3_ZeroCrossingRate	MA_LEye_W3_ZeroCrossingRate
MMW_REye_W3_EntropyEnergyBins	MA_LEye_W3_EntropyEnergyBins
MMW_REye_W3_25SPF	MA_LEye_W3_PW0-3
MMW_REye_W3_PW3-6	MA_LEye_W3_PW3-6
MMW_REye_W3_DominantFrequency	MA_LEye_W3_DominantFrequency
MMW_Mouth_W3_ENR	MA_LEye_W3_SpectralRollOff
MMW_Mouth_W3_Minimum	MA_REye_W3_VTI

MMW_Mouth_W3_Median_Boost
MMW_Mouth_W3_Variance_Boost
MMW_Mouth_W3_StandardDeviation_Boost
MMW_Mouth_W3_InterquartileRange
MMW_Mouth_W3_Skewness
MMW_Mouth_W3_DominantFrequency
SM_Eyes_W3_Median_Boost
SM_Eyes_W3_InterquartileRange
SM_Eyes_W3_Skewness
SM_LEye_W3_VTI
SM_LEye_W3_ENR
SM_LEye_W3_Skewness
SM_LEye_W3_25SPF
SM_LEye_W3_EntropySpectralBins
SM_REye_W3_VTI
SM_REye_W3_Median_Boost
SM_REye_W3_InterquartileRange
SM_REye_W3_Skewness
SM_REye_W3_EntropyEnergyBins
SM_REye_W3_EntropySpectralBins
SM_Mouth_W3_VTI
SM_Mouth_W3_Maximum
SM_Mouth_W3_Skewness
SM_Mouth_W3_EntropyEnergyBins
THP_Eyes_W3_VTI
THP_Eyes_W3_Maximum
THP_Eyes_W3_Median_Boost
THP_Eyes_W3_Kurtosis
THP_Eyes_W3_EntropyEnergyBins
THP_Eyes_W3_PW3-6
THP_LEye_W3_VTI
THP_LEye_W3_Maximum
THP_LEye_W3_Mean_Boost
THP_LEye_W3_Skewness
THP_LEye_W3_Kurtosis
THP_LEye_W3_ZeroCrossingRate
THP_LEye_W3_EntropyEnergyBins
THP_LEye_W3_PW3-6
THP_REye_W3_VTI
THP_REye_W3_ENR
THP_REye_W3_Maximum
THP_REye_W3_MaximumMinusMinimum
THP_REye_W3_Median_Boost
THP_REye_W3_InterquartileRange
THP_REye_W3_Kurtosis
THP_REye_W3_EntropyEnergyBins
THP_REye_W3_PW0-3
THP_REye_W3_DominantFrequency
THP_REye_W3_EntropySpectralBins
THP_Mouth_W3_VTI
THP_Mouth_W3_MaximumMinusMinimum
THP_Mouth_W3_Median_Boost
THP_Mouth_W3_Skewness
PBFS_Eyes_W3_Maximum
PBFS_Eyes_W3_MaximumMinusMinimum
MA_REye_W3_Minimum
MA_REye_W3_Median_Boost
MA_REye_W3_InterquartileRange
MA_REye_W3_Skewness
MA_REye_W3_Kurtosis
MA_REye_W3_PW3-6
MA_REye_W3_SpectralRollOff
MA_REye_W3_SpectralCentroid
MA_Mouth_W3_Minimum
MA_Mouth_W3_Maximum
MA_Mouth_W3_Variance_Boost
MA_Mouth_W3_InterquartileRange
MA_Mouth_W3_MeanCrossingRate
MA_Mouth_W3_EntropyEnergyBins
MA_Mouth_W3_25SPF
MA_Mouth_W3_PW3-6
MXM_Eyes_W3_VTI
MXM_Eyes_W3_Median_Boost
MXM_Eyes_W3_Variance_Boost
MXM_Eyes_W3_StandardDeviation_Boost
MXM_Eyes_W3_Skewness
MXM_Eyes_W3_MeanCrossingRate
MXM_LEye_W3_ENR
MXM_LEye_W3_Maximum
MXM_LEye_W3_MaximumMinusMinimum
MXM_LEye_W3_25SPF
MXM_REye_W3_Median_Boost
MXM_REye_W3_ZeroCrossingRate
MXM_REye_W3_PW3-6
MXM_Mouth_W3_VTI
MXM_Mouth_W3_ENR
MXM_Mouth_W3_Maximum
MXM_Mouth_W3_InterquartileRange
MXM_Mouth_W3_Skewness
MXM_Mouth_W3_Kurtosis
MXM_Mouth_W3_EntropyEnergyBins
MXM_Mouth_W3_PW3-6
AMXM_Eyes_W3_VTI
AMXM_Eyes_W3_Median_Boost
AMXM_Eyes_W3_Variance_Boost
AMXM_Eyes_W3_StandardDeviation_Boost
AMXM_Eyes_W3_Kurtosis
AMXM_Eyes_W3_MeanCrossingRate
AMXM_Eyes_W3_SpectralRollOff
AMXM_LEye_W3_VTI
AMXM_LEye_W3_MaximumMinusMinimum
AMXM_LEye_W3_Variance_Boost
AMXM_LEye_W3_Skewness
AMXM_LEye_W3_25SPF
AMXM_LEye_W3_PW0-3
AMXM_LEye_W3_PW3-6
AMXM_REye_W3_VTI
AMXM_REye_W3_Minimum
AMXM_REye_W3_Variance_Boost
AMXM_REye_W3_StandardDeviation_Boost

PBFS_Eyes_W3_Median_Boost	AMXM_REye_W3_InterquartileRange
PBFS_Eyes_W3_PW0-3	AMXM_REye_W3_Kurtosis
PBFS_LEye_W3_Maximum	AMXM_REye_W3_MeanCrossingRate
PBFS_LEye_W3_MeanCrossingRate	AMXM_REye_W3_DominantFrequency
PBFS_LEye_W3_PW3-6	AMXM_Mouth_W3_VTI
PBFS_REye_W3_Maximum	AMXM_Mouth_W3_ENR
PBFS_REye_W3_Kurtosis	AMXM_Mouth_W3_Minimum
PBFS_REye_W3_PW0-3	AMXM_Mouth_W3_MaximumMinusMinimum
PBFS_REye_W3_DominantFrequency	AMXM_Mouth_W3_Median_Boost
PBFS_Mouth_W3_VTI	AMXM_Mouth_W3_ZeroCrossingRate
PBFS_Mouth_W3_MaximumMinusMinimum	AMXM_Mouth_W3_EntropyEnergyBins
PBFS_Mouth_W3_Mean_Boost	AMXM_Mouth_W3_PW0-3
PBFS_Mouth_W3_Kurtosis	AMXM_Mouth_W3_EntropySpectralBins
PBFS_Mouth_W3_PW3-6	AMXM_Mouth_W3_SpectralRollOff
ATHP_Eyes_W3_VTI	MXMW_Eyes_W3_VTI
ATHP_Eyes_W3_Median_Boost	MXMW_Eyes_W3_Minimum
ATHP_Eyes_W3_Variance_Boost	MXMW_Eyes_W3_Maximum
ATHP_Eyes_W3_Skewness	MXMW_Eyes_W3_MaximumMinusMinimum
ATHP_LEye_W3_VTI	MXMW_Eyes_W3_Median_Boost
ATHP_LEye_W3_ENR	MXMW_Eyes_W3_InterquartileRange
ATHP_LEye_W3_Minimum	MXMW_Eyes_W3_Skewness
ATHP_LEye_W3_Median_Boost	MXMW_Eyes_W3_Kurtosis
ATHP_LEye_W3_Kurtosis	MXMW_LEye_W3_VTI
ATHP_REye_W3_Median_Boost	MXMW_LEye_W3_Maximum
ATHP_REye_W3_Variance_Boost	MXMW_LEye_W3_MaximumMinusMinimum
ATHP_REye_W3_StandardDeviation_Boost	MXMW_LEye_W3_Median_Boost
ATHP_REye_W3_Skewness	MXMW_LEye_W3_Skewness
ATHP_REye_W3_ZeroCrossingRate	MXMW_LEye_W3_ZeroCrossingRate
ATHP_REye_W3_SpectralRollOff	MXMW_LEye_W3_EntropySpectralBins
ATHP_Mouth_W3_VTI	MXMW_REye_W3_VTI
ATHP_Mouth_W3_Minimum	MXMW_REye_W3_Maximum
ATHP_Mouth_W3_MaximumMinusMinimum	MXMW_REye_W3_MaximumMinusMinimum
ATHP_Mouth_W3_InterquartileRange	MXMW_REye_W3_Median_Boost
ATHP_Mouth_W3_Skewness	MXMW_REye_W3_Skewness
ATHP_Mouth_W3_Kurtosis	MXMW_REye_W3_PW3-6
ATHP_Mouth_W3_ZeroCrossingRate	MXMW_REye_W3_EntropySpectralBins
ATHP_Mouth_W3_25SPF	MXMW_Mouth_W3_VTI
ATHP_Mouth_W3_PW0-3	MXMW_Mouth_W3_EntropyEnergyBins
ATHP_Mouth_W3_PW3-6	MXMW_Mouth_W3_PW3-6
ATHP_Mouth_W3_DominantFrequency	MXMW_Mouth_W3_SpectralCentroid
MA_Eyes_W3_Minimum	

5.2.15 Experiment 6 - Selected features from all patients

Table 5.21: Experiment 6: Selected features from all patients.

MMW_Eyes_W3_Minimum	MA_Eyes_W3_SpectralCentroid
MMW_Eyes_W3_Median_Boost	MA_LEye_W3_VTI
MMW_Eyes_W3_DominantFrequency	MA_LEye_W3_Minimum
MMW_LEye_W3_VTI	MA_LEye_W3_Median_Boost
MMW_LEye_W3_Median_Boost	MA_LEye_W3_InterquartileRange
MMW_LEye_W3_25SPF	MA_LEye_W3_25SPF
MMW_REye_W3_VTI	MA_LEye_W3_PW0-3
MMW_REye_W3_DominantFrequency	MA_LEye_W3_DominantFrequency

SM_Eyes_W3_Minimum	MA_REye_W3_VTI
SM_Eyes_W3_Maximum	MA_REye_W3_Minimum
SM_REye_W3_PW3-6	MA_REye_W3_Median_Boost
THP_Eyes_W3_PW3-6	MA_REye_W3_MeanCrossingRate
THP_LEye_W3_EntropyEnergyBins	MA_REye_W3_EntropySpectralBins
THP_LEye_W3_PW3-6	MA_Mouth_W3_Minimum
THP_REye_W3_VTI	MA_Mouth_W3_Maximum
THP_REye_W3_ENR	MA_Mouth_W3_MaximumMinusMinimum
THP_REye_W3_MaximumMinusMinimum	MA_Mouth_W3_Kurtosis
THP_Mouth_W3_Maximum	MA_Mouth_W3_PW0-3
THP_Mouth_W3_Median_Boost	MA_Mouth_W3_PW3-6
PBFS_Eyes_W3_VTI	MXM_Eyes_W3_Variance_Boost
PBFS_Eyes_W3_Maximum	MXM_Eyes_W3_Kurtosis
PBFS_Eyes_W3_MaximumMinusMinimum	MXM_LEye_W3_Skewness
PBFS_Eyes_W3_InterquartileRange	MXM_LEye_W3_Kurtosis
PBFS_Eyes_W3_DominantFrequency	AMXM_Eyes_W3_Kurtosis
PBFS_Eyes_W3_SpectralRollOff	AMXM_LEye_W3_Minimum
PBFS_LEye_W3_Maximum	AMXM_LEye_W3_MaximumMinusMinimum
PBFS_LEye_W3_StandardDeviation_Boost	AMXM_LEye_W3_Variance_Boost
PBFS_LEye_W3_25SPF	AMXM_LEye_W3_PW3-6
PBFS_REye_W3_Median_Boost	AMXM_Mouth_W3_ENR
PBFS_REye_W3_DominantFrequency	AMXM_Mouth_W3_Minimum
PBFS_Mouth_W3_VTI	AMXM_Mouth_W3_Median_Boost
PBFS_Mouth_W3_PW0-3	AMXM_Mouth_W3_SpectralRollOff
PBFS_Mouth_W3_PW3-6	MXMW_Eyes_W3_InterquartileRange
ATHP_Eyes_W3_Median_Boost	MXMW_Eyes_W3_Skewness
ATHP_Eyes_W3_Variance_Boost	MXMW_LEye_W3_VTI
ATHP_Eyes_W3_InterquartileRange	MXMW_LEye_W3_MaximumMinusMinimum
ATHP_Eyes_W3_Kurtosis	MXMW_REye_W3_VTI
ATHP_LEye_W3_Skewness	MXMW_REye_W3_Skewness
ATHP_REye_W3_Variance_Boost	MXMW_Mouth_W3_ENR
MA_Eyes_W3_Variance_Boost	MXMW_Mouth_W3_Skewness
MA_Eyes_W3_InterquartileRange	

References

[1] Haar cascades repository, 2011. URL `http://alereimondo.no-ip.org/OpenCV/34`.

[2] U.R. Acharya, F. Molinari, S.V. Sree, Chattopadhyay S., Ng K.H., and Suri J.S. Automated diagnosis of epileptic eeg using entropies. *Biomedical Signal Processing and Control*, 7(4):401–408, 2012.

[3] D. Aha and D. Kibler. Instance-based learning algorithms. machine learning. *Machine*, 6:37–66, 1991.

[4] S. Altunay, Z. Telatar, and O. Erogul. Epileptic eeg detection using the linear prediction error energy. *Expert Systems with Applications*, 37(8):5661–5665, 2010.

[5] S. Benbadis. The differential diagnosis of epilepsy: A critical review. *Epilepsy & Behavior*, 15(1): 15–21, May 2009. ISSN 1525-5069.

[6] A.T. Berg and I.E. Scheffer. New concepts in classification of the epilepsies: Entering the 21st century. *Epilepsia*, 52(6):1058–1062, 2011.

[7] A.T. Berg, S.F. Berkovic, M.J. Brodie, J. Buchhalter, J.H. Cross, W. van Emde Boas, J. Engel, J. French, T.A. Glauser, G.W. Mathern, S.L. Moshé, D Nordli, P Plouin, and I.E. Scheffer. Revised terminology and concepts for organization of seizures and epilepsies: Report of the ILAE Commission on Classification and Terminology, 2005–2009. *Epilepsia*, 51(4):676–685, 2010.

[8] A.M. Beun, T Gutter, and J. Overweg. Home EEG and video monitoring in epilepsy: first experiences. *Clinical Neurology and Neurosurgery*, 96:257–260, 1994.

[9] R.R. Bouckaert. Bayesian network classifiers in weka for version 3-5-7. Technical report, University of Waikato, New Zealand, 2008.

[10] G. Bradski. The OpenCV Library. *Dr. Dobb's Journal of Software Tools*, 2000.

[11] Gary Bradski and Adrian Kaehler. *Learning OpenCV*. O'Reilly Media, 2008.

[12] M. Castrillón-Santana, O. Déniz-Suárez, L. Antón-Canalís, , and J. Lorenzo-Navarro. Face and facial feature detection evaluation. In *International Conference on Computer Vision Theory and Applications*, 2008.

[13] D. Chadwick and D. Smith. The misdiagnosis of epilepsy. *British Medical Journal*, 324(7336): 495–496, March 2002.

[14] Munshi S (2009) Chandaka S, Chatterjee A. Cross-correlation aided support vector machine classifier for classification of eeg signals. *Expert Systems with Applications*, 36(2):1329–1336, 2009.

[15] V. Chandola, A. Banerjee, and V. Kumar. Anomaly Detection: A Survey. *ACM Computing Surveys*, 41(3):15:1–15:58, 2009.

[16] L. Chen, X. Yang, Y. Liu, D. Zeng, Y. Tang, B. Yan, X. Lin, L. Liu, H. Xu, and D. Zhou. Quantitative and trajectory analysis of movement trajectories in supplementary motor area seizures of frontal lobe epilepsy. *Epilepsy & Behavior*, 14:344–353, 2009.

[17] L. Chisci, A. Mavino, G. Perferi, M. Sciandrone, C. Anile, G. Colicchio, and F. Fuggetta. Real-time epileptic seizure prediction using ar models and support vector machines. *IEEE Transactions on Biomedical Engineering*, 57(5):1124–1132, 2010.

[18] J.F. Cohn. Foundations of human computing: Facial expression and emotion. In T. Huang, A. Nijholt, M. Pantic, and A. Pentland, editors, *Artifical Intelligence for Human Computing*, volume 4451 of *LNCS*, pages 1–16. Springer, Berlin, Heidelberg, 2007.

[19] Commission on Classification and Terminology of the International League Against Epilepsy. Proposal for Revised Clinical and Electroencephalographic Classification of Epileptic Seizures. *Epilepsia*, 22:489–501, 1981.

[20] Commission on Classification and Terminology of the International League Against Epilepsy. Proposal for Revised Classification of Epilepsies and Epileptic Syndromes. *Epilepsia*, 30(4):389–399, 1989.

[21] G. Cooper and E. Herskovitz. A bayesian method for the induction of probabilistic networks from data. *Machine Learning*, 9:330–347, 1992.

[22] J. P. S. Cunha, J. M. Fernandes, V.F. Bento, L. M. Paula, E. Dias, C. Bilgin, and S. Noachtar. 2D versus 3D approaches to movement quantification in epileptic seizures: Simulations and real seizures comparative evaluation. *Epilepsia*, 51, suppl. 4:56, 2010.

[23] J.P.S. Cunha, C. Vollmar, Z. Li, J. Fernandes, B. Feddersen, and S. Noachtar. Movement quantification during epileptic seizures: a new technical contribution to the evaluation of seizure semiology,. In *25th Annual International Conference of the IEEE EMBS*, pages 671–673, 2003.

[24] J.P.S. Cunha, J. Fernandes, V. Bento, L. Paula, F. Oliveira, C. Bilgin, and S. Noachtar. 3D movement quantification in epilepsy: new contribution for quantitative semiology analysis. *Epilepsia*, 50, suppl. 10:84, 2009.

[25] J.P.S. Cunha, C. Vollmar, J.M. Fernandes, and S. Noachtar. Automated epileptic seizure type classification through quantitative movement analysis. In *Medical Physics and Biomedical Engineering World Congress*, volume 25, pages 1435–1438, 2009.

[26] J.P.S. Cunha, J.M. Fernandes, A. Peters, C. Bilgin, J. Rémi, Z. Mirzadjanona, J.A. Gonzalez-Victores, and S. Noachtar. Quantitative analysis of upper limb automatisms in temporal and frontal lobe epilepsy. *Epilepsia*, 51, suppl. 4:53, 2010.

[27] J.P.S. Cunha, L.M. Paula, V.F. Bento, C. Bilgin, E. Dias, and S. Noachtar. Movement quantification in epileptic seizures: A feasibility study for a new 3D approach. *Medical Engineering & Physics*, 2012.

[28] K. Cuppens, L. Lagae, and B. Vanrumste. Towards automatic detection of movement during sleep in pediatric patients with epilepsy by means of video recordings and the optical flow algorithm,. In *4th European Conference of the International Federation for Medical and Biological Engineering*, volume 22, pages 784–789, 2008.

[29] K. Cuppens, L. Lagae, B. Ceulemans, S. Van Huffel, and B. Vanrumste. Automatic video detection of body movement during sleep based on optical flow in pediatric patients with epilepsy. *Medical & Biological Engineering & Computing*, 2010.

[30] K. Cuppens, B. Vanrumste, L. Lagae, B. Ceulemans, and S. Van Huffel. Detection of epileptic seizures using video data. In *6th International Conference on Intelligent Environments*, 2010.

[31] M.L.C. Dal-Cól, V.C. Terra-Bustamante, T.R. Velasco, J.A.C. Oliveira, A.C. Sakamoto, and N. Garcia-Cairasco. Neuroethology application for the study of human temporal lobe epilepsy: From basic to applied sciences. *Epilepsy & Behavior*, 8:149–160, 2006.

[32] W. Dargie. Analysis of time and frequency domain features of accelerometer measurements. In *18th Internatonal Conference on Computer Communications and Networks*, 2009.

[33] N. Degtyarev and O. Seredin. Comparative testing of face detection algorithms. In A. Elmoataz, O. Lezoray, F. Nouboud, D. Mammass, and J. Meunier, editors, *Image and Signal Processing*, LNCS 6134, pages 200–209. Springer-Verlag Berlin Heidelberg, 2010.

[34] P. Ekman and W. Friesen. *Facial Action Coding System: A Technique for the Measurement of Facial Movement*. Consulting Psychologists Press, Palo Alto, 1978.

[35] J. Engel. A Proposed Diagnostic Scheme for People with Epileptic Seizures and with Epilepsy: Report of the ILAE Task Force on classification and Terminology. *Epilepsia*, 42(6):769–803, 2001.

[36] J. Engel. ILAE classification of epilepsy syndromes. *Epilepsy Research*, 70S:5–10, 2006.

[37] R. Esteller, G. Vachtsevanos, J. Echauz, and B. (2001) Litt. A comparison of waveform fractal dimension algorithms. *IEEE Transactions on Circuits and Systems I: Fundamental Theory and Applications*, 48(2):177–183, 2001.

[38] G. Farnebäck. Two-frame motion estimation based on polynomial expansion. In *13th Scandinavian Conference on Image Analysis*, volume 2749 of *LNCS*, 2003.

[39] T. Fathima, M. Bedeeuzzaman, O. Farooq, and Y. Khan. Wavelet based features for epileptic seizure detection. *MES Journal of Technology and Management*, 2(1):108–112, 2011.

[40] P. Faure and H. Korn. Is there chaos in the brain? I. Concepts of nonlinear dynamics and methods of investigation. *Comptes Rendus de l'Académie des Sciences - Series III - Sciences de la Vie*, 324 (9):773–793, 2001.

[41] R.S. Fisher, W van Emde Boas, W. Blume, C. Elger, P. Genton, P. Lee, and J. Engel. Epileptic Seizures and Epilepsy: Definitions Proposed by the Inernational League Against Epilepsy (ILAE) and the International Bureau for Epilepsy (IBE). *Epilepsia*, 46(4):470–472, 2005.

[42] R.S. Fisher, C. Acevedo, A. Arzimanoglou, A. Bogacz, J.H. Cross, C.E. Elger, J. Engel, L. Forsgren, J.A. French, M. Glynn, D.C. Hesdorffer, B.I. Lee, G.W. Mathern, S.L. Moshé, E. Perucca, I.E. Scheffer, T. Tomson, M. Watanabe, and S. Wiebe. ILAE Official Report: A practical clinical definition of epilepsy. *Epilepsia*, 55(4):475–482, 2014. ISSN 1528-1167. URL `http://dx.doi.org/10.1111/epi.12550`.

[43] L. Forsgren, E. Beghi, A. Õun, and M. Sillanpää. The epidemiology of epilepsy in Europe – a systematic review. *European Journal of Neurology*, 12(4):245–253, 2005. ISSN 1468-1331. doi: 10.1111/j.1468-1331.2004.00992.x.

[44] Y Freund and R.E. Schapire. Experiments with a new boosting algorithm. In *Thirteenth International Conference on Machine Learning*, pages 148–156, 1996.

[45] M. Galassi, J. Davies, J. Theiler, B. Gough, G. Jungman, P. Alken, M. Booth, and F. Rossi. *GNU Scientific Library Reference Manual - Third Edition*. Network Theory Ltd., 3rd edition, 2009.

[46] G. Giannakakis, V. Sakkalis, M. Pediaditis, and M. Tsiknakis. *Neuromethods, Chapter 68 - Methods for Seizure Detection and Prediction: An Overview.* Springer Science+Business Media New York, 2014.

[47] J. Gotman, J.R. Ives, P. Gloor, A. Olivier, and L.F. Quesney. Changes in interictal eeg spiking and seizure occurrence in humans. *Epilepsia*, 23(4):432–433, 1982.

[48] N.F. Güler, E.D. Übeyli, and İ. , Güler. Recurrent neural networks employing Lyapunov exponents for EEG signals classification. *Expert Systems with Applications*, 29(3):506–514, 2005.

[49] M. Hall, E. Frank, G. Holmes, B. Pfahringer, P. Reutemann, and I.H. Witten. The WEKA Data Mining Software: An Update. *SIGKDD Explorations*, 11(1), 2009.

[50] M.A. Hall. *Correlation-based Feature Subset Selection for Machine Learning.* PhD thesis, Univeristy of Waikato, New Zealand, 1999.

[51] H Hassanpour, M. Mesbah, and B. Boashash. Time-frequency based newborn eeg seizure detection using low and high frequency signatures. *Physiological Measurement*, 25(4):935–944, 2004.

[52] W.A. Hauser, J.F. Annegers, and L.T. Kurland. Prevalence of epilepsy in Rochester, Minnesota: 1940–1980. *Epilepsia*, 32:429–445, 1991.

[53] L.D. Iasemidis, D.S. Shiau, W. Chaovalitwongse, J.C. Sackellares, P.M. Pardalos, J.C. Principe, P.R. Carney, A. Prasad, B. Veeramani, and K. Tsakalis. Adaptive epileptic seizure prediction system. *IEEE Transactions on Biomedical Engineering*, 50(5):616–627, 2003.

[54] R. Jain and I. Chlamtac. The P^2 algorithmus for dynamic calculation of quantiles and histograms without storing observations. *Communications of the ACM*, 28(10):1076–1085, 1985.

[55] G.H. John and P. Langley. Estimating continuous distributions in bayesian classifiers. In *Eleventh Conference on Uncertainty in Artificial Intelligence, San Mateo*, pages 338–345, 1995.

[56] K. Jostschulte, A. Amer, M. Schu, and H. Schröder. A subband based spatio-temporal noise reduction technique for interlaced video signals. In *IEEE International Conference on Consumer Electronics*, 1998.

[57] P. KaewTraKulPong and R. Bowden. An improved adaptive background mixture model for real-time tracking with shadow detection. In *2nd European Workshop on Advanced Video Based Surveillance Systems*, Sept. 2001.

[58] S Kalitzin, G Petkov, D Velis, B Vledder, and F.L. da Silva. Automatic segmentation of episodes containing epileptic clonic seizures in video sequences. *IEEE Transactions on Biomedical Engineering*, 59(12):3379–3385, 2012.

[59] H. Kantz and T. Schreiber. *Nonlinear time series analysis.* Cambridge University Press, 2004.

[60] N.B. Karayiannis. Advancing videometry through applications: quantification of neonatal seizures from video recordings. In *14th International Conference on Digital Signal Processing*, 2002.

[61] N.B. Karayiannis and G. Tao. Extraction of temporal motion velocity signals from video recordings of neonatal seizures by optical flow methods. In *25th Annual International Conference of the IEEE EMBS*, 2003.

[62] N.B. Karayiannis and G. Tao. Improving the extraction of temporal motion strength signals from video recordings of neonatal seizures. In *IEEE Conference on Advances in Video and Signal Based Surveillance*, 2003.

[63] N.B. Karayiannis and G. Tao. An improved procedure for the extraction of temporal motion strength signals from video recordings of neonatal seizures. *Image and Vision Computing*, 24(1): 27–40, 2006.

[64] N.B. Karayiannis and Y. Xiong. Extraction of temporal motor activity signals from video recordings of neonatal seizures by feature tracking methods based on deformable motion models. In *25th Annual International Conference of the IEEE EMBS*, 2003.

[65] N.B. Karayiannis, S. Srinivasan, R. Bhattacharya, M.S. Wise, J.D. Frost Jr., and E.M. Mizrahi. Extraction of motion strength and motor activity signals from video recordings of neonatal seizures. *IEEE Transactions on Medical Imaging*, 20(9):965–980, 2001.

[66] N.B. Karayiannis, A. Sami, J.D. Frost Jr., M.S. Wise, and E.M. Mizrahi. Quantifying motion in video recordings of neonatal seizures by feature trackers based on predictive block matching. In *26th Annual International Conference of the IEEE EMBS*, 2004.

[67] N.B. Karayiannis, G Tao, B. Varughese, J.D. Frost Jr., M.S. Wise, and E.M. Mizrahi. Discrete optical flow estimation methods and their application in the extraction of motion strength signals from video recordings of neonatal seizures. In *26th Annual International Conference of the IEEE EMBS*, 2004.

[68] N.B. Karayiannis, A. Sami, J.D. Frost Jr., M.S. Wise, and E.M. Mizrahi. Automated extraction of temporal motor activity signals from video recordings of neonatal seizures based on adaptive block matching. *IEEE Transactions on Biomedical Engineering*, 52(6):676–686, 2005.

[69] N.B. Karayiannis, G. Tao, Y. Xiong, A. Sami, B. Varughese, J.D. Frost Jr., and E.M. Wise, M.S. Mizrahi. Computerized motion analysis of videotaped neonatal seizures of epileptic origin. *Epilepsia*, 46(6):901–917, 2005.

[70] N.B. Karayiannis, B. Varughese, G. Tao, J.D. Frost Jr., M.S. Wise, and E.M. Mizrahi. Quantifying motion in video recordings of neonatal seizures by regularized optical flow methods. *IEEE Transactions on Image Processing*, 14(7):890–903, 2005.

[71] N.B. Karayiannis, J.D. Xiong, Y. amd Frost Jr., M.S. Wise, and E.M. Mizrahi. Quantifying motion in video recordings of neonatal seizures by robust motion trackers based on block motion models. *IEEE Transactions on Biomedical Engineering*, 52(6):1065–1077, 2005.

[72] N.B. Karayiannis, Y. Xiong, J.D. Frost Jr., M.S. Wise, and E.M. Mizrahi. Improving the accuracy and reliability of motion tracking methods used for extracting temporal motor activity signals from video recordings of neonatal seizures. *IEEE Transactions on Biomedical Engineering*, 52(4): 747–749, 2005.

[73] N.B. Karayiannis, G. Tao, J.D. Frost Jr., M.S. Wise, R.A. Hrachovy, and E.M. Mizrahi. Automated detection of videotaped neonatal seizures based on motion segmentation methods. *Clinical Neurophysiology*, 117(7):1585–1594, 2006.

[74] S.P. Kumar, Sriraam. N., P.G. Benakop, and B.C. Jinaga. Entropies based detection of epileptic seizures with artificial neural network classifiers. *Expert Systems with Applications*, 37(4):3284–3291, 2010.

[75] M. Le Van Quyen, C. Adam, J. Martinerie, M. Baulac, S. Clemenceau, and F. Varela. Spatio-temporal characterizations of nonlinear changes in intracranial activities prior to human temporal lobe seizures. *European Journal of Neuroscience*, 16(6):2124–2134, 2000.

[76] Z. Li, A. Martins da Silva, and J. P. S. Cunha. Movement quantification in epileptic seizures: a new approach to video-EEG analysis. *IEEE Trans. Biomed. Eng.*, 49(6):565–573, 2002.

[77] R. Lienhart and J. Maydt. An extended set of haar-like features for rapid object detection. In *IEEE International Conference on Image Processing*, pages 900–903, 2002.

[78] R Lienhart, A Kuranov, and V. Pisarevsky. Empirical analysis of detection cascades of boosted classifiers for rapid object detection. In *Pattern Recognition*, volume 2781 of *LNCS*, pages 297–304. Springer Berlin Heidelberg, 2003.

[79] B. Litt, R. Esteller, J. Echauz, M. DŠAlessandro, R. Shor, T. Henry, P. Pennell, C. Epstein, R. Bakay, M. Dichter, and G. Vachtsevanos. Epileptic seizures may begin hours in advance of clinical onset: a report of five patients. *Neuron*, 30(1):51–64, 2001.

[80] A. Liu, J.S. Hahn, G.P. Heldt, and R.W. Coen. Detection of neonatal seizures through computerized eeg analysis. *Electroencephalography and Clinical Neurophysiology*, 82(1):30–37, 1992.

[81] Q. Liu, R.J. Scalabassi, and M. Sun. Change detection in epilepsy monitoring video based on markov random field theory. In *International Symposium on Intelligent Signal Processing and Communication Systems*, 2004.

[82] H. Lu, H.L. Eng, B. Mandal, D.W.S. Chan, and Y.L. Ng. Markerless video analysis for movement quantification in pediatric epilepsy monitoring. In *33rd Annual International Conference of the IEEE EMBS*, 2011.

[83] B.D. Lucas and T. Kanade. An iterative image registration technique with an application to stereoscopic vision. In *International Conference of Artificial Intelligence*, 1981.

[84] E. Magiorkinis, S. Kalliopi, and A. Diamantis. Hallmarks in the history of epilepsy: epilepsy in antiquity. *Epilepsy & Behavior*, 17(1):103–108, 2010.

[85] T. Maiwald, M. Winterhalder, R. Aschenbrenner-Scheibe, H.U. Voss, A. Schulze-Bonhage, and J. Timmer. Comparison of three nonlinear seizure prediction methods by means of the seizure prediction characteristic. *Physica D-Nonlinear Phenomena*, 194(3–4):357–368, 2004.

[86] P. Maurel. *Shape gradients, shape warping and medical application to facial expression analysis.* PhD thesis, École Doctorale de Sciences Mathématiques de Paris Centre, 2008.

[87] P. Maurel, A. McGonigal, R. Keriven, and P. Chauvel. 3d model fitting for facial expression analysis under uncontrolled imaging conditions. In *19th International Conference on Pattern Recognition*, 2008.

[88] P.E. McSharry, L.A. Smith, and L. Tarassenko. Comparison of predictability of epileptic seizures by a linear and a nonlinear method. *IEEE Transactions on Biomedical Engineering*, 50(5):628–633, 2003.

[89] A. Meier, J.P.S. Cunha, C. Mauerer, C. Vollmar, and S. Noachtar. Quantified analysis of wrist and trunk movements differentiates between hypermotor and automotor seizures. *Epilepsia*, 46, suppl. 6:157, 2005.

[90] Z. Mirzadjanona, A.S. Peters, J. Rémi, C. Bilgin, J.P.S. Cunha, and S. Noachtar. Significance of lateralization of upper limb automatisms in temporal lobe epilepsy: A quantitative movement analysis. *Epilepsia*, 51(10):2140–2146, 2010.

[91] T. Moeslund and E. Granum. A survey of computer vision-based human motion capture. *Computer Vision Image Understanding*, 81:231–268, 2001.

[92] T.B. Moeslund, A. Hilton, and V. Krüger. A survey of advances in vision-based human motion capture and analysis,. *Computer Vidion Image Understanding*, 104:90–126, 2006.

[93] F. Mormann, T. Kreuz, R.G. Andrzejak, P. David, K. Lehnertz, and C.E. Elger. Epileptic seizures are preceded by a decrease in synchronization. *Epilepsy Research*, 53(3):173–185, 2003.

[94] F. Mormann, T. Kreuz, C. Rieke, R.G. Andrzejak, A. Kraskov, P. David, C.E. Elger, and K. Lehnertz. On the predictability of epileptic seizures. *Clinical Neurophysiology*, 116(3):569–587, 2005.

[95] L. Mündermann, S. Corazza, and T.P. Andriacchi. The evolution of methods for the capture of human movement leading to markerless motion capture for biomechanical applications,. *Journal of Neuroengineering and Rehabilitation*, 3, 2006.

[96] G. M. K. Ntonfo, G. Ferrari, R. Raheli, and F. Pisani. Low-complexity image processing for real-time detection of neonatal clonic seizures. *IEEE Transactions on Information Technology in Biomedicine*, 16(3):375–382, 2012.

[97] G. M. K. Ntonfo, F. Lofino, G. Ferrari, R. Raheli, and F. Pisani. Video processing-based detection of neonatal seizures by trajectory features clustering. In *2012 IEEE International Conference on Communications - Selected Areas in Communications Symposium*, 2012.

[98] R O'Dwyer. *Quantitative Analysis of Ictal Head Movements in Temporal Lobe Epilepsy.* PhD thesis, Ludwigs-Maximilians-Universität zu München, 2007.

[99] R. O'Dwyer, J.P.S. Cunha, C. Vollmar, C. Mauerer, R.C. Burgess, A. Ebner, and S. Noachtar. Lateralizing significance of quantitative analysis of versive head movements during seizures of patients with temporal lobe epilepsy. *Epilepsia*, 46, suppl. 6:304, 2005.

[100] R. O'Dwyer, J.P.S. Cunha, C. Vollmar, C. Mauerer, B. Feddersen, R.C. Burgess, A. Ebner, and S. Noachtar. Lateralizing significance of quantitative analysis of head movements before secondary generalization of seizures of patients with temporal lobe epilepsy. *Epilepsia*, 48(3):524–530, 2007.

[101] Alan V. Oppenheim, Roland W. Schafer, and John R. Bruck. *Discrete-time signal processing.* Prentice-Hall, 2nd edition, 1999.

[102] N. Paivinen, S. Lammi, A. Pitkanen, J. Nissinen, M. Penttonen, and T. Gronfors. Epileptic seizure detection: a nonlinear viewpoint. *Computer Methods and Programs in Biomedicine*, 79(2):151–159, 2005.

[103] P.R. Pal, P. Khobragade, and R. Panda. Expert system design for classification of brain waves and epileptic-seizure detection. In *Students' Technology Symposium (TechSym), IEEE*, pages 187–192, Jan 2011. doi: 10.1109/TECHSYM.2011.5783822.

[104] C. P. Panayiotopoulos. Typical absence seizures and related epileptic syndromes: Assesment of current state and directions for future research. *Epilepsia*, 49(8):2131–2147, 2008.

[105] C. P. Panayiotopoulos. *Epilepsies Vade Mecum.* MEDICANAE, 2009.

[106] C. P. Panayiotopoulos, T. Obeid, and G. Waheed. Differentiation of typical absence seizures in epileptic syndromes. A video EEG study of 224 seizures in 20 patients. *Brain*, 112:1039–1056, 1989.

[107] Y. Park, L. Luo, K.K. Parhi, and T. Netoff. Seizure prediction with spectral power of EEG using cost-sensitive support vector machines. *Epilepsia*, 52(10):1761–1770, 2011.

[108] M. Pediaditis, M. Tsiknakis, P. Vorgia, D. Kafetzopoulos, V. Danilatou, and D. Fotiadis. Vision-based human motion analysis in epilepsy - Methods and challenges. In *10th IEEE International Conference on Information Technology and Applications in Biomedicine (ITAB)*, pages 1–5, 2010.

[109] M. Pediaditis, M. Tsiknakis, V. Bologna, and P. Vorgia. Model-free vision-based facial motion analysis in epilepsy. In *10th International Workshop on Biomedical Engineering (BioEng)*, 2011.

[110] M. Pediaditis, M. Tsiknakis, L. Koumakis, M. Karachaliou, S. Voutoufianakis, and P. Vorgia. Vision-based absence seizure detection. In *34th Annual International Conference of the IEEE EMBS*, 2012.

[111] M. Pediaditis, M. Tsiknakis, V. Kritsotakis, M. Góralczyk, S. Voutoufianakis, and P. Vorgia. Exploiting advanced video analysis technologies for a smart home monitoring platform for epileptic patients: Technological and legal preconditions. In *International Conference on Telecommunications and Multimedia (TEMU)*, 2012.

[112] M. Pediaditis, M. Tsiknakis, and N. Leitgeb. Vision-based motion detection, analysis and recognition of epileptic seizures - A systematic review. *Computer methods and programs in biomedicine*, 108(3):1133–1148, 2012.

[113] G. Peeters. A large set of audio features for sound description (similarity and classification) in the cuidado project. Technical report, IRCAM, Analysis/Synthesis Team, 2004.

[114] F. Pisani, C. Spagnoli, C. Pavlidis, E. amd Facini, G.M. Kouamou Ntonfo, G. Ferrari, and R. Raheli. Real-time automated detection of clonic seizures in newborns. *Clinical Neurophysiology*, 125: 1533–1540, 2014.

[115] J. Platt. *Advances in Kernel Methods - Support Vector Learning - Fast Training of Support Vector Machines using Sequential Minimal Optimization.* 1998.

[116] K. Polat and S. Güneş. Classification of epileptiform eeg using a hybrid system based on decision tree classifier and fast fourier transform. *Applied Mathematics and Computation*, 187(2):1017–1026, 2007.

[117] R. Poppe. Vision-based human motion analysis: an overview. *Computer Vision Image Understanding*, 108:4–18, 2007.

[118] H. Qu and J. Gotman. A patient-specific algorithm for the detection of seizure onset in long-term EEG monitoring: possible use as a warning device. *IEEE Transactions on Biomedical Engineering*, 44(2):115–122, 1997.

[119] R. Quinlan. *C4.5: Programs for Machine Learning.* Morgan Kaufmann Publishers, San Mateo, CA, 1993.

[120] E. Ramasso, C. Panagiotakis, D. Pellerin, and M. Rombaut. Human action recognition in videos based on the Transferable Belief Model. *Pattern Analysis and Applications*, 11(1):1–19, 2008.

[121] J. Rémi, J.P.S. Cunha, C. Vollmar, Ö.B. Topçuoğlu, A. Meier, S. Ulowetz, P. Beleza, and S. Noachtar. Quantitative movement analysis differentiates focal seizures characterized by automatisms,. *Epilepsy & Bahavior*, 20:642–647, 2011.

[122] J. Rémi, P. Wagner, R. O'Dwyer, Cunha J.P.S., C. Vollmar, I. Krotofil, and S. Noachtar. Ictal head turning in frontal and temporal lobe epilepsy. *Epilepsia*, 52(8):1447–1451, 2011.

[123] Z. Rogowski, I. Gath, and E. Bental. On the prediction of epileptic seizures. *Biol Cybern*, 42(1): 9–15, 1981.

[124] H. Rowley, S. Baluja, and T. Kanade. Neural network-based face detection. *IEEE Transactions on Pattern Analysis and Machine Intelligence*, 20(1):23–38, 1998.

[125] V. Sakkalis, C.D. Giurcaneanu, Xanthopoulos P., M.E. Zervakis, Tsiaras V., Yang Y., Karakonstantaki E., and S. Micheloyannis. Assessment of linear and nonlinear synchronization measures for analyzing eeg in a mild epileptic paradigm. *IEEE Trans Inform Tech Biomed*, 13(4):433–441, 2009.

[126] A. Sami, N.B. Karayiannis, J.D. Frost Jr., M.S. Wise, and E.M. Mizrahi. Automated tracking of multiple body parts in video recordings of neonatal seizures. In *2004 IEEE International Symposium on Biomedical Imaging: Nano to Macro*, 2004.

[127] B. Schäling. *The Boost C++ Libraries.* XML Press, 2011.

[128] S.J.M. Smith. EEG in the diagnosis, classification and management of patients with epilepsy. *Journal of Neurology, Neurosurgery and Psychiatry*, 76 (Supplement 2):2–7, 2005.

[129] V. Srinivasan, C. Eswaran, and N. Sriraam. Artificial neural network based epileptic detection using time-domain and frequency-domain features. *Journal of Medical Systems*, 29(6):647–660, 2009.

[130] C.J. Stam. Nonlinear dynamical analysis of eeg and meg: review of an emerging field. *Clinical Neurophysiology*, 116(10):2266–2301, 2005.

[131] H. Steg, H. Strese, C. Loroff, J. Hull, and S. Schmidt. Europe is facing a demographic challenge - ambient assisted living offers solutions. Technical report, compiled within the Specific Support Action "Ambient Assisted Living Ũ preparation of an article 169-initiative", 2006.

[132] Y. Tian, T. Kanade, and J. Cohn. Facial expression analysis. In S.Z. Li and A.K. Jain, editors, *Handbook of Face Recognition*, pages 247–275. Springer, New York, 2005.

[133] C. Tomasi and T. Kanade. Detection and tracking of point features. Technical Report CMU-CS-91-132, Carnegie Mellon University, Pittsburgh, 1991.

[134] A.T. Tzallas, M.G. Tsipouras, D.G. Tsalikakis, E.C. Karvounis, L Astrakas, S. Konitsiotis, and M. Tzaphlidou. *Epilepsy - Histological, Electroencephalographic and Psychological Aspects, Chapter 4 - Automated Epileptic Seizure Detection Methods: A Review Study.* InTech, 2012.

[135] E.D. Übeyli. Lyapunov exponents/ probabilistic neural networks for analysis of eeg signals. *Expert Systems with Applications*, 37(2):985–992, 2010.

[136] S. Ulowetz, J.P.S. Cunha, C. Mauerer, C. Vollmar, B. Feddersen, and S. Noachtar. Quantitative movement analysis of extent of wrist movements identifies hypermotor seizures in a non-selected sample of focal epileptic motor seizures. *Epilepsia*, 46, suppl. 6:157, 2005.

[137] W. van Drongelen, S. Nayak, D.M. Frim, M.H. Kohrman, V.L. Towle, H.C. Lee, A.B. McGee, M.S. Chico, and K.E. Hecox. Seizure anticipation in pediatric epilepsy: use of Kolmogorov entropy. *Pediatric Neurology*, 29(3):207–213, 2003.

[138] P. Vannemreddy, Stone J.L., and Slavin K.V. Frederic Gibbs and his contributions to epilepsy surgery and electroencephalography. *Neurosurgery*, 70(3):774–782, 2012.

[139] G. Vavoulas, M. Pediaditis, C. Chatzaki, E. G. Spanakis, and M. Tsiknakis. The MobiFall Dataset: Fall Detection and Classification with a Smartphone. *International Journal of Monitoring and Surveillance Technologies Research (IJMSTR)*, 2(1):44–56, 2014.

[140] S.S. Viglione and G.O. Walsh. Epileptic seizure prediction. *Electroencephalography and Clinical Neurophysiology*, 39:435–436, 1975.

[141] P Viola and M.J. Jones. Rapid object detection using a boosted cascade of simple features. In *IEEE Computer Society Conference on Computer Vision and Pattern Recognition*, 2001.

[142] P. Wagner, J.P.S. Cunha, C. Vollmar, C. Mauerer, R. Burgess, A. Ebner, and S. Noachtar. Comparison of quantified ipsilateral and contralateral head movements in patients with frontal and temporal lobe epilepsy. *Epilepsia*, 45, suppl. 7:268–269, 2004.

[143] M. Winterhalder, T. Maiwald, H.U. Voss, R. Aschenbrenner-Scheibe, J. Timmer, and A. Schulze-Bonhage. The seizure prediction characteristic: a general framework to assess and compare seizure prediction methods. *Epilepsy & Behavior*, 4(3):318–325, 2003.

[144] X. Yang, L. Chen, Y. Liu, D. Zeng, Y. Tang, B. Yan, X. Lin, L. Liu, H. Xu, and D. Zhou. Motor trajectories in automatisms and their quantitative analysis. *Epilepsy Research*, 83:97–102, 2009.

[145] Q. Yuan, W. Zhou, Y. Liu, and J. Wang. Epileptic seizure detection with linear and nonlinear features. *Epilepsy & Behavior*, 24(4):415–421, 2012.

[146] E.I. Zacharaki and A. Bezerianos. Segmentation of pathology by statistical modeling and distributed estimation. In *10th International Workshop on Biomedical Engineering (BioEng)*, 2011.

[147] A.S. Zandi, G.A. Dumont, M. Javidan, and R. Tafreshi. An entropy-based approach to predict seizures in temporal lobe epilepsy using scalp eeg. In *31st Annual International Conference of the IEEE EMBS*, pages 228–231, 2009.

[148] Mi Zhang and A.A. Sawchuk. A feature selection-based framework for human activity recognition using wearable multimodal sensors. In *6th International Conference on Body Area Networks*, 2011.